UNIVERSITY OF CALIFORNIA, SAN DIEGO

Effects of Slurry Chemistry on the Rate of Agglomeration of Alumina Nanoparticles for Chemical Mechanical Planarization

A dissertation submitted in partial satisfaction of the requirements for the degree of

Doctor of Philosophy

in

Materials Science and Engineering

by

Neil Anjan Brahma

Committee in charge:

Professor Jan B. Talbot, Chair
Professor Guarav Arya
Professor Eric Fullerton
Professor Joanna McKittrick
Professor Andrea Tao

2013

The dissertation of Neil Anjan Brahma is approved, and it is acceptable in quality and form for publication on microfilm and electronically:

Chair

University of California, San Diego

2013

Dedicated to my parents and

brother

TABLE OF CONTENTS

LIST OF FIGURES

LIST OF TABLES

ACKNOWLEDGEMENTS

First, I would like to thank Professor Jan Talbot for her support as chair of my committee and her invaluable support with the experiments, data analysis, writing, and editing of the numerous publications and presentations. I also extend my gratitude to the University of California, Berkeley IMPACT program for its support along with the partner companies: Applied Materials, AMSL, Ebara Technologies, Global Foundries, IBM, Intel Corporation, KLA-Tencor, Marvell, Mentor Graphics, Novellus Systems, Panoramic Tech, SanDisk, Synopsys, Tokyo Electron Limited, and Xilinx Inc, along with matching support by the UC Discovery Grant ele07-10283.

I would also like to thank Mimi Wang for her help with the mathematical analysis along with Kasia Matusik and Robin Ihnfeldt for her support with the particle size distribution and aggregation rate measurements. Also, I would like to thank Ryan Anderson and Aruni Suwarnasarn for their help with the SEM and ESEM experiments. Their invaluable guidance with using the SEM instrument is much appreciated. Additionally I extend my thanks to the Nano3 facility at CalIT2 along with its entire staff for providing and supporting the SEM used for imaging experiments. I also would like to acknowledge Cabot Corporation for their supply of the alumina dispersion used in experiments. Finally I would like to thank all of my friends from my materials science class and beyond, who are too many to name now, whose support and advice throughout my graduate career has been inestimable.

Chapter 2 is a reprint of the material as it appears in Chemical Mechanical Polishing 10, Neil Brahma, Mike Chan, and Jan B. Talbot, Vol 19 (2009), along with

material as it appears in Chemical Mechanical Polishing 11, Neil Brahma and Jan B. Talbot, Vol 33 (2010). The dissertation author was the primary investigator and author of this material.

Chapter 3 in part is currently being prepared for submission for publication of the material; Neil Brahma and Jan B. Talbot. The dissertation author was the primary investigator and author of this material.

Chapter 4, in full, is a reprint of the material as it appears in the Proceedings of the International Conference of Planarization/CMP Technology, Neil Brahma and Jan B. Talbot, (2010). The dissertation author was the primary investigator and author of this material.

Chapter 5 in part is currently being prepared for submission for publication of the material; Neil Brahma and Jan B. Talbot. The dissertation author was the primary investigator and author of this material

Chapter 7 in part is currently being prepared for submission for publication of the material; Neil Brahma and Jan B. Talbot. The dissertation author was the primary investigator and author of this material

VITA

2008	Bachelor of Science and Engineering, Case Western Reserve University
2008-2013	Graduate Student Researcher, University of California, San Diego
2011-2012	Teaching Assistant, Department of NanoEngineering, University of California, San Diego
2009	Master of Science, University of California, San Diego
2013	Doctor of Philosophy, University of California, San Diego

PUBLICATIONS

“Effect of Copper CMP Slurry Chemistry on the Rate of Agglomeration of Alumina Particles,” N. Brahma, M. Chan, J. B. Talbot, *Chemical Mechanical Polishing 10*. **19** (7), 25-30 (2009).

“Effect of Copper CMP Slurry Chemistry on the Rate of Agglomeration of Alumina Particles”, N. Brahma, M.C. Chan, and J.B. Talbot, Abstract No. 732, 215th Electrochemical Society Meeting, San Francisco (Oct. 2009).

“Effects of CMP Slurry Additives on the Rate of Agglomeration of Alumina Particles,” N. Brahma and J. B. Talbot, *Chemical Mechanical Polishing 11*. **33**(10), 53 (2010).

“Effects of CMP Slurry Additives on the Rate of Agglomeration of Alumina Particles,” N. Brahma and J.B. Talbot, Abstract No. 1465, The Electrochemical Society Meeting, Las Vegas (Oct. 2010).

“Effects of CMP Slurry Chemistry on the Isoelectric Point of Alumina Particles,” N. Brahma and J. B. Talbot, *Proceedings of International Conference on Planarization/CMP Technology*, Phoenix, AZ (2010).

"Effect of Chemical Additives on the Agglomeration and Zeta Potential of Alumina Nanoparticles", N. Brahma and J.B. Talbot, Abstract No. 2511. The Electrochemical Society Meeting, Honolulu (Oct. 2012).

“Effects of CMP Slurry Additives on the Agglomeration of Alumina Nanoparticles I: General Aggregation Behavior,” N. Brahma and J. B. Talbot, to be submitted to *J. Colloid Interface Sci.*

“Effects of CMP Slurry Additives on the Agglomeration of Alumina Nanoparticles II: Aggregation Rate Analysis,” N. Brahma and J. B. Talbot, to be submitted to *J. Colloid Interface Sci.*

"Time Dependent Modeling of Copper CMP Using Colloidal Behavior of the Alumina Slurry ," N. Brahma and J. B. Talbot, to be submitted to *J. Electrochem. Soc.*

PRESENTATIONS

"Modeling of Copper Chemical Mechanical Planarization (CMP)," N. Brahma, R. Ihnfeldt, and J. B. Talbot, 2nd Impact Workshop, Advanced Micro Devices, Sunnyvale, CA, 29 Oct, 2008, Poster.

2009 Department Best Poster Finalist – "Modeling of Copper Chemical Mechanical Planarization," N. Brahma and J. B. Talbot, 2009 Jacobs School of Engineering Research Expo, University of California, San Diego, 19 Feb, 2009, Poster.

"Modeling of Copper Chemical Mechanical Planarization (CMP)," N. Brahma, and J. B. Talbot, 3rd Impact Workshop, Advanced Micro Devices, Sunnyvale, CA, 15 Apr, 2009, Poster.

"Effect of Copper CMP Slurry Chemistry on the Rate of Agglomeration of Alumina Particles," N. Brahma, 215th Electrochemical Society Meeting, San Francisco, CA, 25 May, 2009, Presentation.

"Effects of CMP Slurry Additives on the Agglomeration of Alumina Particles," N. Brahma and J. B. Talbot, 4th Impact Workshop, Mentor Graphics, Fremont, CA, 2 Nov, 2009, Poster.

"Effect of Particle Concentration on the Agglomeration of Alumina Particles" N. Brahma and J. B. Talbot, 5th Impact Workshop, Applied Materials, Mountain View, CA, 2 Apr, 2010, Poster.

"Effect of Particle Concentration on the Agglomeration of Alumina Particles," N. Brahma and J. B. Talbot, 2010 Jacobs School of Engineering Research Expo, University of California, San Diego, 15 Apr, 2010, Poster.

"Effects of CMP Slurry Additives on the Rate of Agglomeration of Alumina Particles," N. Brahma, 218th Electrochemical Society Meeting, Las Vegas, NV, 11 Oct, 2010. Presentation.

"Effect of CMP Slurry Chemistry on Isoelectric Point of Alumina Particles," N. Brahma and J. B. Talbot, 6th Impact Workshop, KLA-Tencor, Milpitas, CA, 5 Nov, 2010, Poster.

"Effect of CMP Slurry Chemistry on Isoelectric Point of Alumina Particles," N. Brahma and J. B. Talbot, 2010 International Conference on Planarization/CMP Technology, The Biltmore, Phoenix, AZ, 14-17 Nov, 2010, Poster.

“Effect of Copper CMP Slurry Chemistry on Agglomeration of Alumina Particles,” N. Brahma and J. B. Talbot, Intel Webinar, 28 Jan, 2011, Presentation.

“Effects of CMP Slurry Chemistry on Isoelectric Point of Alumina Particles,” N. Brahma and J. B. Talbot, 2011 Jacobs School of Engineering Research Expo, University of California, San Diego, 14 Apr, 2011, Poster.

“Effects of Chemical Additives on the Agglomeration and Zeta Potentials of Alumina Nanoparticles,” N. Brahma and J. B. Talbot, 8th Impact Workshop, Gobalfoundries, Milpitas, CA 27 Jan, 2012, Poster.

“Effects of Chemical Additives on the Agglomeration Rate of Alumina Nanoparticles, N. Brahma and J. B. Talbot, 2012 Jacobs School of Engineering Research Expo, University of California, San Diego, 12 Apr, 2012, Poster.

ABSTRACT OF THE DISSERATION

Effects of Slurry Chemistry on the Rate of Agglomeration of Alumina Nanoparticles for Chemical Mechanical Planarization

by

Neil Anjan Brahma

Doctor of Philosophy in Materials Science and Engineering

University of California, San Diego, 2013

Professor Jan B. Talbot, Chair

Chemical mechanical planarization (CMP) is a polishing process used during the manufacture of microelectronic integrated circuits. During fabrication of multilevel circuitry, excess deposited material must be removed and the wafer surface globally planarized for proper function of devices. This is especially necessary with copper interconnects, thus, copper CMP was the focus of this study. CMP requires the use of a slurry containing nanometer-sized abrasive particles along with a variety of chemical additives. The particles and chemicals act synergistically to mechanically and chemically remove material and provide a near globally planar surface. For optimal CMP performance, the effective abrasive particle size must be controlled. If particles aggregate, CMP performance may diminish and possibly even cause defective devices. The chemistry of the slurry (pH, ions present, etc) can not only affect the mean aggregate size of the abrasive particles, but also growth of aggregate over time.

This research investigated the aggregation behavior of suspensions of 150 nm alumina particles in 1mM KNO_3 with various additives (glycine, H_2O_2, benzotriazole, and sodium dodecyl sulfate) used in CMP of copper through effective particle (agglomerate) size versus time and zeta potential measurements. Aggregate size rate data were analyzed to elucidate the mechanism of aggregation, as well its effect on the structure of the resultant aggregate. The effects of temperature of the slurry were also explored. Finally, particle size distribution data collected at various stages of aggregation were incorporated into the Luo and Dornfeld model of CMP to investigate the dynamic nature of the CMP process.

CHAPTER 1

BACKGROUND OF CHEMICAL MECHANICAL PLANARIZATION

1.1 Introduction

Chemical mechanical planarization (CMP) is a polishing process used in the fabrication of integrated circuits (ICs) to produce a globally planarized wafer surface. Borrowing heavily from glass polishing, the CMP process involves rotating the wafer while pressing it against a rotating polishing pad (typically polyurethane). An aqueous slurry containing abrasive particles and other chemicals is dispensed onto the rotating pad and a synergistic effect produced by the chemicals and abrasives within the slurry actively removes material both chemically and mechanically [1]. A schematic of a typical CMP process is shown in Figure 1.1.

CMP was implemented beginning in the 1980's by IBM as a method to planarize inter-level dielectrics [2]. The need for a smooth surface increased as device dimensions shrunk and multi-level metallization was implemented to reduce the interconnect delay that dominates as the feature sizes reduced to sub-micron (<0.5 μm) [3]. As subsequent layers are added to the device, topography buids up on the surface, causing defects and depth of focus issues during photolithography [1]. Increased topography also reduces yield in the photolithography and dry etch processing steps. Reduced feature sizes has also required a smoother substrate surface [4].

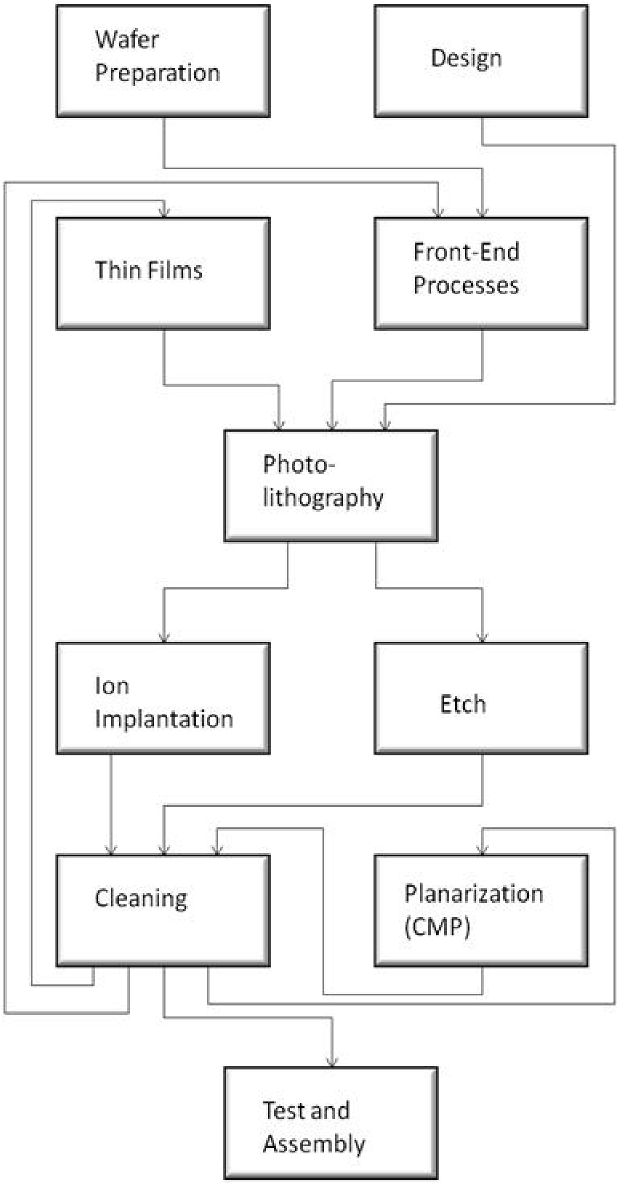

Figure1.1. A typical wafer processing flow diagram that shows CMP is an integral part of the manufacturing process [from 1].

Other planarization techniques besides CMP have been used. Such techniques include spin coating of a material in liquid form (including low-k dielectrics, polymeric dielectrics, etc) which then dry, and reactive ion etching of a surface and etch back (where an IC pattern is etched onto the substrate followed by spin-coating of a photoresist to fill in trenches and vias leaving hills in the patterns exposed for further etching by plasma, a process typically used to etch SiO_2 and other dielectrics) [4]. Each technique has its advantages but also numerous drawbacks. For example, the dielectric materials used in spin coating can absorb moisture leading to cracking and peeling, while reactive ion and etch back utilizes high energy ion bombardment which can damage devices and artifacts resulting from the lithography step may require further planarization [4]. Of all planarization techniques employed in industry, only CMP is able to provides the near to complete global planarity that is required for processing ICs and is robust enough to use on many different materials (including silicon, tungsten, copper, etc) for a multitude of applications (interconnects, interlayer dielectrics, diffusion barriers, etc) [4].

The work of this dissertation is a continuation of the colloidal studies of the alumina particles used in copper CMP slurries by Gopal [15, 16] and Ihnfeldt [17-20]. Gopal's work investigated the effects of common copper CMP additives on the colloidal behavior of the slurries through measurements of zeta potential and particle size distributions as a function of slurry chemistry [15]. Ihnfeldt continued Gopal's work by further studying the colloidal behavior of the alumina slurries with different CMP additives as a function of chemistry also through zeta potential and particle size measurements [17]. Ihnfeldt focused on the effect of copper in solution on the colloidal behavior of the slurry [17]. Both Gopal and Ihnfeldt incorporated their experimental results into the Luo and Dornfeld model of CMP in order to predict material removal rate for copper CMP[16, 18]. Ihnfeldt also investigated the effects of slurry chemistry on the nanohardness of copper to include in the model [19, 20]. A more detailed review of Gopal and Ihnfeldt's work is presented in Chapter 2.

During particle size measurements, Ihnfeldt ultrasonicated the suspensions after preparation to break up any aggregates that may have formed during the preparation procedure [2]. Ihnfeldt observed growing agglomerate sizes for alumina dispersed in 1mM KNO_3 at pH 7.5, aggregating to average sizes >5 μm within 2 hours [2]. Because CMP slurries can reside on the wafer for up to 10 minutes before being replaced with fresh slurry [2], Ihnfeldt had used this data to determine that it was necessary to measure particle sizes 10 minutes after ultrasonication to obtain data comparable to the copper CMP process. These results indicated that aggregation of the slurry particles could occur at measureable rates; however the phenomenon has not been studied in much detail by her or others.

The main focus of this study was to investigate rate of aggregation of the slurry particles. The individual effects of each additive on the zeta potential and dispersion of the alumina particles was studied. Additives and their concentrations for the study were chosen based on those used by Gopal and Ihnfeldt, which were also used in measurements of material removal rates for copper CMP [2, 15-20]. In this study, for steadily aggregating suspensions, aggregation rates were measured and analyzed by determining a stability ratio, a measure of the effectiveness of the energy barrier (detailed in section 1.5) to prevent aggregation, and by using fractal dimension analysis which can give information about the openness of the aggregate structure.

This dissertation is organized as follows. The following sections in this chapter present a background of the CMP process. The process steps will be described along with common process parameters and variables. The CMP slurry is described along with discussion of the effects of particle size on CMP performance. A brief discussion of the theory of particle aggregation will also be presented.

Chapter 2 presents a detailed review of Ihnfeldt's and Gopal's work on the colloidal behavior of alumina nanoparticles. Preliminary aggregation rate measurements and fractal dimension analysis is also presented.

Chapter 3 presents systematic measurements of the aggregate size and zeta potentials of various alumina slurries composed of various mixtures of chemical additives and a range of pH. A literature review is presented of work on the effects of solution chemistry on colloidal stability.

Chapter 4 discusses the effects of temperature on the colloidal behavior of alumina. A literature review of the effects of temperature on the colloidal behavior of nanoparticles is presented followed by a presentation of zeta potential measurements of alumina nanoparticles as a function of pH and temperature.

Chapter 5 contains aggregate size measurements over time for the various suspensions investigated in Chapter 3. A review of aggregation rate literature is presented focusing on methods of analysis. The application of these analysis methods to the collected data is also presented.

Chapter 6 presents scanning electron microscopy images of the alumina aggregates. A discussion of the challenges inherent in the imaging process as well as potential solutions including use of an environmental scanning electron microscope is also presented.

Chapter 7 presents the results of incorporating the collected aggregation rate data into the Luo and Dornfeld model of CMP. A brief review of CMP models is presented along with a discussion of the Luo and Dornfeld model. Finally, model predictions using experimental particle size distribution data at various stages of aggregation is presented.

Chapter 8 presents final conclusions of the study. Proposed future work that can further the understanding of the aggregation phenomenon is also discussed.

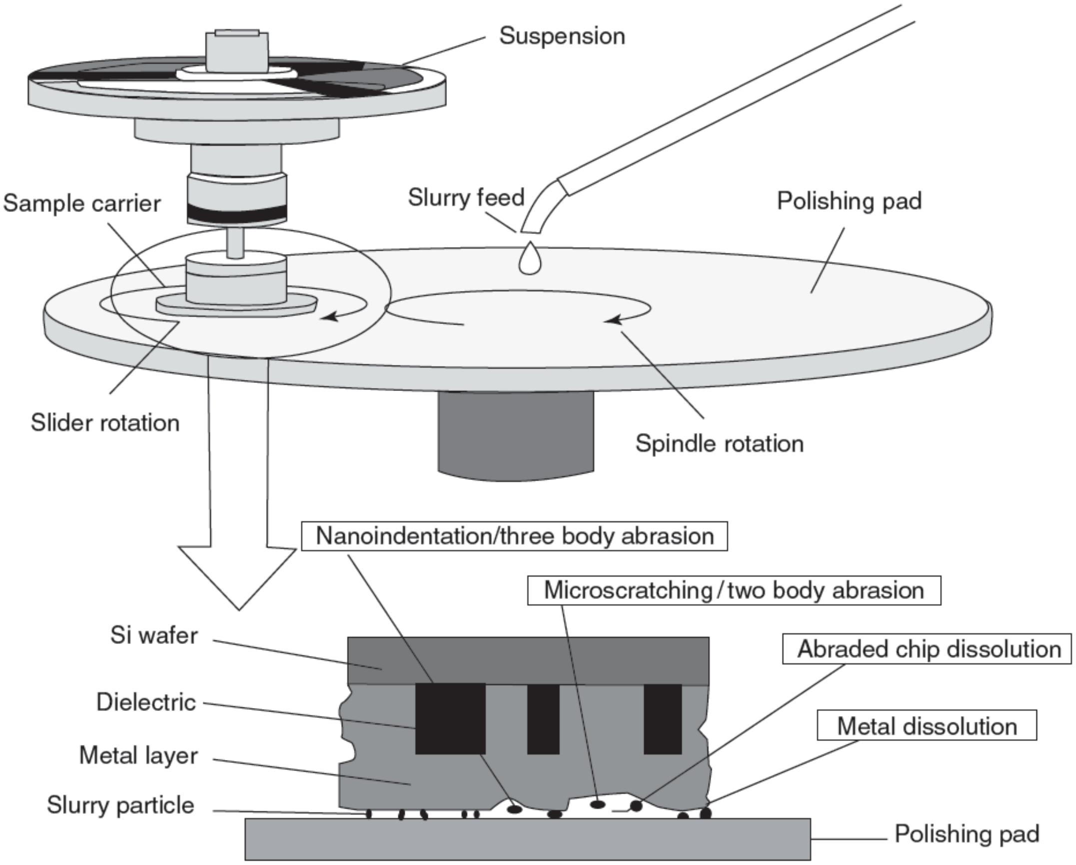

Figure1.2. Schematic of the CMP process [from 5].

1.2 CMP Process

The first step during the CMP process is fixing the wafer to the wafer carrier. The wafer carrier holds and rotates the substrate against a rotating polishing pad, typically made of polyurethane, and applies down pressure to activate the mechanical polishing. An aqueous slurry is dispensed onto the surface of the pad [1].

The polishing pad serves two functions; to transport the slurry to the substrate surface and to press the abrasive particles to the substrate. Asperities on the pad surface force the particles against the substrate and, due to the pressure applied by the pad, material is mechanically removed. Additives in the slurry chemically react with the substrate surface to chemically soften, passivate, or etch material. Other additives are used for complexation with removed metal (aiding in dissolution of removed material) to prevent redeposition or excessive scratching by undissolved material. This synergistic effect between the mechanical and chemical nature of the process is credited for producing the near global planarity of the wafer surface [9]. The role of the CMP slurry will be discussed in more detail in Section 1.4.

As planarization proceeds the polishing pad becomes fouled and glazes over time [9]. This occurs as slurry particles become embedded in the pad and fill in the features. This is typically remedied by utilizing a diamond grit conditioner head that is applied in situ onto the pad to remove embedded particles and the top layer of the pad itself. A careful balance must be met that enough pad material is removed to restore its polishing performance without unnecessarily reducing the lifetime of the pad.

Table 1.1 shows the multitude of operating parameters for the CMP process. Typical wafer head and pad rotation velocities range from 30 to 120 rpm, while carrier down pressure can range from 1 to 9 psi. Slurry flow rates range from 50 to 300 ml/min. The slurry flow is continuous and the residence time of the slurry on the substrate surface is ~10 minutes. Conditioner head pressures can range from 1 to 5 psi with diamond grit sizes ranging from 70 to 180 μm [6]. Conditioners can also have various shapes (crosses, open circle, closed circle) and diamond attachment methods (electroplated nickel over diamonds, chemical brazing, etc.) [7, 8]. CMP slurry performance is typically quantified by material removal rates (MRR) and typical MRR for copper CMP range from 50 to 1000 nm/min [2]. Other performance measures include within-wafer nonuniformity (WIWNU) and wafer-to-wafer nonuniformity (WTWNU) [1].

With all the variables inherent to the CMP process, extensive experimentation is required to determine the best operating conditions and the slurry chemistry must be developed for each material to be planarized [2]. As new materials are introduced, CMP process parameters must again be determined. A more fundamental understanding of the process and variables themselves would be therefore invaluable in the development of improved consumables, such as the slurry and pad. Details regarding the CMP slurry will be discussed in Section 1.4.

CMP is classified into two types: oxide CMP and metal CMP [2]. Oxide CMP consists of polishing of the polysilicon or dielectric materials used to insulate circuitry. Metal CMP is utilized during the production of damascene structures that serve as connections of transistors manufactured in underlying layers [1]. These types of CMP have been described in greater detail elsewhere [1]. Metal CMP is the most complex as it involves removal of several types of material (dielectric, barrier layers, etc.), as well as metal; types of metal CMP include shallow trench isolation, tungsten CMP, and copper CMP. During the manufacture of integrated circuits multiple CMP steps are necessary and both types of CMP (oxide and metal) may be required.

Table 1.1. Summary of CMP process parameters [from 4].

Input Variables

Machine Parameters:
- Down Pressure
- Linear Velocity
- Slurry Flow

Slurry Characteristics:
- Particle Characteristics
  - Size
  - Size Distribution
  - Shape
  - Mechanical Properties
  - Chemistry
  - Dispersion
  - Concentration
  - Agglomeration
  - Oversize Particles
- Slurry Chemistry
  - Oxidizers
  - pH and pH Drifts
  - pH Stabilizers
  - Complexing Agents
  - Dispersants
  - Concentration

Pad Characteristics:
- Mechanical Properties
- Topography
- Conditioning
- Pad Uniformity

Substrate Characteristics:
- Feature Size
- Feature Density

Micro Scale Parameters

Pad:
- Contact Area
- Pad Pressure

Particles on Pad:
- Pressure
- Coverage

Chemical Concentration

Distribution

Contact Mode:
- Direct
- Hydroplaning
- Mixed

Nanoscale Parameters

Chemical Etching

Mechanical Removal

Chemo-Mechanical:
- Surface Layer Formation
- Thickness
- Uniformity
- Rate of Formation
- Layer Removal

Output Parameters

Removal Rate

Planarization

Surface Finish

End Point

Selectivity

Wafer to Wafer Uniformity

Within Wafer Uniformity

Dishing and Erosion Resistance

1.3 Why Copper?

Since the early 1990's copper has been the interconnect material of choice for its high thermal conductivity and low electrical resistivity, replacing aluminum [10, 11]. Because copper does not form a volatile compound at low pressures, it cannot be deposited by reactive ion etching, a process used to deposit aluminum. Instead a damascene process is used. This process begins with the deposition of the dielectric material followed by etching of the layer to produce the circuitry patterns. Vias (conductive connections between layers) can also be etched after the initial etching of the circuitry, reducing the number of steps in the patterning process. To prevent electromigration of copper into the dielectric material, a barrier layer, typically composed of Ta or TaN, is first deposited followed by copper electrodeposition [1]. Copper CMP typically follows electrodeposition to remove the overburden of copper and obtain a nearly globally planar surface for subsequent layers of circuitry. The copper damascene process does not require the metal mask steps needed by aluminum interconnect [12]. Recent advances in metallization schemes have also enabled the fabrication of low resistance contacts of copper by filling in the high aspect ratio contacts without voids replacing tungsten at the contact level for 22 nm technology nodes and reducing the number of CMP steps necessary [14].

1.4 Slurry Chemistry

The CMP slurry is directly responsible for removing material and polishing the surface. A typical metal CMP slurry includes abrasive particles, typically in the nanometer size range; etching agents to soften metal and ease material removal; complexing agents to prevent re-deposition of material onto the surface; passivation agents to protect lower layers from excessive polishing; and surfactants for stability of the particles in solutions [5, 9]. Each component is included for a specific role, but each may have an effect on the overall MRR [40]. For example, MRR for 200 mm copper wafers measured by Armini et al. for slurries containing 90 nm silica abrasives varied considerably depending on the additives present; a MRR of only 7 nm/min was measure for 1 vol% H_2O_2, while a MRR of 425 nm/min was measured for 1 vol% H_2O_2 with 1 wt% glycine. When a combination of 0.018 wt% BTA was added to glycine and H_2O_2 with no abrasives, a MRR of 150 nm/min was measured [40].

The pH of the slurry affects the MRR of the CMP process in a few ways. The primary effect of pH is the altering of the surface charge of both the abrasive particles as well as the wafer surface. A strong surface charge of like polarity is desirable on all particles so that significant electrostatic repulsion prevents aggregation [9]. The pH can be adjusted such that the particles and wafer are of opposite polarity causing the wafer to attract the particles, useful for achieving high material removal rates [9]. Another significant effect of the pH is on the chemical dissolution rate of the metal and oxide surfaces and, for metal CMP, pH can affect the oxidation behavior of the metal surface. The oxidation state of the copper surface can alter the surface hardness [19] and consequently, the MRR [20].

The additives present in the slurry serve a multitude of roles. For metal CMP, oxidizing agents (such as hydrogen peroxide, nitric acid, or ammonium hydroxide) are added to oxidize the metal surface. The oxidizing reagent oxidize the recessed portions of the wafer, passivating it from wet etching while also dissolving exposed metal from the protruding regions [40]. This cycle of passivation, removal, and repassivation continues until the desired planarity and thickness is produced [40]. Nitric acid was first used as an oxidizer in copper CMP slurries, however the oxide layer was unstable and no passivation of the underlying metal occurred [25]. For most metal CMP, when hydrogen peroxide has been used, the metal surface evenly oxidized and the underlying layers are passivated without dissolution of the oxide layer on top [9]. During copper CMP, dissolved Cu^{2+} ions can catalyze the decomposition of H_2O_2 into OH^* radicals (a process known as the Fenton cycle), which are stronger oxidizers than H_2O_2 alone, increasing the uniformity and speed of formation of the passivation layer [26].

To further control the oxide layer, a corrosion inhibitor is typically added. This inhibitor does not prevent the oxidation of the metal from occurring, but rather aids in stabilizing the oxide layer and prevent detachment [9], a necessity for uniform polishing. This is achieved by the chemisorption of the inhibitor to the oxide surface [9]. For copper CMP, benzotriazole (BTA) is most commonly used, however more environmentally benign additives (such as ammonium dodecyl sulfate) are currently being studied as a potential alternative [9].

Other additives also include chelating and stabilizing agents. The chelating agents (typically glycine for copper CMP) are used to dissolve polishing debris to reduce the risk of scratching by the debris and to prevent redeposition of already removed material back onto the wafer surface [9]. As mentioned, glycine (H_2NCH_2COOH) is a common chelating agent used in copper CMP that can form soluble complexes with copper depending on pH; The predominant complexes range from $Cu(H_3NCH_2COO)^{2+}$ at pH 2, $Cu(H_2NCH_2COO)^{+}$ at pH 4, $Cu(H_3NCH_2COO)_2$ between pH 6 to 9, and $Cu(H_3NCH_2COO)_2^{-}$ at pH > 9.5 [2, 41]. Solubilized copper is desirable since then the copper will not redeposit onto the wafer surface or cause excessive scratching during the planarization process. Ethylenediaminetetraacetic acid (EDTA) is also commonly used as a complexing agent that can form soluble complexes with positive metal ions [2, 15]. Stabilizing agents are also added to ensure long slurry lifetime and stability by preventing abrasive particle aggregation [26]. For copper CMP the most common is stabilizer is sodium dodecyl sulfate (SDS), an anionic surfactant [9]. SDS typically adsorbs to the surface of particles and can sterically stabilize the dispersion [27].

The abrasive particles mechanically remove material from the surface. The choice of the particle (silica, alumina, ceria, etc) can vary depending on the type of CMP (oxide or metal) [1]. In colloidal systems, aggregation of particles is a common issue. The slurry industry differentiates agglomerates as two types: hard agglomerates (large size particles) and soft agglomerates (aggregates of smaller abrasive particles) [23]. The presence of either type of agglomerate is detrimental to the CMP process. Studies have shown that larger agglomerates can affect removal rates, increase surface roughness, and, if large enough, cause deep scratches [21, 23, 24, 35, 36]. The hard agglomerates greater than 2 μm in size can be easily filtered out of the slurries before use. Soft agglomerates, however, may form after the filtration step.

During CMP, aggregation of the abrasive particles can occur depending on the conditions of the process. It was shown that agglomerates can withstand the shear forces present during the CMP process and do not break up (unless agglomerate sizes are greater than ~4.5 μm) [19]. Studies on the effect of effective particle size on CMP are limited. Bielmann et al. investigated the effects of alpha alumina particle size on tungsten CMP and observed that increased average abrasive size corresponded with decreased material removal rates, however the overall surface roughness was identical for all particles sizes studied [21]. For example, a 2.2-2.4 μm particle size at 2 wt% solids loading yielded MRRs of ~120 nm/min, while particle sizes of 100-300 nm yielded removal rates of ~500 nm/min. They concluded that smaller average effective particle sizes typically gave a higher MRR [21]. Basim et al. investigated the effects of particle size on the MRR of p-type silicon wafers with a 1.5 μm SiO_2 layer deposited by plasma-enhanced chemical vapor deposition. The slurries used were prepared with commercial fumed silica (mean size of 140 nm) spiked with 0.5, 1.0, and 1.5 μm sol-gel silica particles at concentrations varying from 0.2 to 1.3 wt% [23]. They also observed decreased MRR when larger particles were added (however, increased MRR was observed when 1.5 μm particles when 1.1 wt% was added) and that the roughness of the surface increased significantly when larger particles were present for all conditions. However, Jung and Singh observed that, for copper CMP with silica particles, removal rates increased with increasing particle size from 100 to 1000 nm [35]. Li et al. observed no correlation between MRR of Cu and silica particle size (sizes 13 to 35 nm and concentrations from 1 to 2 wt%) at low down pressures of 1.5 psi and rotational velocities of 0.46 m/s, but noted higher MRR with larger abrasive sizes of 35 nm at higher down pressures of 2.5 psi and velocities of 1.09 m/s [36].

Particle size has also been observed to affect the overall number of defects from the CMP process. Tateyama et al. studied the number of defects on wafers polished with slurries of differing concentrations of ceria particles. They measured secondary particle sizes (larger particles formed by aggregation of smaller primary particles) and counted defects produced during polishing of blanket plasma-enhanced tetraethyl-orthosilicate (PE-TEOS) oxide deposited on silicon wafers. The number of scratches was significantly affected by the secondary particle size and, if the mean particle size was greater than 340 nm, the number of scratches increased dramatically from 10 to 100 counts per wafer [24].

Many slurry recipes have been developed and are uniquely tailored for the many types of CMP currently used in industry. Leading slurry manufacturers include Cabot Microelectronic Corporation, Dow Electronic Materials, Fuji Film Electronic Materials, DuPont Air Products Nano Materials LLC, Fujimi Corporation, Hitachi Chemicals Company, JSR Corporation, Cheil, and BASF [5].

The stability of the slurry is dependent on the chemistry. Ions present in the slurry can interact with the abrasive particle surface, altering surface charge and potentially destabilizing the slurry. Aggregation can occur during storage of the slurry before use and filtration is commonly employed to remove up to 80% of aggregates > 2 μm [39]. However, excessive aggregation can lead to reduced particle concentrations in the slurry once dispensed onto the polishing pad. Additionally, aggregation may occur during the CMP process itself where the slurry has a typical residence time of ~10min. The aggregation phenomenon will be discussed in further detail in the following section.

1.5 Particle Aggregation

A metal oxide surface in a liquid environment will develop an electrical double layer [27]. The surface charge on the surface originates from the acidic or basic dissociation of the metal hydroxide groups on the metal surface. In an acidic environment, where an excess of H^+ ions are present, an OH group on the surface may be protonated and then dissociate from the surface, forming water and leaving a net positive charge site. Conversely, when an excess of OH^- ions are present, as in a basic environment, an OH group may be de-protonated, again forming water but leaving an O^- site. The extent of net dissociation is governed by the concentration of H^+ or OH^- ions in the suspensions (pH) [28]. In this manner, the surface of the metal oxide becomes charged.

When a charged surface is present in a solution an electrical double layer forms. This double layer is modeled by the Guoy-Chapman-Stern-Grahame model [27] and a schematic representation is shown in Figure 1.2. The first layer (inner Helmholtz plane) is composed of directly adsorbed ions to the particle surface, while the second (outer Helmholtz plane) is composed of dissolved ions attracted to the metal oxide surface through Coulombic forces. Ions within this layer are trapped within the shear plane of the particle and screen the surface charge of the inner layer [27]. The layer beyond the outer Helmholtz plane is known as the diffuse layer, the thickness of which, also called the Debye length, is inversely dependent on the ionic strength of the solution. Increasing the solution ionic strength (a greater concentration of dissolved ions) will compress the diffuse layer [29]. Beyond these layers is the bulk liquid. The electrical potential between the outer Helmholtz plane and the bulk liquid is the zeta potential (ζ) and the pH where the zeta potential is zero is known as the isoelectric point (IEP) [30].

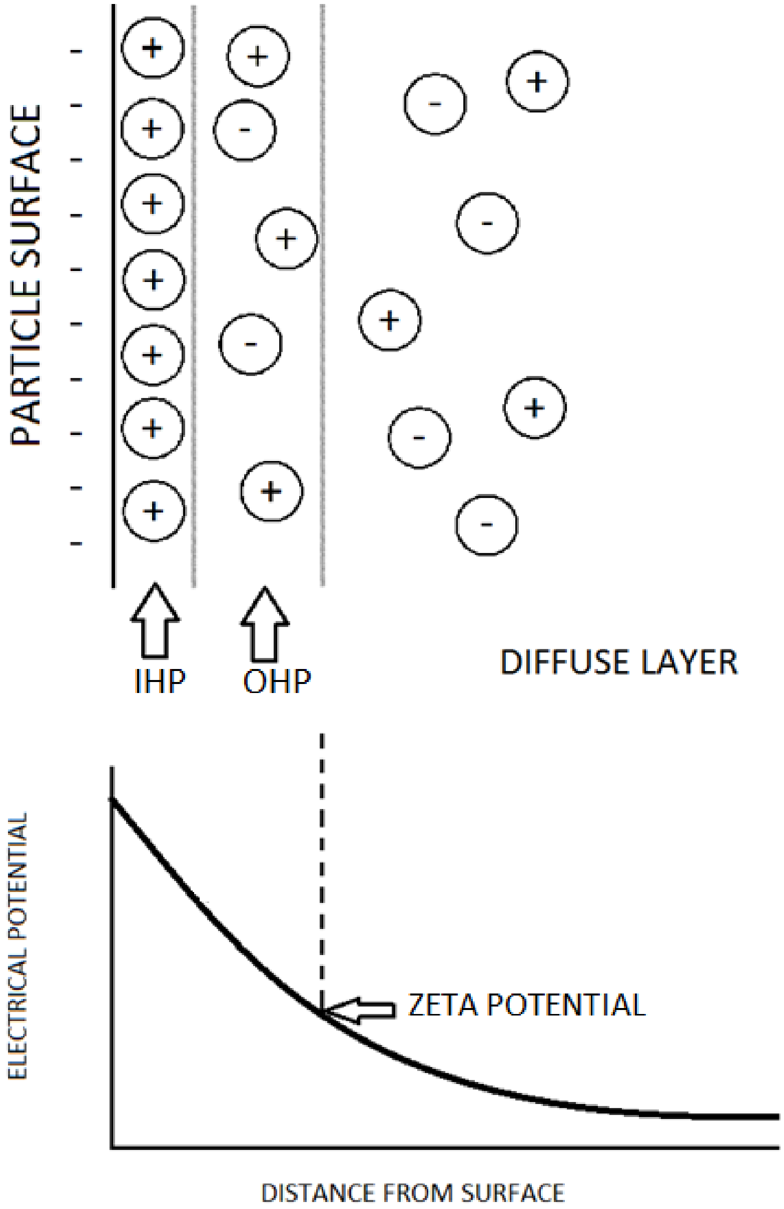

Figure 1.3. Schematic representation of the electrical double layer as depicted by the Guoy-Chapman-Stern-Grahame model with the inner Helmholtz plane (IHP) and the outer Helmholtz plane (OHP) depicted. The zeta potential is defined to be the electrical potential at the OHP as shown in the chart of electrical potential as a function of distance from the particle surface.

The interaction between the electrical double layer repulsion and the van der Waals attraction is treated by DLVO theory, named after Darjaguin, Landau, Verwey, and Overbeek. When the summation of these two forces is shown as a function of distance from the surface, an energy barrier may be observed. This energy barrier is also a barrier for particle attraction. When an energy barrier of potential energy E_B is present, aggregation will not occur if E_B is significantly greater than the thermal energy of the particle (k_BT). The magnitude of the energy barrier is affected by the colloidal chemistry (adsorbed ion, charge screening, etc) and can be reduced by altering the colloid. When E_B is comparable to or larger than k_BT, many collisions must occur before particles may stick. The rate in this case is limited by the probability the particles will overcome the repulsive barrier or:

$$P \sim \exp(E_B / k_B T) \qquad [1.1]$$

where P is the probability, k_B is the Boltzmann constant, and T is the temperature. This type of aggregation is termed reaction-limited aggregation (RLA). When $E_B \ll k_BT$, typical at the isoelectric point, every collision results in sticking and aggregation is limited only by the diffusion of the particles; this type of aggregation is termed diffusion-limited aggregation (DLA) [38].

The overall interaction energy can be affected by other types of forces as well. These forces include magnetic attraction caused by the alignment of electron spins, hydrophobic interactions caused by entropic effects of separating the hydrogen bonds of water, osmotic repulsion caused by a concentration of ions trapped between two particles, electro-steric repulsion in which molecules on a particles surface resist the loss of entropy due to compaction, and bridging attraction caused by surface molecules bonding with each other and bridging particles [29].

It has been observed that the particle point of zero charge (the pH where the surface charge is zero) can be affected by the particle size itself [31]. For metal oxide particles, the point of zero charge and the isoelectric point are identical if H^+ and OH^- are the only potential determining ions [34]. Other ions present in the suspension can interact with the particle surface in a few ways. Some ions may adsorb onto the metal oxide surface by chemical means, directly altering the surface charge. These ions can reverse the polarity of the surface. Ions that do not adsorb onto the surface are referred to as indifferent ions and do not alter the surface charge. Instead, these ions will position themselves within the outer Helmholtz plane surrounding the particle appropriately based on the surface charge. This has no effect on the particle surface charge, but will reduce the zeta potential. Therefore indifferent electrolytes can reduce zeta potential, but will not affect the isoelectric point [34].

The phenomenon of particle aggregation has been studied and described in numerous texts. A theoretical analysis of aggregation and modeling along with experimental verification is presented in the book by Elimelech et al. [32]. Hunter's books on colloid science [27, 33] discuss in depth the theoretical nature of particle aggregation including interparticle surface forces. Israelachvilli's textbook reviews the surface chemistry aspects during aggregation [37].

The chemical effects of slurry additives on the colloidal behavior of alumina particles and its effects on copper CMP performance has been studied by Gopal and

Ihnfeldt [15-20]. Gopal and Ihnfeldt measured particle size distributions and zeta potentials of the particles as a function of slurry chemistry [15, 17]. Ihnfeldt also made preliminary measurements of the aggregate growth over time of the alumina particles [16]. Gopal and Ihnfeldt also incorporated their colloidal data into the Luo and Dornfeld mechanical model of material removal rates [16, 18] and found that this improved model predictions for copper CMP. Ihnfeldt also measured the effects of the slurry additives on the copper etching and used her findings to further improve the Luo and Dornfeldt model [19, 20]. A more detailed review of the work by Gopal and Ihnfeldt is presented in Chapter 2. A review of the literature regarding particle aggregation and chemical adsorption on particle surfaces, specifically its relationship to particle agglomeration, is also presented in Chapter 2. A review of literature on the rate of particle aggregation is presented in Chapter 3.

References

1. Y. Li, *Microelectronic Applications of Chemical Mechanical Planarization*, John Wiley and Sons Inc., Hoboken, New Jersey (2008).

2. R. Ihnfeldt, PhD Thesis, University of California, San Diego (2008).

3. S.P. Murarka, Metallization: *Theory and Practice for VLSI and ULSI*, Butterworth-Heinemann, Boston, Massachusetts (1993).

4. P. B. Zantye, A. Kumar and A.K. Sikder, *Materials Science and Engineering: R: Reports*, **45** (3-6), 89-220 (2004).

5. G. Banerjee, “Chemical Mechanical Planarization for Cu-Low-k Integration”, M. R. Baklanov, P. S. Ho, and E. Zschech (eds.), *Advanced Interconnects for ULSI Technology,* John Wiley and Sons Ltd., West Sussex, UK (2012).

6. J. M. Steigerwald, S. P. Murarka, and R. J. Gutman, *Chemical Mechanical Planarization of Microelectronic Materials*, John Wiley and Sons, New York (1997).

7. T. Ohi, *Industrial Diamond Review*, **1**, 14-21 (2004).

8. A. H. Tan and Y. C. Cheng, *Wear*, **262**, 693-698 (2007).

9. L. Nolan, K. Cadien, “Chemical Mechanical Polish for Nanotechnology”, M. Stepanova and S. Dew (eds.), *Nanofabrication*, Springer, Vienna, New York (2012).

10. R. Ihnfeldt and J.B. Talbot, *J. Electrochem. Soc.*, **155** (6), H412-H420 (2008).

11. M. G. Song, J. Lee, Y. G. Lee, and J. Koo, *J. Colloid and Interface Sci.,* **300**, 603-611 (2006).

12. W. R. Morrison, S. Joshi, and R. Tolles, *Copper and STI CMP Technology: The Challenges and the Cost*, Future Fab International, Volume 11 (2001).

13. M. R. Oliver, *Chemical-Mechanical Planarization of Semiconductor Material*, Springer-Verlag, Berlin, Germany (2004).

14. V. M. Dubin, “Copper Electroplating for On-Chip Metallization”, M. R. Baklanov, P. S. Ho, and E. Zschech (eds.), *Advanced Interconnects for ULSI Technology,* John Wiley and Sons Ltd., West Sussex, UK (2012).

15. T. J. Gopal and J. B. Talbot, *J. Electrochem. Soc.,* **153**(7), G622-G625 (2006).

16. T. J. Gopal and J. B. Talbot, *J. Electrochem. Soc.,* **154**(6), H507-H511 (2007).

17. R. Ihnfeldt and J. B. Talbot, *J. Electrochem. Soc.,* **153**(11), G948-G955 (2006).

18. R. Ihnfeldt and J. B. Talbot, *J. Electrochem. Soc.,* **154**(12), H1018-H1026 (2007).

19. R. Ihnfeldt and J. B. Talbot, *J. Electrochem. Soc.,* **155**(6), H412-H420 (2008).

20. R. Ihnfeldt and J. B. Talbot, *J. Electrochem. Soc.,* **155**(8), H582-H588 (2008).

21. M. Bielmann, U. Mahajan, and R. K. Singh, *Electrochem. and Solid-State Lett.*, **2**, 401–403 (1999).

22. S. Jung and R. K. Singh, *Mat. Res. Soc. Symp. Proc.*, 816, K.1.8.1-4 (2004).

23. G. B. Basim, J. J. Adler, U. Mahajan, R. K. Singh, and B. M. Moudgil, *J. Electrochem. Soc.*, **147**(9), 3523-3538 (2000).

24. Y. Tateyama, T. Hirano, T. Ono, N. Miyashita, T. Yoda, *Chemical Mechanical Polishing (IV)*, The Electrochemical Society, Pennington, New Jersey (2001).

25. R. Carpio, J. Farkas, and R. Jairath, *Thin Solid Films*, **266**(2), 266-238 (1995).

26. P. Wardman and L. P. Candeias, *Radiat. Res.,* **145**(5), 523-532 (1996).

27. R. J. Hunter, “Foundations of Colloid Science,” Oxford University Press Inc., New York (2001).

28. S. M. Ahmed, *Canadian Journal of Chemistry,* **44**, 1663-1670 (1966).

29. E. M. Hotze, T. Phenrat, and G. V. Lowry, *J. Environ. Qual.*, **39**, 1909-1924 (2010).

30. M. Shane, PhD Thesis, University of California, San Diego (1994).

31. Y. T. He, J. Wan, and T. Tokunaga, *J. Nanopart. Res.*, **10**, 321-332 (2008).

32. M. Elimelech, X. Jia, J. Gregory, and R. Williams, “Particle Deposition and Aggregation: Measurement, Modeling and Simulation,” Butterworth-Heinemann, Woburn, MA (1995).

33. R. J. Hunter, “Introduction to Modern Colloid Science,” Oxford University Press, Oxford (1993).

34. R. J. Hunter, “Zeta Potential in Colloid Science: Principles and Applications,” Academic Press Inc., London (1981).

35. S. Jung and R. K. Singh, *Mat. Res. Soc. Symp. Proc.*, 816, K.1.8.1-4 (2004).

36. Z. Li, K. Ina, P. Lefevre, I. Koshiyama, and A. Philipossian, *J. Electrochem. Soc.*, **152** (4), G299-G304 (2005).

37. J. Israelachvili, “Intermolecular and Surface Forces,” Academic Press (1992).

38. M. Y. Lin, H. M. Lindsay, D. A. Weitz, R. C. Ball, R. Klein, and P. Meakin, *Physical Review A,* **41**(4), 2005-2020 (1990).

39. R. K. Singh, *Semiconductor International,* **9** (64), (2005).

40. S. Armini, C. M .Whelan, M. Moinpour, and K. Maex, *Mater. Res. Soc. Symp. Proc.,* **1079** (11), N11-04 (2008).

41. S. Seal, S. C. Kuiry, and B. Heinmen, *Thin Solid Films,* **423**, 243-251 (2003).

CHAPTER 2

PRELIMINARY STUDY OF ALUMINA NANOPARTICLE AGGREGATION

2.1 Introduction

Preliminary work by our group investigated the colloidal behavior of 20 nm alumina particles, with a mean aggregate diameter of 150 nm in pure DI water, as affected by the chemistry of the typical copper CMP suspensions. Gopal measured effective particle size (agglomerate size) and zeta potential for alumina with 1mM KNO_3 as a supporting electrolyte as a function of pH. Zeta potential ranged from a maximum of 58 mV at pH 3.5 to -24 mV at pH 10. Particle sizes were consistently in the size range of 182 to 192 nm with a standard deviation < 10 nm for pH < 8, but aggregated up to 3.1 µm at pH 9 [1]. Particle size distributions show unimodal distributions of alumina, with a maximum size of 197 nm at pH 4.5 and 2.8 µm at pH 8.5 [1]. For suspensions of alumina also containing glycine with concentrations ranging from 10^{-1} to 10^{-3}, isoelectric points (IEP) of 8.9 to 9.3 were measured. Large average agglomerate sizes (~2-3 µm) were measured for pH > 8 with the maximum sizes observed at the IEP (~9) and small average particle sizes (~200 nm) at pH <7 for all concentrations of glycine. Zeta potentials ranged from 61 mV at pH 3.5 to -16 mV at pH 10. Gopal noted less variation of the zeta potential at a given pH (±2%) with even the smallest concentration of glycine versus with no glycine present (±8%), concluding that glycine stabilizes the zeta potential. The least amount of variation (±3 mV) was observed with 10^{-1} M glycine at pH 3.5 to 6 [1].

Measurements with 1mM KNO_3 and 0.1M glycine and 0.1wt% H_2O_2 yielded zeta potentials ranging from 27 mV at pH 3.5 to -47 mV at pH 10, with stabile zeta potentials (~30 ± 3 mV) and consistent particle sizes (166 to 185 nm) at pH <7 and an IEP of 8.8. Gopal observed broader particle size distributions (standard deviation of 200 to 800 nm) at pH > 8 and an average aggregate diameter of ~2 µm at the IEP, lower than the 3 µm observed at the IEP when H_2O_2 was not present [1]. When the H_2O_2 concentration was increased to 2%, measured zeta potentials ranged from 39 mV at pH 3.5 to 1 mV at pH 10. Consistent average aggregate diameters were measured (133 to 136 nm) at pH < 6 and 2.5 µm at pH 8.5, but decreased to 1.9 µm at pH 9. Zeta potentials were less stable with 2 wt% H_2O_2 present so a precise IEP could not be measured, however it was determined to be between 8 and 10 [1].

Gopal also investigated suspensions of alumina with 1mM KNO_3 and 1mM SDS, noting negative yet stable zeta potentials (±7 mV), ranging from -41 mV at pH 3.5 to -34 mV at pH 8 [1]. Yuehua and Guanzho also observed negative zeta potentials for alumina particles in this pH range with SDS present in solution and attributing the adsorption of SDS onto the alumina surface as the cause of the negative zeta potentials [2]. Measured particle sizes were relatively constant ranging from 218 to 229 nm at pH 10 and 5, respectively. Yuehua and Guanzho also noted similar reduced particle sizes for alumina and believe this resulted from the hydrophobic interactions between alumina particles with adsorbed SDS, in accordance with the DLVO theory (discussed in chapter 1) [2].

Gopal also made measurements of slurry with a mixture of additives. An alumina slurry containing 0.1 M glycine, 0.01 wt % BTA, 1 mM SDS, and 0.1 wt % H_2O_2 yielded negative zeta potentials for the entire pH range and agglomerate sizes ranging from 520 nm to 1.8 µm at pH 3.5 and pH 8, respectively. Measurements of a slurry with a mixture of 0.01 M EDTA, 0.01 wt % BTA, 1 mM SDS, and 0.1 wt % H_2O_2 again showed negative zeta potentials, although in a narrower range from -13 to -25 mV. Large aggregate diameters ranging from 3.3 to 2.1 µm were observed at pH 3.5 and 8, respectively, with standard deviations of ~500 nm. By measuring slurries containing only 0.01 wt% BTA and 0.01M EDTA, it was determined aggregation occurred due to the presence of EDTA in the slurry [1].

Gopal incorporated her experimental data into the Luo and Dornfeld model of CMP. The Luo and Dornfeld model is a mechanical model of CMP, which incorporates both particle–particle and particle–surface interactions of the abrasives and the wafer surface through the average abrasive size, the standard deviation of the abrasive size distribution, and the wafer surface hardness, to predict the MRR. A detailed derivation of the Luo and Dornfeld model can be found elsewhere [4, 5]. The Luo and Dornfeld model accounts for the chemical activity of the slurries through the abrasive size and distribution, hardness and chemical etch rate. After incorporating experimental particle size data, Gopal found the model to be very sensitive to the standard deviation of the particle sizes for average particle sizes < 500 nm. The model also under predicted material removal rates (MRR), which was thought to be due to using a constant wafer surface hardness [3].

Ihnfeldt continued Gopal's investigation of the colloidal behavior of alumina, notably studying the effect of the presence of copper in the slurry. In suspensions of only

1mM KNO_3, Ihnfeldt measured an IEP at pH ~6.5 for alumina and ~6.7 when copper was present. She noted that these pH levels are lower than the reported value of 9.2 [6] and concluded that the presence of KNO_3 was the likely cause of the discrepancy. In general Ihnfeldt observed that for low pH, the repulsive forces of the dissolved Cu^+ ions and the positively charged alumina reduced aggregation. As pH increased, mostly likely CuO formed and attracted the alumina (up to pH 10) due to opposing charges. At pH greater than 10, CuO and alumina are both negatively charged and repel, thereby decreasing the extent of alumina aggregation [6]. Ihnfeldt did measure some large agglomerates in the acidic slurries ranging from 500-5000 nm with no copper present, but the size decreased to 300-800 nm when copper was added. In the alkaline slurries, the large alumina aggregate sizes were between 700-7000 nm with no copper, but increase to 2000-9000 nm with copper.

With the addition of glycine, Ihnfeldt also found the alumina suspension was more stable. A highly soluble Cu-glycine can form at $pH < 4$ and $pH > 9$ and can reduce agglomeration by electrostatically repelling the alumina particles. Ihnfeldt did notice a change in IEP (increased to ~9) when glycine and copper were present, but did not observed any such change if copper was not added. Zeta potentials ranged from >25 mV at $pH < 7$ and 0-20 mV at $pH > 7$ with no copper present. Aggregate sizes were similar for with and without copper, ranging from ~2 µm at pH 6 to 9 and < 1.5 µm for $pH < 6$). Ihnfeldt also investigated the addition of H_2O_2 to the KNO_3 and glycine suspension. The addition of 0.1 wt% H_2O_2 caused a >5 mV decrease in zeta potential, promoting greater particle aggregation and the presence of copper broadened the alumina aggregate size distribution. Using a H_2O_2 concentration of 2.0 wt% with glycine, KNO_3 and copper, Ihnfeldt observed a reduction of aggregate sizes without copper. She attributed the reduction in sizes to the interaction of the alumina with the Cu-glycine complex as well as $Cu(OH)_2$, formed by the oxidation of the copper by H_2O_2 [6]. Zeta potential measurements were not possible due to electrolysis at the cell electrode due to the high concentration of H_2O_2 [6].

Finally, Ihnfeldt looked at the behavior of a slurry containing a mixture of additives, the first of which being a combination of 0.1M glycine, 0.1 wt% H_2O_2, 1 mM SDS, and 0.01 wt% BTA. Ihnfeldt measured negative zeta potentials for all pH regardless of the presence of copper (except for pH 9 with copper) and concluded this was due to the adsorption of SDS to the alumina. She noted that when copper is not present, the combination of these additives increases the aggregation of alumina at all pH values. However, when copper was present, large agglomerates were not observed, and alumina particle sizes were similar to those seen without any additives [6]. When using 0.01M EDTA instead of glycine, more negative zeta potentials were measured (-2 to -12 mV and -4 to -27 mV for without and with copper, respectively) than with glycine (-10 to 5 mV regardless of the presence of copper). Particle size distributions were identical for with and without copper suggesting EDTA eliminates the effect of copper which is consistent with literature since EDTA is known to complex with positively charged metal ions [6].

Ihneldt also calculated the shear forces on abrasive particles in a CMP slurry during the process. She determined that the shear forces are not sufficient to break up the aggregates and therefore aggregate size measurements are appropriate to use in CMP models [7]. Because of the availability of CMP MRR data, Ihnfeldt also focused on the Luo and Dornfeld model. She studied the effects of additives on the surface chemistry of copper and since that the chemistry can affect the oxidation state of the copper surface, hardness was measured. With incorporation of the particle size and hardness data into the model, copper CMP MRR predictions improved. However, the model could not predict MRRs for highly chemically active slurries; slurries at acidic pH or with high etch rates (> 7nm/min) [8].

The following experiments were a continuation of Ihnfeldt's initial investigation into the rate of aggregation of alumina nanoparticles. As discussed in Chapter 1, Ihnfeldt noted that for alumina slurries dispersed in 1mM KNO_3 at pH 7.5, aggregation can occur at a measureable rate. The purpose of this study was to determine if the presence of chemical additives can affect the rate.

2.2 Experimental

The experiment was performed by preparing 100 ml solutions of 1 mM KNO_3 with filtered distilled water. Additives of interest were also added to the solution before pH adjustment. Solutions of pH 4, 7.5 and 10 were prepared using either KOH or HNO_3 to adjust pH, measured by an Orion model SA 720 pH meter. When the solution was adjusted to the proper pH, ~89 µl of alumina slurry were added to the solution. The alumina used was a dispersion manufactured by Cabot Corporation containing 40 wt% α-alumina in de-ionized water. The alumina particles have a primary diameter of 20 nm and a median aggregate diameter of 150 nm. The solution was then stirred to ensure proper mixing of the alumina in solution. In addition, the solution was placed in a Bransonic

Cleaner model 1200 sonicator for 5 minutes before measurement. Then the solution was removed from the sonicator and approximately 4.5 ml of the solution was pipetted into cuvettes with caps. The cuvettes were filled fully with solution to ensure minimization of trapped air that might change the pH. Similar procedures were followed for samples with copper added. For these samples, when the solution reached the desired pH, copper nanoparticles (Sigma Aldrich) with a particle diameter less than 100 nm, was added to the solution (0.12mM) and mixed.

These solutions were then placed into a ZetaPlus particle size analyzer (Brookhaven Instruments Corporation). Measurements were taken every minute for the first 25 min and then at 30, 45, 60, 120, 240, 1440 and 2880 min. This machine utilizes a quasi-elastic light scattering technique to measure the diameter of the agglomerates.

2.3 Results and Discussion

The average agglomerate size data over time for 1 mM KNO_3 solutions at various pH values without copper are displayed in Figure 1. At pH of 4 and 10 the aggregate size reached relatively constant values of 179 ± 28 nm and 408 ± 122 nm, respectively. However at a pH of 7.5, the particles agglomerated from ~690 to ~4400 nm at a rate of ~82 nm/min. This pH is close to the measured isoelectric point of pH 6.5 [1], where the zeta potential of the alumina particles is zero. In contrast, solutions of pH 4 and 10, further from the isoelectric point, had constant agglomerate sizes.

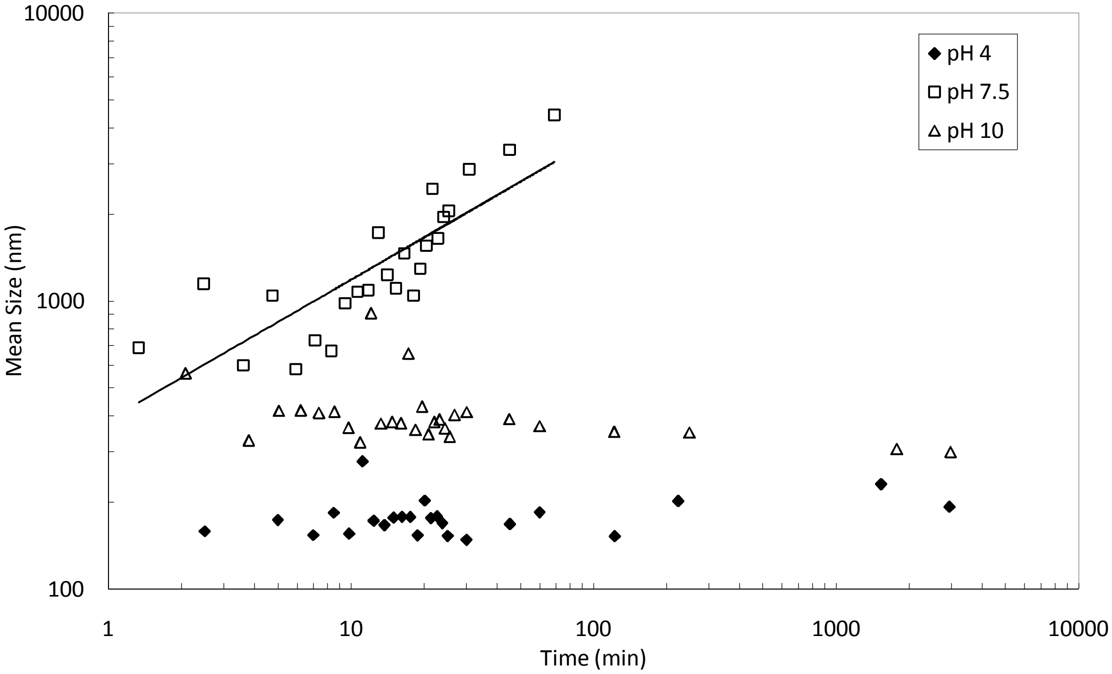

Figure 2.1. Mean agglomerate size vs time for 1 mM KNO_3 solutions of pH 4, 7.5 and 10 without copper.

The presence of copper, as shown in Figure 2, did not seem to make a significant difference at pH 4 with a relatively constant agglomerate size of 187 ± 19 nm. At pH 7.5 and 10 with copper added, the agglomerate sizes increased from ~930 to ~4000 nm (with a large average standard deviation of ~1700 nm) and ~500 to ~ 4800 nm (with an average standard deviation of ~740 nm), respectively. The rates of agglomeration at pH values of 7.5 and 10 were 117 and 42 nm/min, respectively. The variance in the sizes is due to the polydispersive nature of the particles in these suspensions as described in detail elsewhere [1].

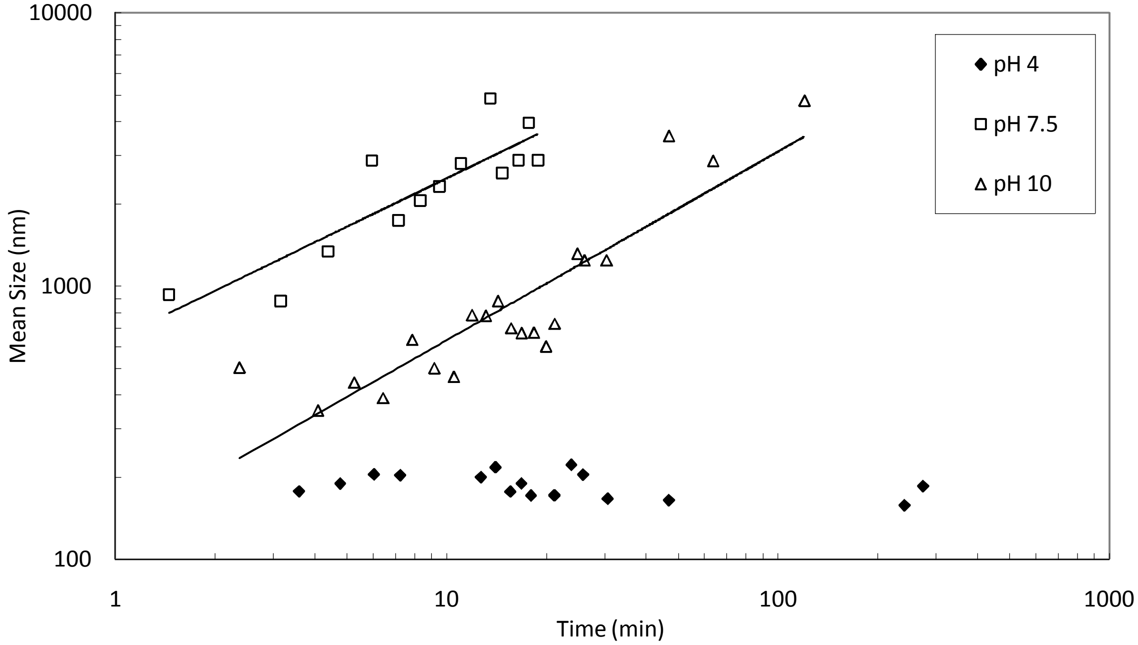

Figure 2.2. Mean agglomerate size vs time for 1 mM KNO_3 solutions of pH 4, 7.5 and 10 with copper.

The mechanisms of aggregation of colloidal particles have been studied by the use of fractal dimension by analyzed light-scattering data [9-11]. It has been shown that colloidal aggregates formed by diffusion-limited aggregation are fractal and therefore, grow by a power law, as shown in Eq. 1:

$$M \propto L^{d_f} \tag{2.1}$$

in which the mass of the aggregate, M, (or number of particles) is proportional to the effective diameter, L, raised to the fractal dimension, d_f. The fractal dimension, which ranges from 1 to 3, is dependent upon the physical and chemical nature of the solution and can infer the structure of the aggregates formed. For example, d_f values close to 2 signify two-dimensional structures, such as flake-like aggregates, while values closer to 3 are characteristic of more spherical structures [9]. The d_f number also infers the density of the aggregates themselves; loosely packed aggregate structures are characterized by low d_f numbers (<2) while denser aggregates are characterized by larger d_f numbers (between 2 and 3) [11].

By using the Smoluchowski equation, which describes aggregation kinetics in terms of cluster-cluster formation [10], with simple scaling arguments for the cluster distributions, a power law governing the agglomeration kinetics can be obtained from equation 2.1 as follows:

$$R(t) = C_1 t^{1/d_f} \qquad [2.2]$$

where R is the particle size (diameter), t is time, and C_1 is a constant. This equation implies that the kinetics is Brownian in nature and the fractal dimension has been used to indicate the agglomeration mechanism [10]. A fast diffusion-limited aggregation (DLA) is indicated by a smaller fractal dimension, which yields open, loosely packed agglomerate structures. Since particle repulsion is small, particles stick together almost as soon as they contact. Slower aggregation, characterized by reaction-limited aggregation (RLA) where particle-particle repulsion has a greater effect, follows an exponential growth as shown in equation 2.3:

$$R(t) = C_2 e^{at} \qquad [2.3]$$

where C_2 and a are constants [10]. Agglomerates produced by the RLA mechanism are more densely packed. This is because the particles can penetrate farther into agglomerate structures without being captured initially. The RLA mechanism gives a higher fractal dimension number. It should be noted that a fractal dimension number cannot be readily calculated by a fit of equation 2.3 to aggregation data. Instead, static light scattering measurements are typically analyzed by plotting the scattering light intensity versus the scattering vector and from the slope determining the d_f for suspensions aggregating by a RLA mechanism [12]. Dynamic and static light scattering studies of agglomeration kinetics have been performed by a number of groups. Cametti et al. reported d_f values of 1.75 ± 0.03 for DLA and 2.1 ± 0.1 for RLA for polystyrene particles with a diameter of 481 ± 5 nm. RLA was observed for a NaCl concentration of 0.075M, while DLA was observed for NaCl concentrations ranging from 0.13 M to 2.6 M [9]. Hoekstra et al. reported d_f values of 1.7 - 1.8 for DLA and values up to 2.0 - 2.1 for RLA of nickel hydroxycarbonate particles with a diameter of 80 - 180 nm. They found that RLA was predominant for low electrolyte concentrations (no additional electrolyte added) and that DLA occurred at higher concentrations (0.1 M $NaNO_3$) [12]. Herrington and Midmore observed a transition from high (RLA) to low fractal dimension (DLA) for the aggregation of 40 nm diameter kaolinite as the pH increased from 3 to 3.5 in water and 3.2 to 4.5 in 1 mM KCl [13]. Hoekstra et al. observed a shift from RLA to DLA for nickel hydroxycarbonate particles in 1.2 mM $Ni(NO_3)_2$ and 2.0 mM Na_2CO_3 once effective aggregate sizes reached approximately 700 nm [12].

The inverse of the slope of the log-log plots in Figures 2.1 and 2.2 gives d_f values as shown in Table 2.1.

Table 2.1. Fractal dimension of alumina solutions at various pH values.

Solution pH	Without Copper	With Copper
4	N/A	N/A
7.5	2.1	1.7
10	N/A	1.4

The solution without copper at pH 7.5 gave a value of 2.1 indicating reaction-limited agglomeration, while those with copper at pH 7.5 and 10 gave d_f values below 2 indicating diffusion-limited agglomeration. The other dispersions at pH 4 and 10 without copper and pH 4 with copper showed reversible aggregation with a relatively constant agglomerate size. As stated, the addition of copper had no effect on agglomeration for a suspension with pH 4. However, at pH 7.5 the aggregation mechanism is observed to change from DLA to RLA with the addition of copper.

The average agglomerate sizes of the alumina particles for 1mM KNO_3 with 0.1M glycine solutions at various pH are shown in Figure 2.3. Solutions with pH 4 and pH 10 both show reversible agglomerate formation with a mean particle size of 155 ± 55 nm and 3620 ± 1800 nm, respectively. For pH 7.5 solutions, agglomeration was observed increasing from ~171 nm to ~3000 nm at a rate of approximately 12 nm/min, slower than solutions of only KNO_3. From calculation of the fractal dimension number, DLA is the mechanism at work. See Table 2.1 for a list of calculated fractal dimension numbers. It is important to note that the DLS machine is most accurate at measuring particle size in the 2 to 3000 nm range.

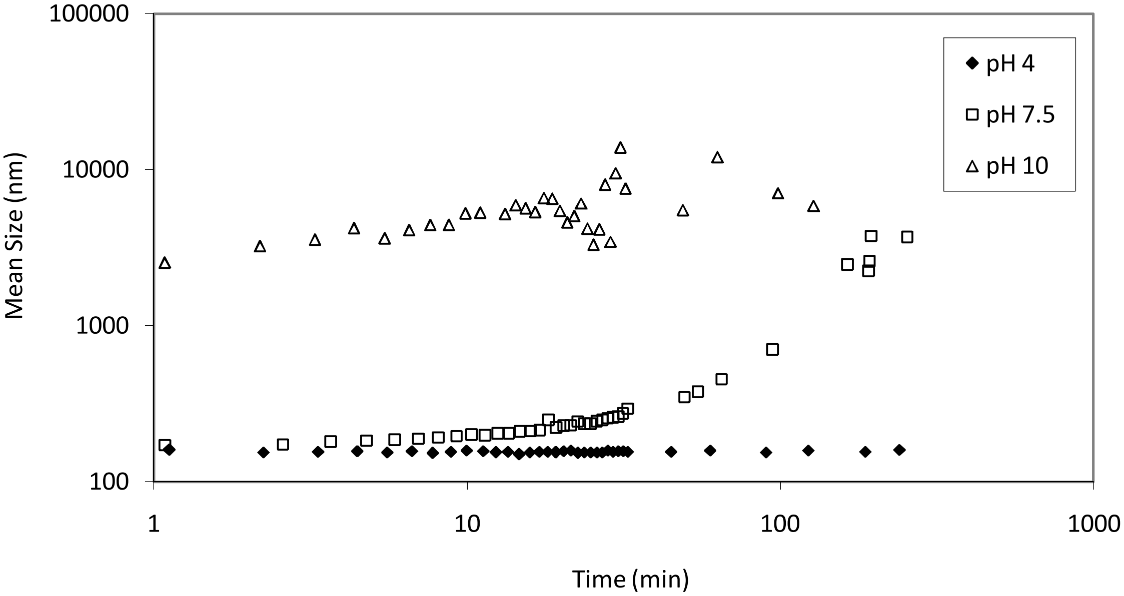

Figure 2.3. Average agglomerate sizes of alumina in solutions of 1mM KNO_3 and 0.1M glycine at various pH values.

Figure 2.4 shows the average agglomerate sizes of the alumina particles for the 1mM KNO_3, 0.1mM glycine, 0.1wt% H_2O_2, 0.01wt% benzotriazole, and 0.1mM sodium dodecyl sulfate solutions at various pH values. In this case, at pH 7.5 particle size appears unaffected by the additional additives compared to the KNO_3 and glycine system, increasing from ~202 nm to ~3000 nm at a rate of 12 nm/min with a DLA mechanism again. Solutions with a pH of 10 still show reversible agglomerate formation with an average size of 6590 ± 1200 nm. Solutions of pH 4 still showed reversible agglomerate formation, however with average sizes of 7740 ± 4250 nm, significantly larger than with the KNO_3 and glycine system.

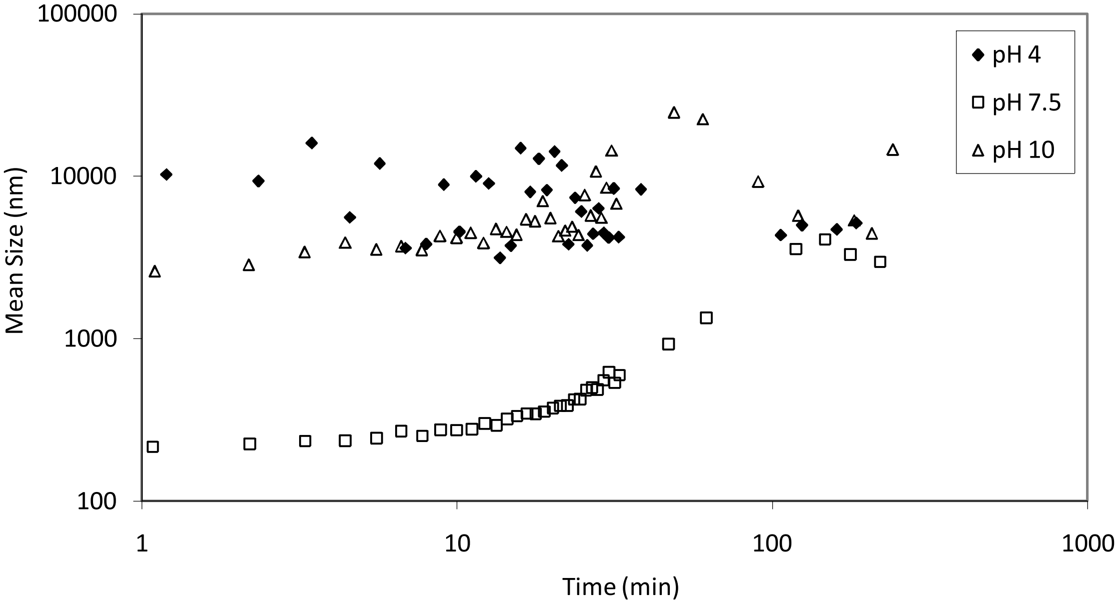

Figure 2.4. Average agglomerate sizes of alumina in solutions of 1mM KNO_3, 0.1mM glycine, 0.1wt% H_2O_2, 0.01wt% benzotriazole, and 0.1mM sodium dodecyl sulfate at various pH values.

The fractal dimension numbers of the agglomeration of the alumina in the various solutions are shown in Table 2.2. The only pH this calculation is applicable to is pH 7.5 as it is the only system with steady aggregation. The fractal dimension numbers calculated indicate a diffusion-limited aggregation mechanism. Based on the data in Figures 2.3 and 2.4, it is possible that reversible agglomeration was occurring in the early times followed by faster, diffusion limited aggregation.

Table 2.2. Fractal dimension of alumina solutions at various pH values.

Solution pH	**KNO_3 + glycine**	**KNO_3, glycine, H_2O_2, SDS, BTA**
4	N/A	N/A
7.5	1.6	1.6
10	N/A	NA

Interestingly, it has been seen that changing the pH of the suspension after agglomeration can significantly alter the sizes and size distribution. For example, it has been seen that changing the pH from 8.5 to 4 in the KNO_3-glycine system lowers the agglomerate sizes from 2880 ± 950 nm to 411 ± 210 nm. As expected, raising the pH from 4 to 8.5 causes an increase in average sizes from 147 ± 47 nm to 2700 ± 1190 nm.

2.4 Conclusions

The presence of copper in suspension appeared to have an effect on the aggregation of alumina nanoparticles. For suspensions without copper, there was no growth of agglomerate sizes for solutions of pH 4 and 10, but a rate of agglomeration of 82 nm/min for pH 7.5 was observed. The addition of copper had no effect on agglomeration at pH 4, but an increased agglomeration rate was observed for the solutions of higher pH. After the addition of copper for the solutions of pH 7.5 and 10, an increase in both agglomeration rates was observed. At pH 7.5 the aggregation mechanism is observed to change from DLA to RLA with the addition of copper.

Comparing the suspensions with glycine to those with no additives, agglomeration was not observed at pH 7.5, but was observed at pH 10. There was no effect at pH 4. The mixture of additives has no additional effect at pH 7.5 compared to the KNO_3 and glycine system, but agglomeration was observed at pH 4 and 10. For suspensions with glycine and the surfactant, a diffusion-limited reaction mechanism was observed for pH 7.5. Both pH 4 and 10 exhibited reversible agglomeration with average aggregate diameters > 3 μm.

Measurements of the zeta potential of the alumina, discussed in Chapter 3, were made to develop a more complete understanding of the effects of the slurry additives. The IEP of a material in solution refers to the pH where the zeta potential (the electrical potential of the dispersed medium and the stationary fluid layer surrounding the particles) is zero. In general, colloids are most stable if the magnitude of the zeta potential is high and will not aggregate appreciably. Particles with a low absolute value of zeta potential will tend to have significant aggregation. Therefore, knowledge of the IEP is critical to the understanding of the agglomeration of particles.

Acknowledgements

This work was supported by University of California, Berkeley IMPACT program for its support along with the partner companies: Applied Materials, AMSL, Ebara Technologies, Global Foundries, IBM, Intel Corporation, KLA-Tencor, Marvell, Mentor Graphics, Novellus Systems, Panoramic Tech, SanDisk, Synopsys, Tokyo Electron Limited, and Xilinx Inc, along with matching support by the UC Discovery Grant ele07-10283. I would also like to thank Mike Chan and Robin Ihnfeldt for their support with the aggregation measurements.

This chapter is a reprint of the material as it appears in Chemical Mechanical Polishing 10, Neil Brahma, Mike Chan, and Jan B. Talbot, Vol 19 (2009), along with material as it appears in Chemical Mechanical Polishing 11, Neil Brahma and Jan B. Talbot, Vol 33 (2010). The dissertation author was the primary investigator and author of this material.

References

1. T. Gopal and J. B. Talbot, *J. Electrochem. Soc.,* **153** (7), G622-5 (2006).

2. H. Yuehua and Q. Guanzhou, *Min. Eng.*, **16**, 1167 (2003).

3. T. Gopal and J. B. Talbot, *J. Electrochem. Soc.,* **154** (6), H507-H511 (2007).

4. J. Luo and D. Dornfeld, *IEEE Trans. Semicond. Manuf.*, **14**, 112, 2001.

5. J. Luo and D. Dornfeld, "Integrated Modeling of Chemical Mechanical Planarization (CMP) for Integrated Circuit Fabrication: from Particle Scale to Feature, Die and Wafer Scales," Springer, Berlin (2004).

6. R. Ihnfeldt and J.B. Talbot, *J. Electrochem. Soc.*, **153,** G948 (2006).

7. R. Ihnfeldt, PhD Thesis, University of California, San Diego (2008).

8. R. Ihnfeldt and J.B. Talbot, *J. Electrochem. Soc.*, **154** (12), H1018-H1026 (2007).

9. M. Elimelech, J. Gregory, X. Jia, R. A. Williams, *Particle Deposition and Aggregation*, Butterworth-Heinemann, Oxford, England (1995).

10. C. Cametti, P. Codastefano, and P. Tartaglia, *Physical Review A*, 36 (10), 4916-4921 (1987).

11. R. J. Hunter, *Fundamentals of Colloid Science.*, Oxford University Press, 2001.

12. L. L. Hoekstra, R. Vreeker, and W. G. M. Agterhof, *J. Colloid Interface Sci.,* 151 (1), 17-25 (1992).

13. T. M. Herrington and B. R. Midmore, *Colloids and Surfaces A: Physiochemical and Engineering Aspects,* 70, 199-202 (1993).

CHAPTER 3

EFFECTS OF CMP SLURRY ADDITIVES ON THE AGGLOMERATION OF ALUMINA NANOPARTICLES: GENERAL AGGREGATION AND ZETA POTENTIAL BEHAVIOR

3.1 Introduction

Chemical mechanical planarization (CMP) is a material processing technique used to polish semiconductors to atomic level smoothness required for microelectronics fabrication. In this process, the semiconductor wafer is pressed against a rotating polishing pad onto which a chemical slurry is dispensed. The pad aids in slurry transport to the wafer surface, while the slurry itself, containing various chemicals and nanometer-sized abrasives, does the polishing [1]. Because the wafer surface contains regions of metal, such as copper, in addition to the semiconductor itself, various chemicals are added to the slurry to improve polishing uniformity by actively etching material, complexing with removed material to prevent redeposition, or passivating softer materials to prevent excessive polishing while the abrasives within the slurry mechanically remove the material. CMP performance is typically characterized by the material removal rate (MRR), surface roughness and defect count [2, 3].

During CMP, aggregation of the abrasive particles can occur depending on the conditions of the process. It was shown that agglomerates can withstand the shear forces present during the CMP process and do not break up (unless agglomerate sizes are greater than ~4.5 μm) [4].

Copper has become the interconnect of choice, replacing aluminum, due to its low electrical resistivity and high thermal conductivity [4, 6]. For copper CMP, alpha alumina is the abrasive particle used due to its colloidal stability as well as hardness [4]. The copper CMP polishing behavior has been studied by numerous researchers [7-11]. Therefore, the focus of our group's research has been on copper CMP [4, 12-14], specifically the effect of the slurry chemistry on alumina particle aggregation.

Copper CMP additives serve a multitude of functions in the slurry. Benzotriazole (BTA) is a copper corrosion inhibitor, and is used to passivate the copper surface, preventing over-polishing of copper features [4]. Hydrogen peroxide is used as an oxidizing agent, accelerating oxidation reactions of the copper surface aiding in uniform material removal [4, 7, 15]. Sodium dodecyl sulfate (SDS) is an anionic surfactant composed of an anionic sulfate head group and a 12 carbon tail. It is used as a slurry stabilizing agent, preventing excessive aggregation of polishing particles [16]. Glycine is a simple amino acid that is used as a complexing agent with copper that has been removed or dissolved from the surface to prevent re-deposition [15]. Ethylenediaminetetraacetic acid (EDTA) is commonly used as a complexing agent as well [9].

The pH of the slurry must be carefully controlled as the efficacy of the chemical additives can be drastically affected [17]. During copper CMP for example, the surface of the copper is typically oxidized and the oxidation state is dependent on the pH of the environment [18]. The presence of chemical additives can affect the copper state, for example glycine can complex with the copper, while BTA will passivate the surface and act as a corrosion inhibitor. The extent of these effects will ultimately affect the copper surface hardness, etch rate, and removal rate [18].

A comprehensive model of CMP material removal rate was developed by Luo and Dornfeld, utilizing a modified version of Preston's equation and a solid-solid abrasion mechanism [20]. Particle size distribution and etch rate data were incorporated into the Luo and Dornfeld's mechanical CMP model which improved material removal rate prediction for copper CMP [7]. The model predictions indicate that a minimum material removal rate is reached at a critical abrasive particle size and the MRR would increase if the average particle size either increased or decreased from that critical size [12]. For example, with a particle size distribution having a narrow standard deviation of 10 nm, a critical particle size of ~300 nm yielded a MRR of 200 nm/min. Either an increase or decrease of the particle size of 200 nm gave a 150 nm/min increase in MRR [18]. The slurry chemistry including pH, additive concentration, etc, determines this critical effective particle size and thus, the MMR.

Aggregation of particles is primarily an electrokinetic phenomenon. The electrostatic force that keeps particles apart and stabilizes the suspension is very sensitive to pH [1]. For metal oxide particles, the surface charge is affected by the presence of ions adsorbed to the particle surface. The excess of H^+ in an acidic solution can protonate the OH groups present on the particle surface forming water and dissociating from the particle surface leaving a net positive charge. In a basic environment, the excess of OH^- will capture the hydrogen from the dangling OH group, leaving a net negative charge

[20]. When the particle surface is neutral, the electrostatic repulsion is negligible and aggregation will occur.

Surface charge of the particles can be altered by the chemical nature of the slurry. The zeta potential (the electrical potential of the dispersed medium and the stationary fluid layer surrounding the particles) can be easily measured and is useful in determining slurry stability [21]. The pH where the zeta potential is zero is referred to as the isoelectric point (IEP). If the particle surface is either significantly positive or negative and the absolute magnitude of the zeta potential is >~25mV, repulsion will be significant enough to keep particles from agglomerating and the suspension will be stable. If the ionic strength of the solution is large, charge screening can occur, consequently reducing the net charge, and therefore, the zeta potential of the particle [24]. In this situation, the electrostatic repulsion will be too weak to keep particles separated and aggregation will occur. Therefore, knowledge of the IEP is critical to the understanding of the agglomeration of particles [25].

Gopal and Talbot investigated the effects of common CMP additives on zeta potential and particle sizes of alumina nanoparticles for copper CMP [8]. It was seen that the addition of glycine stabilized the zeta potential of alumina nanoparticles (mean diameter of 120 nm) over a large pH range (3.5 to 10) and that SDS caused the mean aggregate diameter to increase to ~200 nm, while EDTA increased mean diameters to ~1.2 to 2.0 μm over the entire measured pH range [9].

The effects of chemistry on the colloidal stability of alumina particles have been studied by others. Hu and Dai investigated aggregation of 1 μm alumina particles in the presence of SDS and dodecylamine (DDA) [24]. The particle size, zeta potential, and contact angle measurements were used to determine surfactant adsorption, aggregation, and electrokinetic behavior. They concluded that adsorption of either molecule caused hydrophobic interactions between particles, which promoted aggregation. They also observed that aggregation became significant at an SDS concentration of 0.1 mM [24]. Somasundaran et al. investigated the stability of 1 μm alumina particles in a 2 mM NaCl solution with an SDS concentration ranging from 0.01 mM to 1 mM [25]. Their measurements of surfactant adsorption and stability ratios, calculated from electrophoretic mobility data, led to the conclusion that pH has the greatest effect on SDS adsorption and alumina stability, with adsorption increasing significantly at an SDS concentration of 0.1 mM [25]. Palla and Shah investigated the effects of multiple surfactant systems, specifically SDS and a variety of nonionic polymeric surfactants [16]. They found that high ionic strength slurries (0.1 M potassium ferrocyanide) can promote aggregation even in the presence of surfactants, however a mixture of surfactants, for example SDS with nonionic surfactants such as Sypmeronic A4 (from ICI surfactants), can effectively stabilize the colloid [16].

Luo investigated the adsorption of additives, such as potassium phthalate and citric acid, and its effects on slurry stability of alumina particles (~200 nm) at concentrations of 5 wt% [26]. These results showed that in general, adsorption strength and steric hindrance increases slurry stability, however aggregate size data were not reported [26]. Basim et al. concluded that the adsorption of surfactants and slurry stability are affected by ionic strength of the slurry [27]. Increasing the ionic strength of a slurry leads to increased charge screening of the particles. This charge screening reduces net particle charge and reduces electrostatic repulsion, leading to particle aggregation [27]. Ionic strength of the suspension can also affect SDS adsorption; as the ionic strength increases, greater charge screening of the polar head groups decreases the repulsive forces as well as enhancing the hydrophobic effect of the non-polar tail, further promoting adsorption onto the metal oxide surface [28]. Pavan et al. noted that for suspensions of magnesium/aluminum layered double hydroxide, SDS adsorption more than doubled when the ionic strength increased from 0.0M to 0.1M NaCl [28]. Palla and Shah demonstrated that a 1 wt% alumina suspension at pH 4 with 10 mM SDS did not aggregate with 1 mM potassium ferricyanide, but did when the potassium ferricyanide concentration was increased to 0.1M [16].

Aggregation rates and the mechanism of aggregation may be affected by the slurry chemistry. Previously, our group found that slurry pH has the greatest effect on the zeta potential and thus, on the agglomerate size distribution [8, 9]. With more additives included in the slurry chemistry, the roles of each may become more complex in the agglomeration mechanism as the chemicals may interact with each other in addition to the particles themselves [13, 14]. Our prior work has investigated the aggregation of alumina nanoparticles in 1 mM KNO_3 with and without copper [13]. Copper nanoparticles were added at a concentration of 0.12 mM to simulate the copper removed during CMP [4, 7, 13]. For solutions without copper, alumina agglomeration was greatest at pH of 7.5, near the isoelectric point of 6.5, at an average rate of 82 nm/min, following a reaction-limited mechanism. Solutions with a pH away from the isoelectric point underwent reversible agglomeration, maintaining a small agglomerate size of 150 nm at steady-state. The addition of copper did not affect agglomeration at pH 4. However, an increase in the agglomeration rates at pH 7.5 and 10 was observed with copper in the solutions, following a diffusion-limited mechanism [13].

The rates of agglomeration of alumina particles in various solutions with the additives at three pH values were measured [13]. Two solutions initially investigated were KNO_3 with glycine and KNO_3 with glycine, H_2O_2, BTA, and SDS. The KNO_3 glycine slurry showed no aggregation at pH 4, slow aggregation at an average rate of 12 nm/min for pH 7.5 following a diffusion-limited mechanism, and reversible agglomerate formation at pH 10 with a mean particle diameter greater than 3 µm. For the complex slurry no change in agglomeration behavior at pH 7.5 or pH 10 compared to the simple slurry was seen, however reversible agglomeration at pH 4 with a mean particle size greater than 3 µm was observed [16]. Thus, pH has a significant influence on the aggregation mechanism [14]. Also of note is that the complex slurry, containing all of the usual copper CMP slurry ingredients including SDS, did not prevent aggregation at acidic pH of 4, within the typical pH range of copper CMP slurries, signifying that aggregation of abrasive particles could still occur [5].

This study is an extension of our previous work on the effects of common CMP slurry additives (SDS, BTA, glycine, and hydrogen peroxide) on the aggregation behavior of alumina nanoparticles. These additives (and the specific concentrations) have been used previously in our copper CMP studies [13, 14]. Ionic strength was maintained in this study by using 0.1 mM KNO_3 solutions, so effects of pH and other additives could be readily compared. Zeta potential was measured to aid in understanding the underlying electrokinetic effects due to the individual additives. This chapter discusses the general aggregation behavior observed, whereas chapter 5 focuses on the measurement and analysis of the aggregation rate observed under certain slurry conditions.

3.2 Experimental

Solutions of 1 mM KNO_3 (99%, Fisher) with filtered distilled water were prepared to ensure constant ionic strength of the solutions. Additives were then mixed into the KNO_3 solution in concentrations as listed in Table 3.1, which included glycine (98.5%, Alfa Aesar), benzotriazole (99%, Avocado Research Chemicals), sodium dodecyl sulfate (99%, Roche Diagnostics), hydrogen peroxide (30% in water, Fisher), and copper (99.8% nanoparticles, Sigma Aldrich, particle diameter <100nm). The order of addition was as follows: glycine (if used), additive of interest (SDS, BTA, or H_2O_2), and then copper (if used). The pH was adjusted from 3 to 10 using either KOH or HNO_3, measured by an Orion model SA 720 pH meter. Then alumina particles were added at 0.05 wt% concentration, required for particle size and zeta potential measurements. Although this concentration is less than that present in typical CMP slurries, results are still comparable as particle-particle interactions in the bulk solution and interfacial region are negligible [7]. The alumina used was a dispersion manufactured by Cabot Corporation containing 40 wt% α-alumina in de-ionized water. The alumina particles have a primary diameter of 20 nm and a median aggregate diameter of 150 nm in water. The suspension was then stirred by a magnetic stirrer and then placed in a Bransonic Cleaner model 1200 sonicator for 5 minutes before measurement to ensure complete dispersion of the particles. The suspension was then removed from the sonicator and approximately 4.5 ml of the solution was pipetted into cuvettes and capped. The cuvettes were filled fully with solution to ensure elimination of trapped air that could change the pH.

The samples were placed into a ZetaPlus particle size analyzer (Brookhaven Instruments Corporation). This machine utilizes a quasi-elastic light scattering technique to measure the diameter of the agglomerates. Particle size measurements were taken every 10 seconds for a total of 10 minutes, as that is the typical residence time for slurry during the CMP process [6]. The upper limit for accurate particle size measurement was 3 µm, so suspensions in which larger particle sizes were observed will be indicated as larger than 3 µm. After particle sizing, zeta potential measurements were taken immediately for the sample using the same ZetaPlus instrument which used an electrophoretic light scattering technique. There is some lag from taking the sample off of sonication the first size measurement (averaging ~1 min) due to physical loading of the sample and calibration of the machine.

The polydispersed nature of the suspension leads to some statistical error in measurement of aggregate size in which an average of 10 readings were taken per measurement. Errors reported in Table 3.2 are the standard deviation of the measurement. The zeta potential reported is an average of 5 measurements with an average error of ± 2 mV (also the standard deviation of the measurement). However, when H_2O_2 was present, there was a larger error of ± 5 mV due to oxidation of the palladium electrodes.

Table 3.1. Suspension chemical compositions in 1mM KNO_3. Each suspension was also made with 0.12 mM Cu added.

Suspension	**Additives Present**
A	0.1M glycine
B	0.1 wt% H_2O_2
C	0.01 wt% BTA
D	0.1mM SDS
E	0.1M glycine + 0.1 wt% H_2O_2
F	0.1M glycine + 0.01 wt% BTA
G	0.1M glycine + 0.1mM SDS
H	0.1M glycine + 0.1 wt% H_2O_2 + 0.01 wt% BTA + 0.1mM SDS

3.3 Results and Discussion

In general, three types of behavior were observed, as shown in Figure 3.1. First, there were conditions where no aggregation occurred; the average particle size remained constant at ~150 nm. The second behavior observed was reversible aggregation, with large aggregates forming almost instantaneously to and maintaining an average size >2.5 µm. Finally, the third observed behavior consisted of aggregates steadily growing in size from the initial size of 150 nm. The effects of pH and additives on the aggregation behavior will be discussed in detail. In general, the zeta potential was largely positive (>40 mV) for acidic suspensions (pH range 3 to 7.5) and then negative (in general ~-10 mV) for basic suspensions. However, suspensions containing SDS (suspensions D, G, and H) did not follow this behavior and will be discussed in more detail.

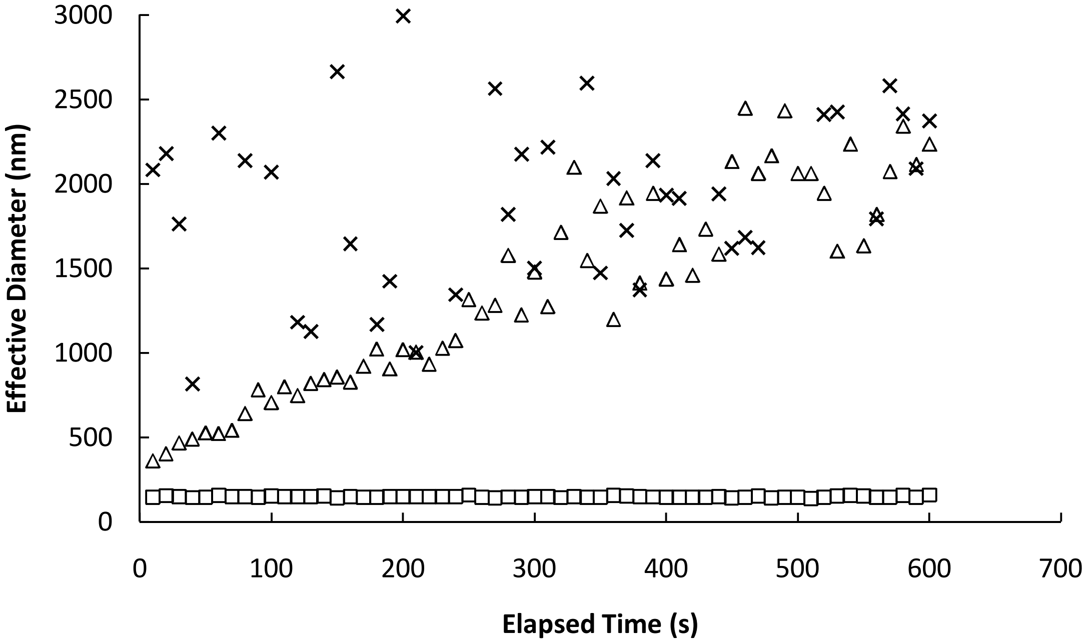

Figure 3.1. Effective aggregate sizes over time for suspension C with Cu at pH 3.0 (squares), suspension C with Cu at pH 8.7 (triangles), and D with Cu at pH 5.8 (x's) displaying no aggregation, steady aggregation, and reversible aggregation respectively.

Table 3.2 displays effective particle size measurements for all suspensions tested; suspensions A-D tested each additive individually with and without the addition of copper and suspensions E-G investigated the combination of glycine with the other three additives. Suspension H consisted of a combination of all additives. As shown in Table 3.2, most of the slurries showed either no agglomeration with an effective size of ~150 nm or immediately agglomerated to a larger size which was maintained over 10 min. A few slurries showed a steadily increasing agglomerate size over time; the final size after 10 min is reported in Table 3.2. These agglomeration rate data will be discussed in chapter 5. The size distributions for the non-aggregating suspensions were mostly monodispersed. For suspensions in which aggregation occurred, monodisperse distributions as well as bimodal distributions, with the smaller peak typically in the smaller particle size range (<1000 nm), were observed. A more detailed analysis of agglomerate size distributions has been done by Ihnfeldt and Talbot [7]. Zeta potential and maximum agglomerate size measurements of the suspensions as a function of pH are presented in Figures 3.2-3.9.

Table 3.2. Summary of agglomerate size measurements. Effective average agglomerate sizes are shown for suspensions when reversible or no aggregation was observed after 10 min. A highlighted box indicates that a steadily increasing agglomerate size over time was observed and the value shown indicates the final average agglomerate size after 10 min.

pH	**Effective Agglomerate Size (nm)**			
	Suspension A	**A with Cu**	**Suspension B**	**B with Cu**
3	151 ± 5	149 ± 5	149 ± 5	149 ± 5
4	152 ± 5	152 ± 5	150 ± 5	148 ± 5
5.5	152 ± 5	151 ± 5	149 ± 5	149 ± 4
6.5	152 ± 6	150 ± 5	151 ± 5	149 ± 5
7.5	153 ± 5	152 ± 8	154 ± 6	150 ± 5
8.5	1590 ± 180	2210 ± 310	149 ± 5	148 ± 5
9.5	>3000	>3000	>3000	>3000
10	2650 ± 590	2970 ± 660	2700 ± 910	>3000
	Suspension C	**C with Cu**	**Suspension D**	**D with Cu**
3	149 ± 5	149 ± 5	>3000	>3000
4	150 ± 6	149 ± 4	>3000	>3000
5.5	149 ± 6	148 ± 5	>3000	>3000
6.5	150 ± 5	150 ± 5	1570 ± 560	162 ± 39
7.5	148 ± 5	149 ± 6	240 ± 9	163 ± 5
8.5	179 ± 18	2240 ± 370	153 ± 6	154 ± 5
9.5	>3000	>3000	163 ± 5	177 ± 6
10	>3000	>3000	>3000	157 ± 9
	Suspension E	**E with Cu**	**Suspension F**	**F with Cu**
3	151 ± 4	152 ± 5	151 ± 4	149 ± 4
4	151 ± 5	153 ± 5	151 ± 5	150 ± 5
5.5	152 ± 5	153 ± 4	152 ± 4	152 ± 5
6.5	151 ± 5	151 ± 5	149 ± 5	153 ± 6
7.5	156 ± 8	155 ± 7	151 ± 5	153 ± 6
8.5	>3000	>3000	2990 ± 370	>3000
9.5	>3000	>3000	>3000	>3000
10	>3000	>3000	>3000	>3000
	Suspension G	**G with Cu**	**Suspension H**	**H with Cu**
3	>3000	>3000	>3000	>3000
4	>3000	>3000	>3000	2890 ± 1100
5.5	2530 ± 810	>3000	1180 ± 500	>3000
6.5	157 ± 6	166 ± 14	152 ± 5	152 ± 4
7.5	2630 ± 570	160 ±6	161 ± 6	156 ± 4
8.5	>3000	>3000	> 3000	>3000
9.5	>3000	>3000	>3000	>3000
10	2320 ± 390	2640 ± 350	2930 ± 600	>3000

Aggregation was not observed for suspensions A with and without copper at acidic and neutral pH values. However, steady aggregation was observed for pH of 8.5 for both suspensions with and without copper. As shown in Figure 3.2, there is no apparent effect of copper during particle aggregation for this suspension with only 0.1M glycine added. Zeta potentials for both suspensions in the acidic to neutral region (3-7.5) are largely positive (>25 mV). As the pH approaches the IEP, the zeta potential decreased and became negative in the basic region reaching -10 mV at pH 10 for both suspensions. An IEP of 9.9 ± 0.1 and 9.7 ± 0.1 was measured for both suspensions. The difference of the IEPs for A with and without copper is statistically insignificant.

The IEP for alumina with no additives is ~9 [7], lower than the measured IEP for suspension A with and without copper. It has been observed previously that, for metal oxide surfaces, KNO_3 acts as an indifferent electrolyte, meaning that its constituent ions do not adsorb onto the surface and alter the surface charge. Although the K^+ and NO_3^- ions can still screen the surface charge (and decrease the magnitude of the zeta potential) they do not alter the IEP [23]. Therefore, the increased IEP for suspension A is due to the presence of glycine. The increase in IEP may be due to the ionic nature of the glycine molecule. Glycine can exist as a cation, zwitterion, or cation depending on the solution pH. The cationic form predominates at pH < 2.35 (pKa_1) and the anionic form is predominant at pH > 9.78 (pKa_2) [34]. As the pH of suspension A increases past the IEP of glycine (6.0) [34] the glycine begins act as a Brønsted acid and loses an H^+ and as the pH increases further a larger number of the glycine molecules lose the H^+ ions. In the condition when no additives are present, the higher concentration of OH^- ions in the suspension will lead to deprotonation of the dangling OH groups on the alumina surface as the hydroxide ion removes it to produce water. However, in the presence of glycine, the hydroxide ions may capture the H^+ ions donated by the glycine molecule instead of the alumina surface. This effect would lead to more positive zeta potentials of the alumina particles in the basic region and shift the IEP to a higher pH.

For suspension B, with and without copper, no aggregation was observed until pH 10, where rapid, reversible aggregation was observed. Zeta potential measurements for B as shown in figure 3.3, with and without copper, are identical, staying mostly positive from acidic to neutral. An IEP of 9.1 ± 0.2 and 8.9 ± 0.2 was measured for B without and with copper respectively, again indicating that the presence of copper has no effect on the IEP. The IEP is also identical to the measured IEP of alumina with no additives, further suggesting that hydrogen peroxide also has no effect on the IEP and aggregation behavior. Of note is that the magnitude of the zeta potential of B in the basic region (>9) is significantly greater than all other suspensions. The pKa of hydrogen peroxide is 11.75 and below that respective pH hydrogen peroxide will predominantly exist in solution as aqueous H_2O_2 [37]. Not until the pH of the solution exceeds 11.75 will the hydrogen peroxide dissociate into H^+ and O_2H^-. Because the pH values of all the suspensions tested are less than the pKa, the hydrogen peroxide does not ionize and therefore does not influence the zeta potential and IEP of the alumina particles.

Aggregation was not observed for suspensions C in acidic and neutral pH. Addition of copper had a minor effect on aggregation. Steady aggregation was observed at pH 8.6 and 10. It is not clear if this is due to the presence of copper or to a high sensitivity of the stability of the suspension to pH in the weakly basic pH region. Zeta potential measurements, shown in figure 3.4, are identical with and without copper. However, a noticeably larger zeta potential value of 52mV without copper at pH 6.5 vs 30mV with copper was measured for suspension C. The difference in zeta potential may be due to inaccuracy of the pH measurement because of the instability of the suspensions as mentioned earlier in the experimental section. Measured IEPs were 10.3 ± 0.3 and 9.9 ± 0.2 for C without and with copper respectively, significantly larger than the IEP of alumina with no additives. BTA has a pKa of 8.2 [31] and will lose a hydrogen to form an anion. Similar to glycine in suspension A, the hydrogen ion produced by the ionization of BTA will be captured by the hydroxide ions present in the basic solution thereby preventing loss of hydrogen ions from the alumina surface, preserving its surface charge.

Suspension D contained SDS and a very different aggregation behavior was observed than for the other tested suspensions. Rapid, reversible aggregation at pH from 3 to 6.2 was observed. No agglomeration was seen at pH 8.5, however steady aggregation was seen at pH 10. Addition of copper had no effect on aggregation in the acidic region. However, no aggregation was observed from pH 6.8 to 10. Zeta potential curves for D in Figure 3.5, with and without copper, are identical in the acidic to weakly basic pH region. Low zeta potential values were measured from pH 3 to 6 where zeta potential begins to increase, corresponding with the decrease in aggregation in this region. At pH 10 a zeta potential of 36 ± 1 mV was measured for suspension D with copper. However, a zeta potential of 0 ± 2 mV was measured for suspension D without copper (indicating an IEP of 10 ± 0.2). This difference may be attributed to the instability of the suspension pH due to the lack of glycine. The cause for the increased IEP from alumina with no additives is unclear. No IEP for D with copper was determined; zeta potentials were positive for all pH values tested. Adsorption of SDS as a function of pH has been investigated by Somasundaran and Fuerstenau [37] and found that adsorption is greatest at low pH (3) and decreases with increasing pH. No adsorption is observed after the pH is increased past the point of zero charge of the alumina (9) [37] and it is therefore thought that the SDS no longer influences the zeta potential of the alumina past this point. Somasundaran and Fuuerstenau observed decreasing electrophoretic mobility from pH of 2 to ~6.7 after which mobility increased sharply [37]. As electrophoretic mobility and zeta potential are directly proportional, the rise in zeta potential observed for suspension D after pH 5.5 is not unexpected. Although SDS is typically used as a dispersant, aggregation occurred in acidic suspensions up to pH 6.5 with it present, regardless of the presence of other additives. A possible explanation is that as pH is decreased, there is greater protonation of OH groups present on the alumina particle surface [32]. These protonated sites are attractive to the anionic head group of the SDS molecules, promoting adsorption. As surface coverage of the particles increases as pH decreases, SDS molecules will begin to bridge the hydrophobic carbon tails with SDS molecules adsorbed to other particles in order to reduce exposure to the aqueous environment and thereby lowering free energy and increasing aggregation [13]. Because of the bridging of the SDS molecules, aggregation can occur even if the magnitude of the zeta potential is large.

The aggregation in suspensions E, with and without copper, behaved similarly. Compared to suspension B, the addition of glycine had no effect on aggregation in the acidic regime; no aggregation was observed for suspension E, with and without copper at pH 3.5 to 6. The addition of glycine did promote aggregation at pH 8.5, with and without copper, for suspension E. Zeta potential measurements were identical for suspension E as shown in figure 3.6, with and without copper, staying mostly positive in the acidic to neutral region, but closer to the IEP values. An IEP of 9.6 ± 0.2 was measured for suspension E without copper and 9.9 ± 0.3 for suspension E with copper. It should be noted that zeta potential measurement error was larger for both suspensions B and E. This is likely due to the slight oxidation of the palladium electrodes caused by the hydrogen peroxide. The glycine present in the suspensions is likely causing the same effect seen in suspension A, and thus responsible for the increased IEP.

For suspension F, with and without copper, the aggregation behavior was similar. Aggregation was noticeably greater in suspension F at pH 8.5 than suspension C, likely due to the high sensitivity of the suspension to pH in this region. The zeta potential curve in figure 3.7 with copper is identical in shape to without copper; however lower zeta potential values were observed, corresponding with the observed aggregation behavior. Identical IEPs were determined for suspension F; 9.7 ± 0.2 and 9.6 ± 0.2 for F without and with copper respectively. Because suspension F contains both glycine and BTA, which both can ionize and produce hydrogen ions at basic pH (>8), it is not surprising that the IEP is higher than that of alumina with no additives.

For suspension G, with and without copper, rapid aggregation was observed for both suspensions at acidic pH (3 to 5.5). For suspension G without copper, steady aggregation began from pH 7.5 and continued to pH 10. After copper was added, aggregation did not occur at pH 7.5; however steady aggregation began at pH 8.5. Zeta potential measurements were identical for suspension G, with and without copper and similar behavior to suspension D was observed. A minimum zeta potential was observed for both at pH 4, followed by a steady increase in zeta potential up to pH 7.5 after which zeta potential began to drop. After pH 7.5, consistently lower values of zeta potential were observed for suspension G without copper than with copper with an IEP of 8.3 ± 0.1, as opposed to an IEP of 8.4 ± 0.2 with copper. It is of note that the IEP of suspension G (without and with copper) is significantly lower than most all other suspensions tested. The effects of the order of addition of the chemicals were investigated, by adding SDS last, after alumina. However, no significant effect on aggregation or zeta potential was observed.

The behavior of suspension H (both without and with copper) were similar to suspension D and G. Aggregation occurred almost instantaneously to large sizes (>3000 nm) after alumina was added to the suspension in acidic pH (3 to 5.5). Suspension H at pH 5.5 did exhibit reversible aggregation for the entire time range; however the mean aggregate diameter was 1180 nm. In this acidic regime, measured zeta potentials were notably positive but less than 25mV. The high magnitudes of aggregation with non-zero zeta potentials suggest that some other forces other than pure electrokinetic forces are present. It is likely that the SDS is promoting aggregation in the acidic region as observed in suspensions D and G. The suspensions near neutral pH (6.5 and 7.5) exhibited no aggregation and zeta potentials >25 mV were measured as expected. For the basic suspensions (8.5 and 10), steady aggregation was observed to sizes exceeding 3000 nm. Zeta potential of pH 8.5 for without and with copper were both positive (~15mV) while at pH 10 zeta potentials were negative, although H with copper was significantly lower than without copper (-12.1 vs -2.6 mV respectively). The IEPs of H with and without copper were markedly different as well; 9.7 ± 0.4 for H without copper and 9.0 ± 0.2 for H with copper. The higher measured IEP for H without copper, compared to when no additives are present, can again be attributed to the effects of glycine and BTA as observed in suspensions A and C. The effect of SDS may dominate over other chemical effects of other additives for acidic suspensions, causing the aggregation observed in more complex slurries where SDS was present. Although greater charge screening of the particles is possible due to the additional sodium ions, the concentration (0.1mM) is an order of magnitude lower than that of the KNO_3 (1mM) and thus negligible.

When copper is present the copper in solution will form copper oxide (CuO) at basic pH but in the presence of H_2O_2 and glycine, the copper will complex further to form $Cu(CH_2NCH_2COO)_2^-$ and $Cu(OH)_2$ [9]. The negatively charged copper-glycine complex may have a higher affinity for H^+ ions than the surface of the alumina and therefore may further increase the deprotonation of the alumina surface. Not all of the glycine complexes with copper since the concentration of copper is significantly lower than glycine. Therefore the effect of the extra deprotonation caused by the copper-glycine complex may be offset by the "shielding" effect of the alumina surface caused by the glycine not complexed as observed in suspension A. Copper can also complex with the BTA in the solution as well, forming a complex polymer $[Cu(BTA)]_n$ at high pH [36]. This copper-BTA complex prevents the BTA from releasing any H^+ ions to the solution, negating its "shielding" effect of preserving the charge on the alumina surface as observed in suspension C and F. The combination of all of these effects may have no net effect on the alumina surface and thus the alumina particles would have an IEP identical to with no additives present.

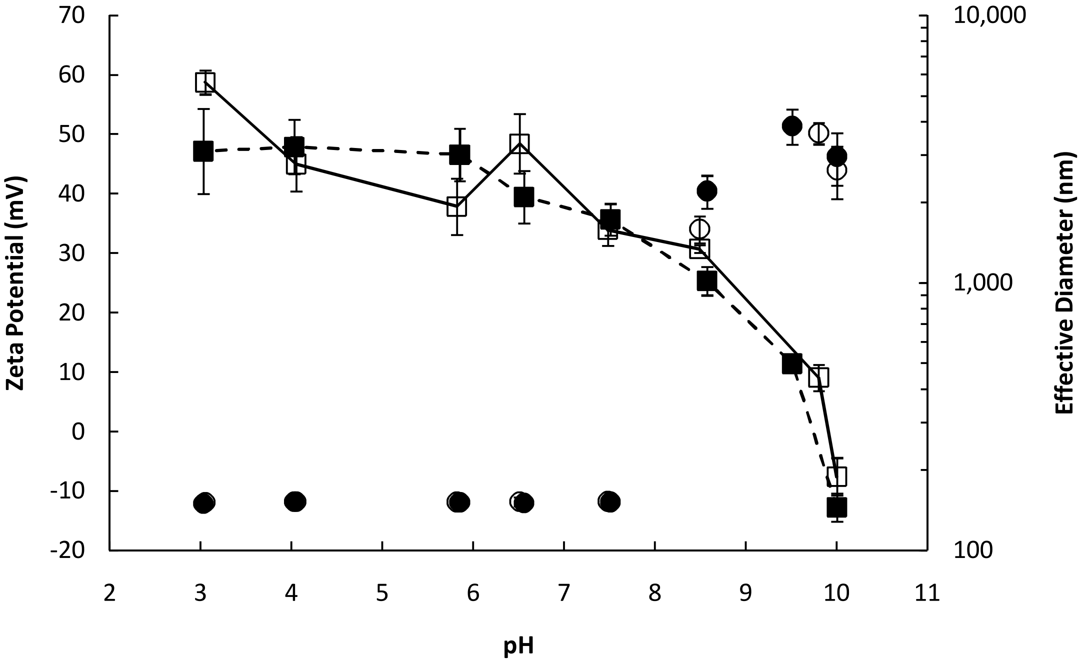

Figure 3.2. Zeta potential (squares) and effective agglomerate sizes (circles) for suspension A without Cu (open points) and with Cu (closed points).

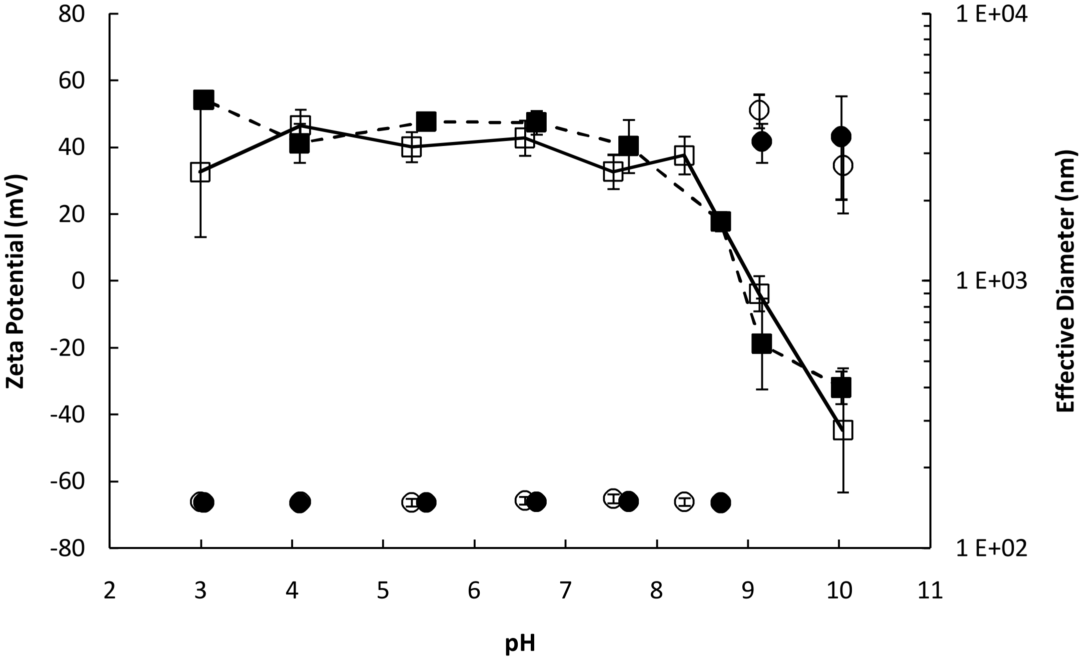

Figure 3.3. Zeta potential (squares) and effective agglomerate sizes (circles) for suspension B without Cu (open points) and with Cu (closed points).

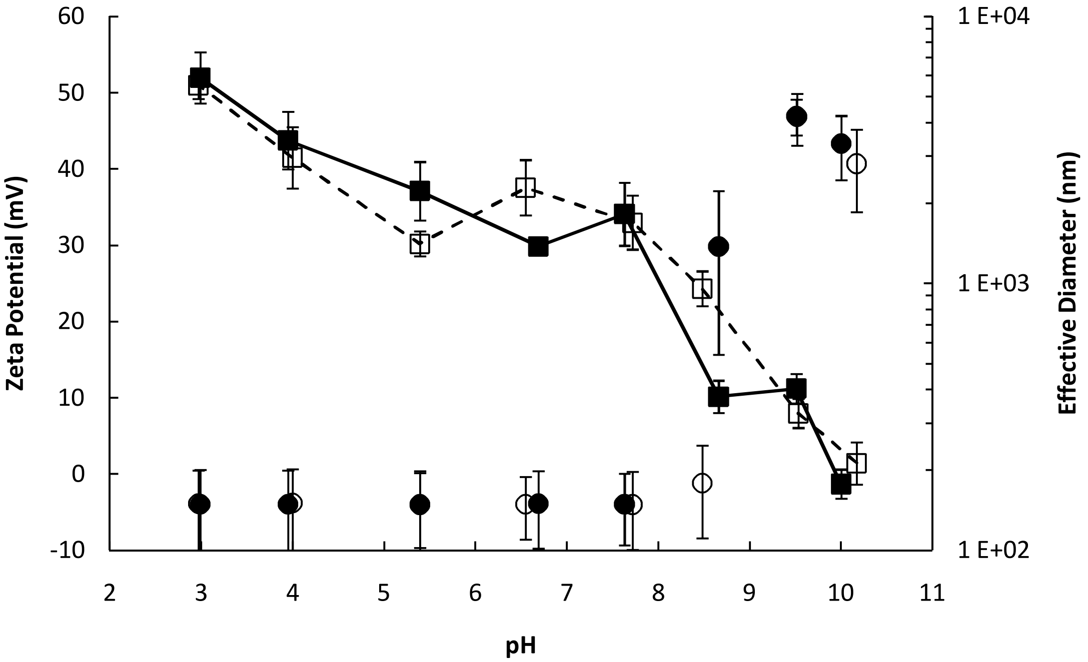

Figure 3.4. Zeta potential (squares) and effective agglomerate sizes (circles) for suspension C without Cu (open points) and with Cu (closed points).

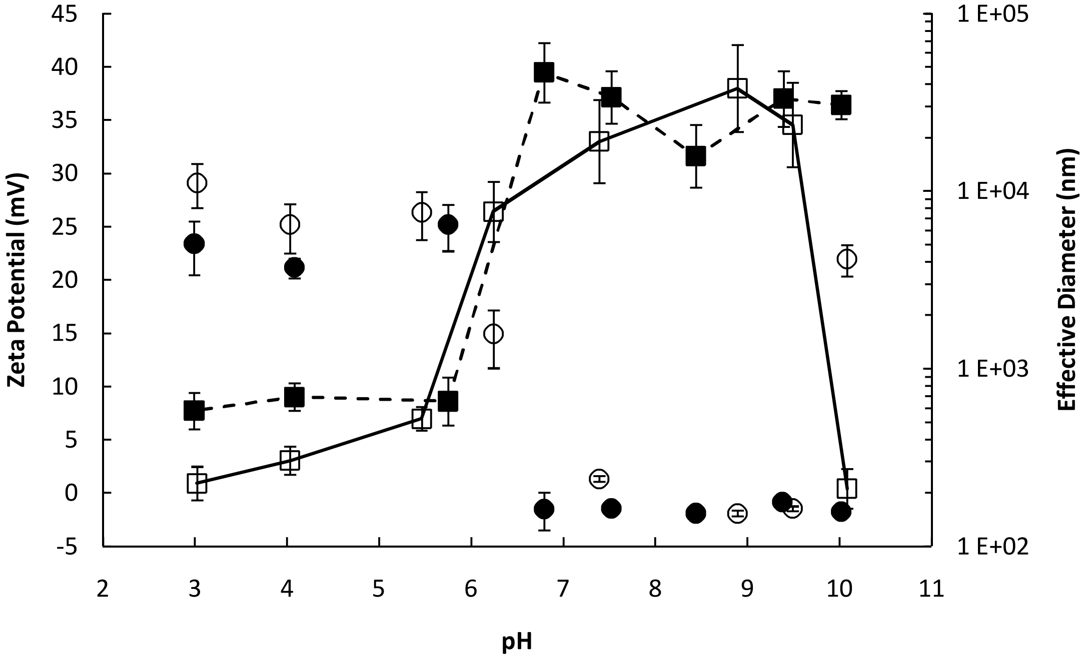

Figure 3.5. Zeta potential (squares) and effective agglomerate sizes (circles) for suspension D without Cu (open points) and with Cu (closed points).

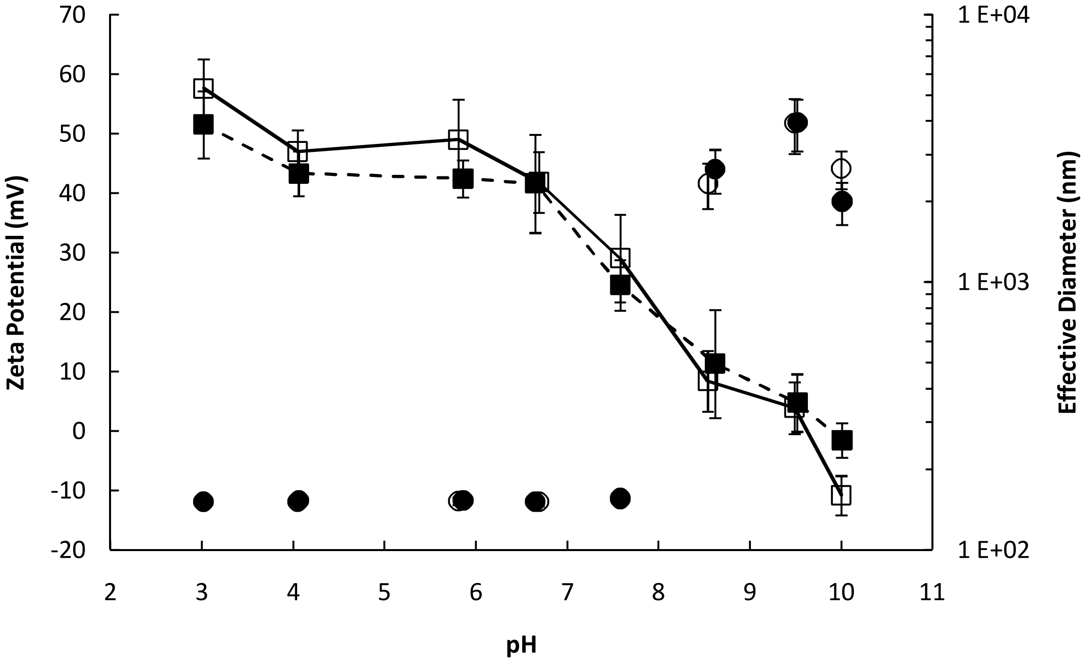

Figure 3.6. Zeta potential (squares) and effective agglomerate sizes (circle) for suspension E without Cu (open points) and with Cu (closed points).

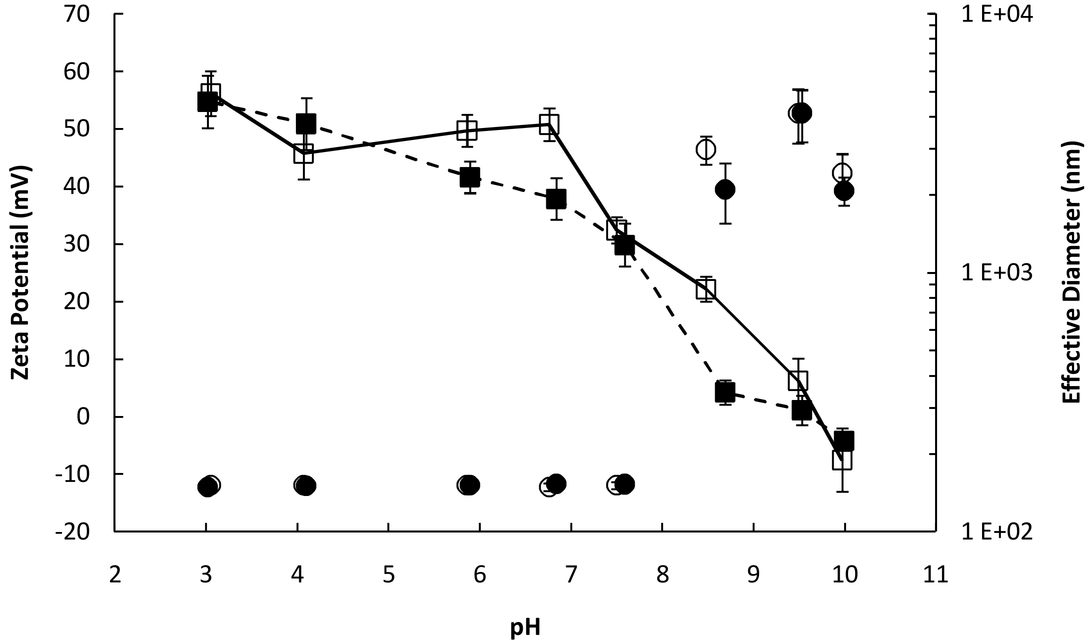

Figure 3.7. Zeta potential (squares) and effective agglomerate sizes (circles) for suspension F without Cu (open points) and with Cu (closed points).

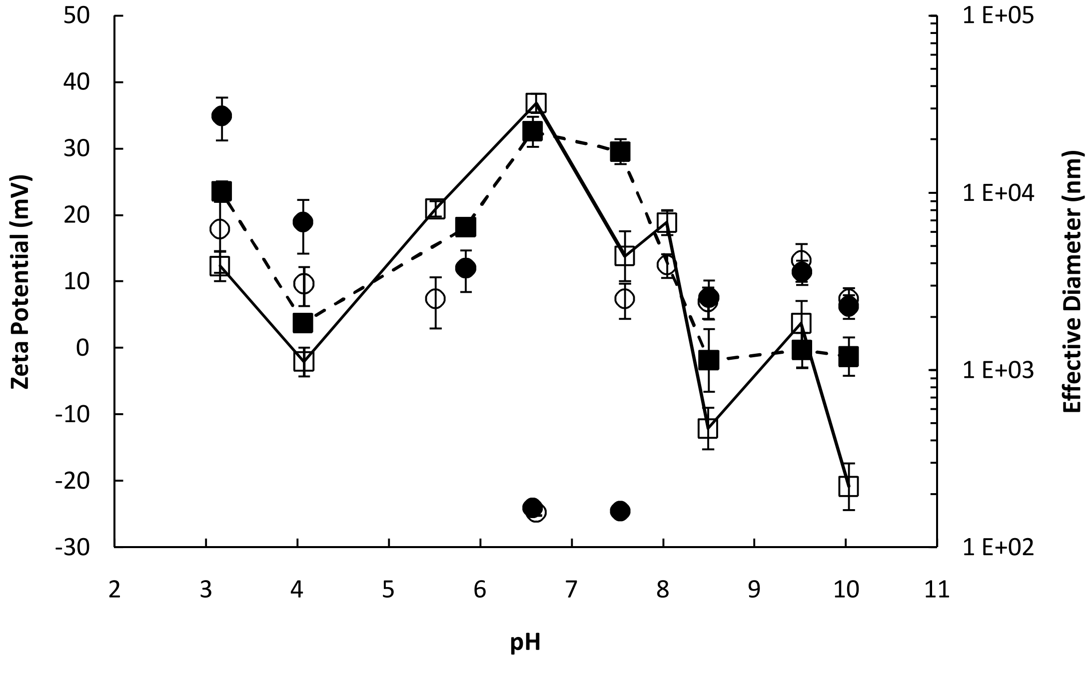

Figure 3.8. Zeta potential (squares) and effective agglomerate sizes (circles) for suspension G without Cu (open points) and with Cu (closed points).

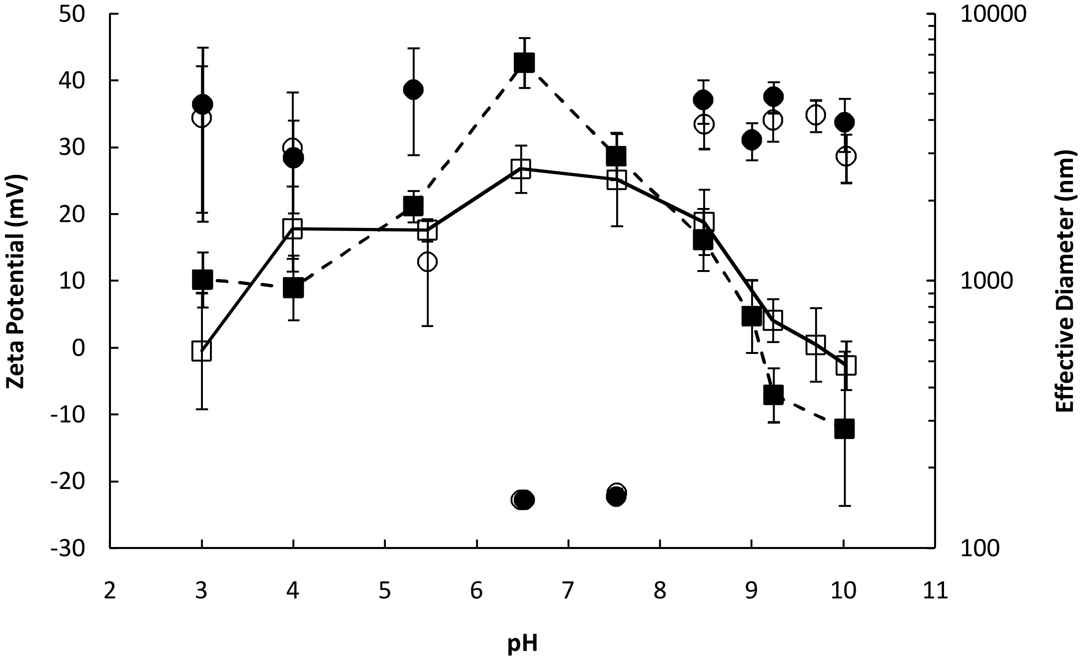

Figure 3.9. Zeta potential (squares) and effective agglomerate sizes (circles) for suspension H without Cu (open points) and with Cu (closed points).

3.4 Conclusions

In our study of the effects of copper CMP slurry additives on the aggregation of 150 nm alumina particles, three behaviors were observed in this study: no aggregation, reversible aggregation where large agglomerates (>2.5 μm) formed almost instantaneously, and steady aggregation from the initial aggregate size. Additives used in CMP slurries play complicated roles in the aggregation behavior of alumina particles. Although SDS is commonly used to disperse nanoparticles, its addition caused a significant increase in agglomeration of alumina in the acidic solutions (3-6.5) as well as a decrease in zeta potential, where agglomeration was not seen in all suspensions tested without SDS. This behavior was seen with SDS in suspensions with and without glycine or copper as well as with all other additives present. The increased aggregation was most likely due to interparticle bridging of SDS molecules. The addition of 0.12 mM copper to the suspensions had a negligible effect on aggregation or zeta potential. Altering the order of addition also had no effect on aggregation behavior or zeta potential. When all additives were present, a lower IEP was measured when copper was present.

Copper had a negligible effect on aggregation and IEP for all other suspensions tested with the exception of suspension H, when all additives are present. H_2O_2 had little effect on IEP as well due to its high pKa. Glycine and BTA both ionize at high pH (>8) losing hydrogen ions to the suspensions. These hydrogen ions may be captured by the hydroxide ions in the basic suspension, preventing loss from alumina surface and preserving the surface charge. This effect is credited to the increase in the IEP of suspensions containing these additives.

Zeta potential was positive in the acidic and neutral suspensions tested for all additives except for SDS, where zeta potentials were close to zero. Isoelectric points in the basic region (ranging from 8 to 10) for all suspensions were also measured, with additives causing shifts in the IEP. All suspensions where aggregation was observed corresponded to zeta potential measurements close to the IEP indicating that the aggregation is occurring via electrokinetic processes.

Overall, pH was the most significant factor causing aggregation of particles. Every suspension tested showed aggregation near the IEP. We have also shown previously that changing the pH can reverse the aggregation and reduce the aggregate sizes [16]. Additionally, this study was conducted with constant ionic strength suspensions to be able to make direct comparisons of effects. Ionic strength is also a factor in aggregation as increased ionic concentrations in suspensions can screen the charge of the particles and alter the zeta potential and IEP values. Chapter 5 will discuss steady aggregation rates observed in this study, and include fractal dimension and stability ratio analysis of the aggregation data.

Acknowledgements

This work was supported by University of California, Berkeley IMPACT program for its support along with the partner companies: Applied Materials, AMSL, Ebara Technologies, Global Foundries, IBM, Intel Corporation, KLA-Tencor, Marvell, Mentor Graphics, Novellus Systems, Panoramic Tech, SanDisk, Synopsys, Tokyo Electron Limited, and Xilinx Inc, along with matching support by the UC Discovery Grant ele07-10283. I would also like to thank Kasia Matusik and Robin Ihnfeldt for their support with the aggregation and zeta potential measurements.

This chapter in part is currently being prepared for submission for publication of the material; Neil Brahma and Jan B. Talbot. The dissertation author was the primary investigator and author of this material.

References

1. T. Ohi, *Trends and Future Developments for Diamond CMP Pad Conditioners*. Industrial Diamond Review; 2004(1): 14-21

2. M. Bielmann, U. Mahajan, and R. K. Singh, *Electrochem. and Solid-State Lett.*, **2**, 401–403 (1999).

3. Y. Tateyama, T. Hirano, T. Ono, N. Miyashita, T. Yoda, *Chemical Mechanical Polishing (IV)*, The Electrochemical Society, Pennington, New Jersey (2001).

4. R. Ihnfeldt and J.B. Talbot, *J. Electrochem. Soc.*, **155** (6), H412-H420 (2008).

5. Z. Li, K. Ina, P. Lefevre, I. Koshiyama, and A. Philipossian, *J. Electrochem. Soc.,* **152** (4), G299-G304 (2005).

6. M. G. Song, J. Lee, Y. G. Lee, and J. Koo, *J. Colloid and Interface Sci.,* **300**, 603-611 (2006).

7. R. Ihnfeldt, PhD Thesis, University of California, San Diego (2008).

8. T. Gopal, PhD Thesis, University of California, San Diego (2004).

9. T. Gopal and J. B. Talbot, *J. Electrochem. Soc.,* **153** (7), G622-5 (2006).

10. R. Ihnfledt and J. B. Talbot, *J. Electrochem. Soc.* **153** (11), G948-G955 (2006).

11. R. Ihnfeldt and J.B. Talbot, *J. Electrochem. Soc.*, **154** (12), H1018-H1026 (2007).

12. R. Ihnfeldt and J.B. Talbot, *J. Electrochem. Soc.*, **155** (8), H582-H588 (2008).

13. N. Brahma, M.C. Chan, and J. B. Talbot, *ECS Trans.,* **19**(7), 25 (2009).

14. N. Brahma and J.B. Talbot*, ECS Trans.,* **33** (10), 53 (2010).

15. P. C. Goonetilleke and D. Roy, *Applied Surface Sci.,* **254** (9), 2696-2707 (2008).

16. B. J. Palla and D. O. Shah, *J. Colloid and Interface Sci.,* **223**, 102-111 (2000).

17. R. K. Singh, S. M. Lee, K. S. Choi, B. B. Basim, W. Choi, Z. Chen, and B. M. Moudgil, *MRS Bulletin,* 752-760, October 2002.

18. P. Moon, V. Chikarmane, K. Fischer, R. Grover, T. A. Ibrahim, D. Ingerly, K. J. Lee, C. Litteken, T. Mule, and S. Williams, *Process and Electrical Results for the On-Die Interconnect Stacks for Intel's 45nm Process Generation*. Intel Technology Journal; 2008, 12(2), 87-92.

19. J. Luo and D. A. Dornfeld, *IEEE Trans. Semiconduct. Manufact.*, **14**, 112–133 (2001).

20. S. M. Ahmed, *Canadian Journal of Chemistry,* **44**, 1663-1670 (1966).

21. J. Luo and D. Dornfeld, *Integrated Modeling of Chemical Mechanical Planarization (CMP) for Integrated Circuit Fabrication: From Particle Scale to Feature, Die and Wafer Scales, Report*, University of California, Berkeley (Oct 2003).

22. Z. Zhou and B. Chu, *J. Colloid and Interface Sci.,* **143**(2), 356-365 (1991).

23. R. J. Hunter, “Zeta Potential in Colloid Science,” Academic Press, London (1981).

24. Y. Hu and J. Dai, *Minerals Engineering,* **16**, 1167-1172 (2003).

25. P. Somasundarun, T. W. Healy, and D. W. Fuerstenau, *J. Colloid and Interface Sci.,* **22**, 599-605 (1966).

26. Q. Luo, *Ind. Eng. Chem. Res.,* **39**, 3249-54 (2000).

27. G. B. Basim, I. U. Vakarelski, and B. M. Moudgil, *J. Colloid and Interface Sci.,* **263** (2), 506-15 (2003).

28. P. C. Pavan, E. L. Crepaldi, G. A. Gomes, and J. B. Valim, *Colloids and Surfaces A: Physiochemical and Engineering Aspects,* **154** (3), 399-410 (1999).

29. A. Khanna, P. Kumar, J. Lee, A. Mishra, A. C. Arjunan, D. Singh, and R. K. Singh, “Analysis of Shear Induced Particle Agglomeration in CMP Slurries.” ECS Meeting Abstracts 2010, Las Vegas, NV

30. S. M. Ahmed, *Canadian Journal of Chemistry,* **44**, 1663-1670 (1966).

31. A. R. Karitzky, S. Rachwal, and G. J. Hitchings, *Tetrahedron*, **47** (16-17), 2683-2732 (1991).

32. D. P. Siegel, B. R. Ware, D. J. Green, and E. W. Westhead, *Biophys J.*, **22**(2), 341-346 (1978).

33. S. Aksi and F. M. Doyle, *J. Electrochem. Soc.*, **149**(6), G352-G361 (2002).

34. S. H. Hilal, S. W. Karickhoff, and L. A. Carreira, *Talenta*, **50**(4), 827-840 (1999).

35. M. G. Evans and N. Uri, *Trans. Faraday Soc.*, **45**, 224-230 (1949).

36. R. Youda, H. Nishihara, and K. Aramaki, *Electrochimica Acta*, **35**(6), 1011-1017 (1990).

37. P. Somasundaran and D. W. Fuerstanau, *J. Phys. Chem.,* **70**(1), 90-96 (1966).

CHAPTER 4

EFFECTS OF TEMPERATURE ON ZETA POTENTIAL OF ALUMINA NANOPARTICLES

4.1 Introduction

The chemical mechanical planarization (CMP) process relies on the simultaneous chemical etching and mechanical abrasion to uniformly planarize a surface. The copper CMP process is sensitive to many variables including abrasive size and size distribution, chemical etch rate, etc. The main goal of the research of our group is to understand the role of slurry chemistry in the copper CMP process. Our studies have focused on alumina abrasive particles, particularly their agglomeration and rate of agglomeration. The ~150 nm size abrasive particles can aggregate to sizes on the order of micrometers. These larger particles can lead to non-uniform polishing, as well as scratches and other defects. Therefore, understanding the mechanism of agglomeration as a function of chemistry could lead to improved chemical slurries with a reduction of particle agglomeration.

Our previous work has studied the role of slurry chemistry on the colloidal behavior of alumina particles in various suspensions [1]. The colloidal behavior was characterized by measuring the particle size distribution and zeta potential. Our particle size and surface hardness data were incorporated into a chemical-mechanical model of Luo and Dornfeld of the CMP process [2]. Recently, we have also initiated a study of the effects of chemistry on the agglomeration and agglomeration rate of alumina particles [3].

The zeta potential, the electrical potential between the stationary fluid layer surrounding the particle and the dispersed medium, plays a role in agglomeration. In general, colloids with large absolute values of the zeta potential (> ~25 mV) tend to be most stable with minimal particle aggregation. Conversely, when the zeta potential is at or close to the isoelectric point (IEP), the pH where the zeta potential is zero, the particles tend to agglomerate significantly. Therefore, knowledge of the IEP is important for the understanding of particle agglomeration.

The zeta potential is affected by adsorption of ions onto the particle surface and the presence of ions in the bulk fluid, hence, most notably solution pH [4]. In a preliminary study on the effect of slurry chemistry on alumina particles, the zeta potential was measured in a 1mM KNO_3 solution and the IEP was found to be 6.5. After the addition of 0.12 mM copper nanoparticles to the solution, no change in the IEP was observed, although the zeta potential values varied at different pHs. The addition of common copper CMP slurry additives have also been shown to alter the IEP of alumina [1]. For example, with the addition of 0.1M glycine, the IEP increased to 9, while with the addition of copper to the solution with glycine, the IEP decreased to 7.5 [1].

The isoelectric point of the particles is greatly dependent on the chemistry of the suspension. For example, a greater concentration of ions in the bulk will allow for higher concentrations of counterions to build up around the particles, altering the magnitude of the zeta potential. Also, the adsorption of surfactants onto the particle surface can increase the effective surface area for charge to build [4]. Not all ions present in a suspension affect the zeta potential of the particles. If the ions do not interact with the particle surface, they are called *indifferent ions*. If they adsorb onto the surface and alter the surface charge, they are *specifically adsorbed ions*. It has already been shown that K^+ and NO_3^- are indifferent ions for metal oxides [4]. The point of zero charge (PZC) is the pH where the surface charge of the particles is zero [4]. If the only potential determining ions are H^+ and OH^-, then the IEP and PZC are equal.

During the CMP process, the temperature of the suspension can increase due to friction from the polishing pad and the substrate and has been measured to increase from room temperature to 40^o C [6]. This increase in temperature can affect the electrokinetic properties of the abrasive particles and promote aggregation.

Although the effects of temperature on metal oxide particle agglomeration have not been studied, temperature has been known to affect colloidal stability for particles sterically stabilized with polymers. This is due to changes of the free energy of mixing of the polymer chains adsorbed onto separate particles. For sterically stabilized polymers a critical flocculation temperature (CFT) exists; a point at which a stable colloid will abruptly begin to flocculate. Polymers that are *enthalpically stabilized*, that is the change in enthalpy of mixing (ΔH^M) and entropy of mixing (ΔS^M) are both positive, will flocculate if the temperature is raised past the CFT. If ΔH^M and ΔS^M are both negative, the colloid is *entropically stabilized* and will flocculate if the temperature is lowered below the CFT. Some colloids may have a positive ΔH^M but a negative ΔS^M and flocculation has no apparent dependence on temperature [7].

Indeed these effects have been observed in experiment. Dederichs et al observed that for hydrophobic boehmite nanoparticles stabilized with dodecyltrimethylammonium broimide ($C_{12}TAB$) elevated temperatures caused a change in colloidal stability. For concentrations of $C_{12}TAB$ up to 55mM, colloidal stability was reduced at higher temperature caused by desorption of the surfactant and CFT was directly proportional to the $C_{12}TAB$ concentration. At $C_{12}TAB$ concentrations > 55 mM, micelles were present at the CFT, which was found to be inversely proportional to $C_{12}TAB$ concentration [8]. Chen et al measured flocculation of prepared platinum nanoparticles stabilized with a variety of vinyl polymers with amide side chains and observed lowered CFT's with increasing concentrations of a divalent electrolyte (Na_2SO_4 for this case). No measurements with monovalent electrolytes were made [9]. Pamies et al measured flocculation of gold nanoparticles stabilized with poly(N-isopropylacrylamide)-block-poly(3-acrylamidopropyl)trimethylammonium chloride polymer also observed that increased temperature promoted flocculation. They proposed that the temperature affected flocculation through a combination of enhanced charge density of the polymer and weakening of the steric hindrance [10].

The effect of temperature on zeta potential is not well understood. Wiśniewska observed greater zeta potentials at all pH for alumina particles in 0.01M NaCl at 35 C than at 15 C (~7-10 mV greater) [11]. Vidojkovic et al studied the electrokinetic properties of magnetite particles (Fe_3O_4) using a custom designed high-temperature zeta meter. They observed a decrease in the isoelectric point of the particles with increasing temperature; measured IEP's were 6.35, 6.00, 5.25, and 5.05 for temperatures of 25, 100, 150, and 200^{o}C. The zeta potential curves were sigmoid in shape and sharper drops from positive to negative zeta potentials occurred for the high temperature samples [12].

Vidojkovic explains the dependence of the zeta potential with temperature as an effect related to the changes in surface oxygen protonation/deprotonation reactions at higher temperatures [12]. Liu et al measured a linear decrease in zeta potentials of gold nanoparticles suspended in 0.09M NaCl from -43.3 to -64.3 mV at temperatures from 10 to 40^{o}C [13]. They also concluded that the effect was due to changes in the surface adsorption/desorption equilibrium but also charge dissociation equilibrium and the diffuse double layer thickness [13]. Jayaweera et al. have shown that for a variety of metal oxides, for higher temperatures up to 235^{o}C, typically both the zeta potential and the PZC of the particles decreased with increasing temperature [14]. Tewari and McLean reported that, for alumina in suspensions of 5 mM to 0.5 M KNO_3, IEP values decreased from 9.2 to 8.8 as temperature increased from 25 to 40°C [15].

This chapter presents measurements of the zeta potential of alumina in the presence of copper CMP slurry additives, such as benzotriazole (BTA), a corrosion inhibitor, and sodium-dodecyl-sulfate (SDS), an anionic surfactant. The zeta potential was also measured at temperatures from 25 – 40^{o}C. The IEPs of alumina in the various solutions as a function of temperature were determined. Particle sizes were also measured to check what effects zeta potential may have on agglomeration.

4.2 Experimental

Suspensions were prepared with distilled water filtered through a 22μm cellulose acetate filter. The following solutions were prepared in 1mM KNO_3 with 0.12mM Cu (as nanoparticles): (a) 0.1M glycine, (b) 0.1M glycine, and 0.1 wt% H_2O_2, and (c) 0.1M glycine, 0.1 wt% H_2O_2, 0.01 wt% BTA, and 0.1mM SDS. The solutions have been previously used in copper CMP studies [1, 2, 3]. The pH of each was then adjusted to the desired value by using KOH and HNO_3, measured by an Orion model SA 720 pH meter. Copper nanoparticles (<100 nm in diameter, from Aldrich) were used instead of copper salts, as to not alter the ionic strength of the suspension. After pH adjustment, 89 µl of alumina from a 40 wt% α-alumina in de-ionized water dispersion, manufactured by Cabot Corporation, was added to produce a 0.05 wt% solution. The alumina particles have a primary diameter of 20 nm and a median aggregate diameter of 150 nm. The solution was then stirred to ensure proper mixing of the alumina in solution and then placed in a Bransonic Cleaner model 1200 sonicator for 5 minutes before measurement. Since the typical copper CMP process has a slurry exposure time of ~5 to 10 minutes [1], the measurements were taken 10 minutes after sonication.

Approximately 4.5 ml of the solution was then pipetted into cuvettes with caps and placed in a ZetaPlus (Brookhaven Instruments Corp.) particle size and zeta potential analyzer which utilizes electrophoretic light scattering [1]. Fresh suspensions were prepared for each pH and temperature tested. For each suspension, both zeta potential and average particle size was measured. The experimental error was determined from an average of 6 measurements. The IEP of α-alumina in water has been reported as 9.2 [1], therefore a pH range from 7 to 11 was initially chosen to adequately characterize the IEP of each suspension.

4.3 Results and Discussion

Figures 4.1 and 4.2 show the zeta potential measurements for suspensions of alumina in two of the solutions at various temperatures and pHs. Figure 4.1 shows that with more acidic pH values, the zeta potential increases to 40 mV and with more alkaline pH values it decreases to -20 mV. The IEP values were estimated from the graphs of zeta potential vs. pH and the error was based on the standard error of the zeta potential measurements. Table 4.1 lists the observed IEP values for the three suspensions and temperatures studied. As also shown in Figure 4.1, the IEP for a suspension with only 0.1M glycine, the IEP ranges from 9.5 - 9.8 for all the temperatures. The zeta potential measurements for alumina in the solution with 0.1M glycine, and 0.1 wt% H_2O_2 (not shown) was similar to those in Figure 4.1, only with slightly shifted curves to lower pH values, resulting in an IEP of 9.1 for all temperatures. The copper particles in solution may oxidize and form different species depending on pH, such as $HCuO_2^-$, CuO_2^-, and CuO [1]. The copper ions may also complex with glycine [1]. At pH 9, as the suspension approaches the IEP, significantly larger particles (~2 μm) formed. Some of these larger particles persisted at higher pH values, although the average particle size decreased as the solutions became more basic and the zeta potential decreased below zero. It should be noted that increased scatter in the zeta potential measurement was observed after the addition of hydrogen peroxide, which is most likely due to its oxidation on the electrodes which produced small bubbles.

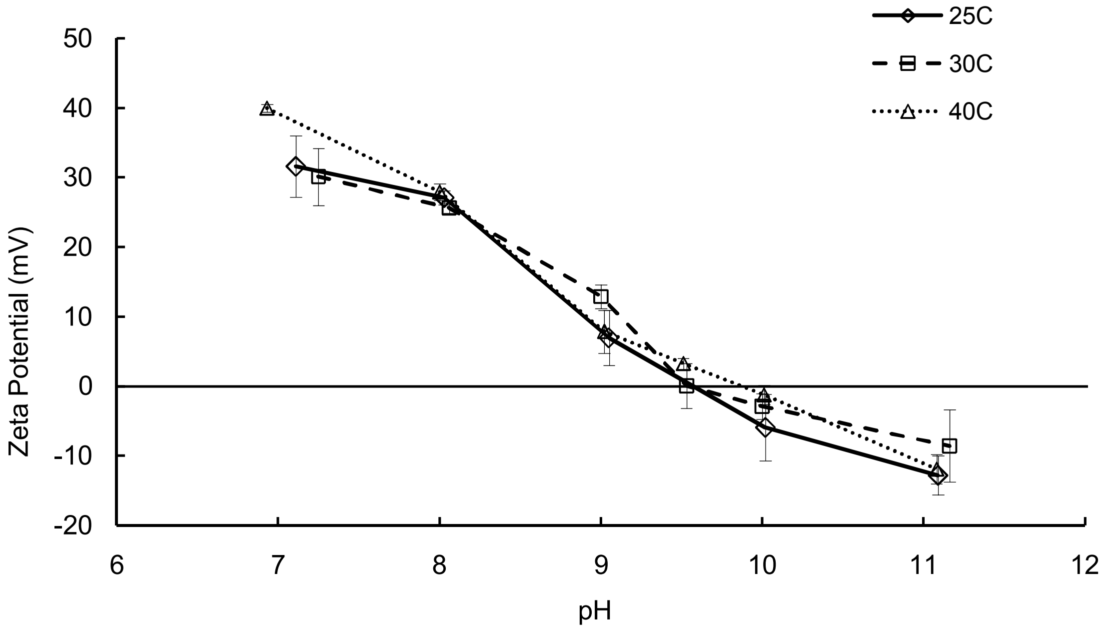

Figure 4.1. Zeta potential vs pH for alumina suspensions with 1mM KNO_3, 0.1M glycine, and 0.12mM copper.

Table 4.1. IEP values for each suspension at temperatures studied.

Additives	**T (^oC)**	**IEP**	**Error (±)**
KNO_3, Glycine, Cu	25	9.5	0.3
	30	9.5	0.4
	40	9.8	0.2
KNO_3, Glycine, H_2O_2, Cu	25	9.1	0.7
	30	9.1	1.1
	40	9.1	0.5
KNO_3, Glycine, H_2O_2, BTA, SDS, Cu	25	9.1	1.8
	30	8.3	3.0
	35	7.5	3.6
	40	7.2	3.8

Figure 4.2 shows zeta potential results for suspensions with KNO_3, glycine, H_2O_2, BTA, SDS, and copper. These measurements showed larger scatter in general than the other suspensions, likely due to the presence of the surfactant and other additives. In this solution as the temperature increased from 25 to 40°C, the IEP values decreased from 9.1 to 7.2. Tewari and McLean reported IEP values that decreased from 9.2 to 8.8 for alumina in this range [15]. The difference in IEP values and the effect of temperature from those reported are likely caused by the presence of ions from the additives used in our suspensions. Therefore the additives present in the suspension affect the variation of IEP with temperature, which in turn will affect particle agglomeration. Slurries at a pH below the IEP at 25°C may not agglomerate, but as the IEP decreases with increasing temperature, agglomeration may become significant.

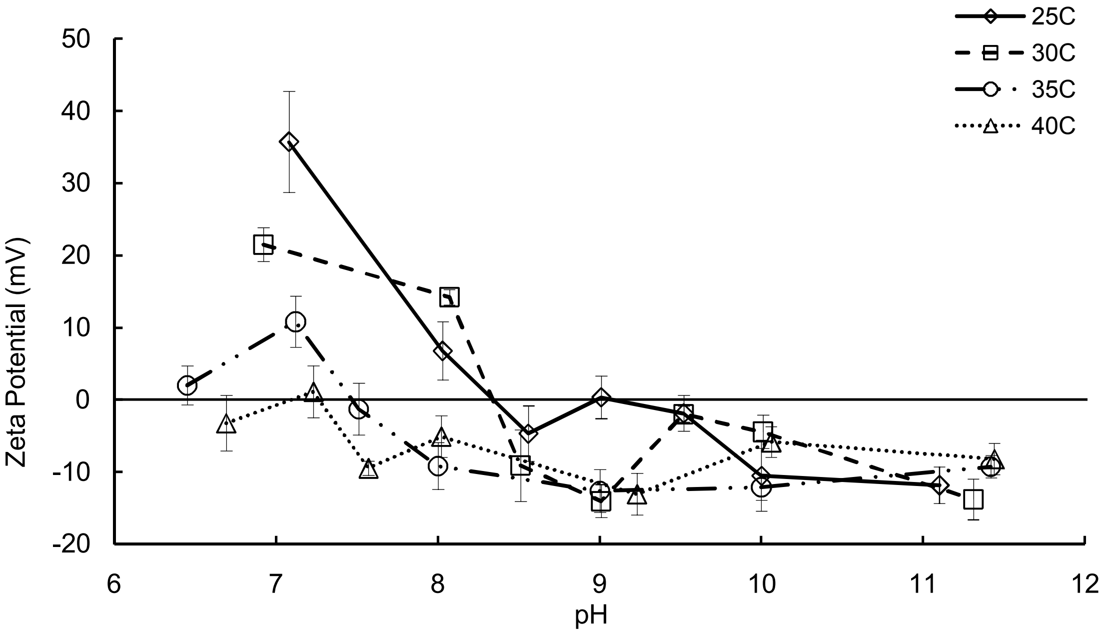

Figure 4.2. Zeta potential vs pH for alumina suspensions with 1mM KNO_3, 0.1M glycine, 0,1wt% H_2O_2, 0.01 wt% BTA, 0.1mM SDS and 0.12mM copper.

4.4 Conclusions

Zeta potentials of alumina particles in solutions with various additives as a function of pH and temperature were measured. For the alumina suspensions with glycine and Cu, and glycine, H_2O_2, and Cu, the IEP was not dependent upon temperature from 25 – 40°C, with values of ~9.1-9.8. The suspension with KNO_3, glycine, H_2O_2, BTA, SDS and Cu did show an effect of temperature, with IEP decreasing from 9.1 to 7.2 as temperature increased.

Future work will be performed to investigate the effect of specific ions present in solution on the zeta potential, specifically to determine which ions are potential determining ions. Titrations of alumina suspensions with a base in various concentrations of KNO_3 can be performed to calculate the surface charge densities at various pHs, and ultimately determine the PZC of alumina [4]. Additional zeta potential and IEP measurements with varying concentration of electrolytes will also be made.

Acknowledgements

This work was supported by University of California, Berkeley IMPACT program for its support along with the partner companies: Applied Materials, AMSL, Ebara Technologies, Global Foundries, IBM, Intel Corporation, KLA-Tencor, Marvell, Mentor Graphics, Novellus Systems, Panoramic Tech, SanDisk, Synopsys, Tokyo Electron Limited, and Xilinx Inc, along with matching support by the UC Discovery Grant ele07-10283.

This chapter, in full, is a reprint of the material as it appears in the Proceedings of the International Conference of Planarization/CMP Technology, Neil Brahma and Jan B. Talbot, (2010). The dissertation author was the primary investigator and author of this material.

References

1. R. Ihnfeldt and J.B. Talbot, *J. Electrochem. Soc.*, **153,** G948 (2006).
2. R. Ihnfeldt and J.B. Talbot, *J. Electrochem. Soc.*, **155**, H582-H588 (2008).
3. N. Brahma, M.C. Chan, and J. B. Talbot, *ECS Trans.,* **19(7),** 25 (2009).
4. R. J. Hunter, "Zeta Potential in Colloid Science," Academic Press, London (1981).
5. N. H. Kim, Y. J. Seo, and W. S. Lee, *Microelectronic Engineering*, **83**, 362-370 (2006).
6. S. Mudhivarthi, P. B. Zantye, A. Kumar, A. Kumar, M. Beerbom, and R. Schalf, *Electrochemical and Solid State Letters*, 8, G241-G245 (2005).
7. R. J. Hunter, "Foundations of Colloid Science," Oxford University Press Inc., New York (2001).
8. T. Dederichs, M. Möller, and O. Weichold, *Langmuir*, **25**(18), 10501-10506 (2009).
9. C. Chen, D. Tano, and M. Akashi, *J. Colloid and Interface Sciences,* **225**, 349-358 (2000).
10. R. Pamies, K. Zhu, S. Volden, A. L. Kjøniksen, G. Karlsson, W. R. Glomm, and B. Nyström, *J. Phys. Chem. C,* **214**, 21960-21968 (2010).
11. M. Wiśniewska, *J. Am. Ceram. Soc.,* **90**(11), 3608-3614 (2007).
12. S. Vidojkovic, V. Rodriguez-Santiago, M. V. Fedkin, D. J. Wesolowski, and S. N. Lvov, *Chemical Engineering Science,* **66**, 4029-4035 (2011).
13. Y. Liu, X. Han, L. He, Y. Yin, *Angew. Chem. Int. Ed.,* **51**, 6373-6377 (2012).
14. P. Jayaweera, S. Hettiarachchim, and H. Ocken, *Colloids and Surfaces* A, **85**, 19-27 (1994).

15. P. H. Tewari and A. W. McLean*,* *J. Colloid and Interface Sciences*, **40**, 267-272 (1972).

CHAPTER 5

EFFECTS OF CMP SLURRY ADDITIVES ON THE AGGLOMRATION OF ALUMINA NANOPARTICLES: AGGREGATION RATE ANALYSIS

5.1 Introduction

Chemical mechanical planarization (CMP) uses a slurry containing a number of additives to passivate and chemically remove material, as well as nanometer sized particles to mechanically remove material. The slurry is dispensed onto the substrate to be polished while a rotating pad applies pressure and transports the slurry across the substrate. CMP performance can be characterized by material removal rate (MRR), post-polishing roughness, and number of defects per wafer, which all are affected by particle size [1, 2].

The agglomeration of 150 nm alumina particles was investigated by measuring the effective particle size and zeta potential in suspensions with various common additives used in copper CMP and is reported in chapter 3. In general, three types of behavior were observed and it was found that pH had a dominant effect on aggregation behavior. However, little is known about the rate of aggregation of CMP slurries. In a typical CMP process, the slurry has a residence time of up to 10 minutes and it has been shown that the shear forces present during the process are not sufficient to break up aggregates [3].

This investigation studied the effects of common CMP slurry additives on agglomeration rate. Fractal dimension analysis was conducted for aggregation occurring via diffusion limited aggregation (DLA). Details of the analysis are presented in Chapter 2. For DLA, the d_f number can also imply whether particle-cluster or cluster-cluster aggregation is occurring. Particle-cluster aggregation can occur during DLA, forming denser aggregates with large d_f numbers (>2). Aggregates formed by cluster-cluster aggregation are typically characterized by d_f numbers < 2 [6].

During reaction-limited aggregation (RLA), an energy barrier prevents particles from aggregating completely [6]. To quantify the effects of the energy barrier on particle aggregation, the stability ratio W is used, which is the ratio of the number of collisions between particles to the number of collisions that result in aggregation [10]. The stability ratio can be determined by an analysis of the rate of doublet formation [11]. By this method, W is calculated as:

$$W = \frac{K_B}{K_{1,1}} \tag{5.1}$$

where K_B is the rate of doublet formation when aggregation is limited by diffusion only (DLA), and $K_{1,1}$ is the rate of doublet formation in the suspension being measured [11]. According to Smoluchowski's theory, K_B can be calculated independently of particle type or size as:

$$K_B = \frac{8k_bT}{3\eta} \tag{5.2}$$

where k_b is the Boltzmann constant, T is temperature and η is the solvent viscosity [20]. $K_{1,1}$, the rate of primary particle aggregation, is given as:

$$\tfrac{dN_1}{dt} = -K_{1,1}N_1^2 \tag{5.3}$$

where N_1 is the number of primary particles. After differentiation, equation 5.3 becomes:

$$N_1(t) = \frac{N_0}{1 + N_0K_{1,1}t} \tag{5.4}$$

where N_0 is the initial number of primary particles. Equation 5.4 can be rewritten as

$$\frac{x}{1-x} = N_0K_{1,1}t \tag{5.5}$$

where x is the conversion of primary particles to doublets:

$$x = \frac{N_0 - N_1}{N_0} \tag{5.6}$$

To estimate x from measurements of the particle size, the measured hydrodynamic radius, R_h, is fit to equation 5.7:

$$< R_h >= \frac{N_1S_1(q) + 4N_2S_2(q)}{N_1S_1(q)R_{h,1}^{-1} + 4N_2S_2(q)R_{h,2}^{-1}} \tag{5.7}$$

where N_2 is the number of doublets. N_1 and N_2 can be expressed as a function of conversion: $N_1 = N_0(1-x)$ and $N_2 = N_0x/2$. $S_1(q)$ and $S_2(q)$ are the structure factors for the primary particles and doublets, respectively. For this analysis $S_1(q) =1$ and $S_2(q)$ is given as:

$$S_2(q) = \tfrac{1}{2}\left(1 + \frac{\sin(2qR_p)}{2qR_p}\right) \tag{5.8}$$

where R_p is the primary particle radius (75 nm) and q is the magnitude of the scattered wave vector given by:

$$q = \tfrac{4\pi n}{\lambda}\sin(\tfrac{\theta}{2}) \qquad [5.9]$$

where n is the index of refraction of the solvent (in this case water), λ is the wavelength of the light, and θ is the scattering angle (90°). After fitting the measured hydrodynamic radius (mean aggregate size as measured by DLS) to that determined by equation 5.7, the conversion can be estimated, followed by the rate of doublet formation from equation 5.5 and finally the stability ratio from equation 5.1 [11]. Values of W can range from 1 to 10^{10}, and can vary by an order of magnitude for suspensions of the same particles with slightly differing electrolyte concentrations [11]. In general, slow agglomeration is observed for $W < 10^4$ [12]. W values ranging from 10^6 to 10^9 are required for a stable suspension [13]. Wiese and Healy studied the behavior of Al_2O_3 and TiO_2 sols, calculating values of W as a function of zeta potential [14]. In their investigations of the fairly unstable sols (W ranging from 1 to 20), they calculated a minimum W (~1) at the IEP of the sols, where the sol aggregates rapidly [14]. However, work by Ottewill and Watanabe in which aggregation of silver iodide sols was induced by cationic surfactants, showed that a minimum of W, and consequently the maximum level of aggregation, can be affected by the surfactants, due to steric and other effects, and may not occur at the IEP [15].

In chapter 3, the effects of pH and chemical additives on aggregate size and zeta potential of 150 nm alumina particles are reported. The additives tested were 0.01 wt% benzotriazole (BTA), 0.1 mM sodium dodecyl sulfate (SDS), 0.1 wt% hydrogen peroxide (H_2O_2), and 0.1 M glycine in a 1 mM potassium nitrate solution used to maintain a constant ionic strength of ~1 mM. The concentrations of these additives were used in our group's previous work on copper CMP [16]. The addition of 0.12 mM copper as nanoparticles to the suspensions was also studied to simulate the copper CMP process. In general, three aggregation behaviors were observed. First, reversible aggregation was observed, where particles aggregated almost instantaneously to mean aggregate sizes > 2.5 μm without further aggregation. A second behavior observed consisted of particles aggregating to mean sizes of ~1 μm almost immediately and then steadily aggregating further over the 10 minute period. The third behavior was steady aggregation from the initial particle size of 150 nm to agglomerates > 1 μm. A detailed discussion of the effects of pH and additives is given in chapter 3.

The purpose of this research was to measure the aggregation rates and to investigate the aggregation mechanisms. Prior to our studies [20, 21], there were no other known data on aggregation rate of abrasives in CMP type slurries. The pH of the suspensions for this study, while not necessarily optimal for CMP, was chosen where aggregation rate analysis could be performed and the effects of each additive could be observed more clearly.

5.2 Experimental

The experimental procedure is the same as discussed in Chapter 3. The suspensions studies are as listed in Table 5.1. Since during copper CMP material is removed and becomes suspended in the slurry, suspensions were tested both with and without copper nanoparticles [16]. The pH was adjusted to ~8 using KOH or HNO_3, measured by an Orion model SA 720 pH meter to ±0.1 pH [17]. The pH of slurries without glycine was difficult to control precisely, which has been observed previously [18]. Particle size measurements were taken every 1 minute for a total of 120 minutes. Although the typical residence time for slurry during the CMP process is less than 10 minutes, a longer total measurement time was used to aid in analysis of the aggregation data [15]. The upper limit for accurate particle size measurement was 3 µm.

In this study, agglomerate sizes of alumina in suspensions with various additives were measured over time for specific conditions listed in Table 5.1 in which the agglomerates were continuously becoming larger. Once aggregates became significantly large, settling occurred and only the size data before settling were analyzed. Not all suspensions detailed in chapter 3 were analyzed; only suspensions that displayed steady aggregation (A, C, E, F, and G) were analyzed.

Table 5.1. Calculated fractal dimension numbers (df) and stability ratios (W) for alumina particles in 1mM KNO3 suspensions with various additives. Initial particle diameter and time to reach 1000 nm is also shown.

	Solution*	pH	Isoelectric Point	Initial Particle Diameter (nm)	Time to reach 1000 nm (min)	d_f	Stability Ratio W
A	0.1M Glycine	8.1	9.9 ± 0.1	233	5.1	1.7 ± 0.1	NA
	0.1M Glycine, 0.12mM Cu	8.2	9.7 ± 0.1	336	22.5	NA	NA
C	0.01wt% BTA	8.4	10.3 ± 0.3	246	125	NA	21.3 ± 3.7
	0.01wt% BTA, 0.12mM Cu	8.8	9.9 ± 0.2	175	36.3	NA	4.2 ± 1.7
E	0.1M Glycine, 0.1wt% H_2O_2	8.0	9.6 ± 0.2	208	17.7	NA	NA
	0.1M Glycine, 0.1wt% H_2O_2, 0.12mM Cu	8.0	9.9 ± 0.3	253	41.4	NA	5.7 ± 1.1
F	0.1M Glycine, 0.01wt% BTA	8.2	9.7 ± 0.2	259	11.4	1.2 ± 0.1	NA
	0.1M Glycine, 0.01wt% BTA, 0.12mM Cu	8.1	9.6 ± 0.2	194	44.7	NA	3.6 ± 1.6
G	0.1M Glycine, 0.1mM SDS	8.1	8.3 ± 0.1	146	65.0	NA	7.1 ± 1.8
	0.1M Glycine, 0.1mM SDS, 0.12mM Cu	8.1	8.4 ± 0.2	179	15.2	1.0 ± 0.1	NA
H	0.1M Glycine, 0.1wt% H_2O_2, 0,01wt% BTA, 0.1mM SDS	7.4	9.7 ± 0.4	251	24.8	1.0 ± 0.1	NA
	0.1M Glycine, 0.1wt% H_2O_2, 0,01wt% BTA, 0.1mM SDS, 0.12mM Cu	7.2	9.0 ± 0.2	255	30.3	0.9 ± 0.1	NA

*** Solution labels corresponds those to Chapter 3**

5.3 Results and Discussion

Figures 5.1-5.6 show aggregate sizes versus time for the suspensions listed in Table 5.1. The aggregation behavior observed was similar for nearly all suspensions. Initial aggregation was slow, but the rate increased as the aggregates grew larger in size. With the addition of copper, some suspensions (A, E, and F in Fig. 5.1, 5.3, and 5.4 respectively) exhibited faster aggregation with 0.12mM copper than without, while others (C and G in Fig. 5.2 and 5.5 respectively) exhibited slower aggregation with copper. For suspension H, negligible difference in aggregation was observed when copper was added.

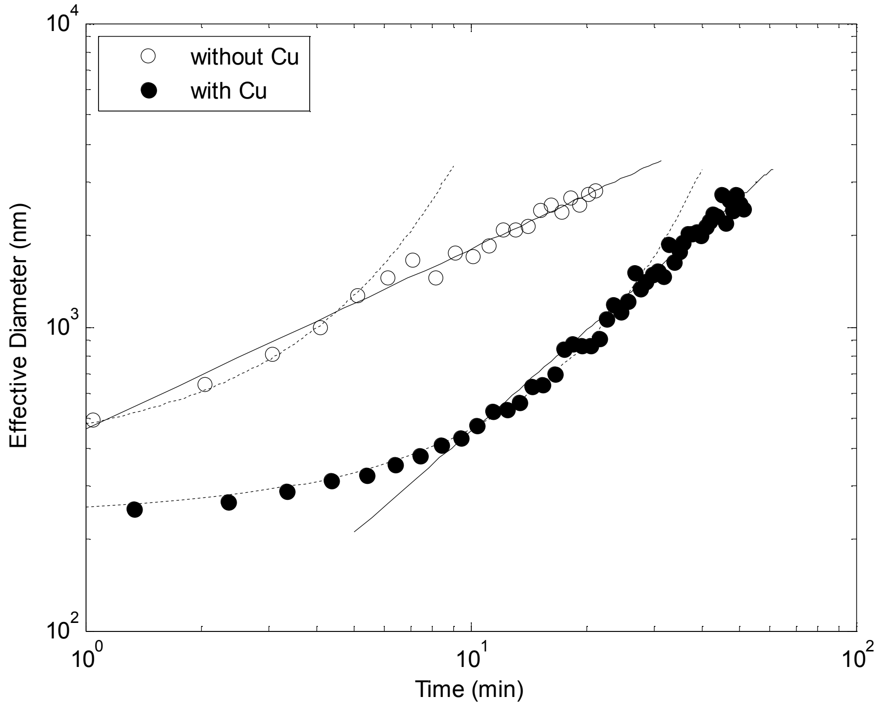

Figure 5.1. Aggregate size versus time for alumina particles in suspension A without and with 0.12mM copper at pH 8.1 and 8.2, respectively. Solid lines are power law fit and dotted lines are exponential fit.

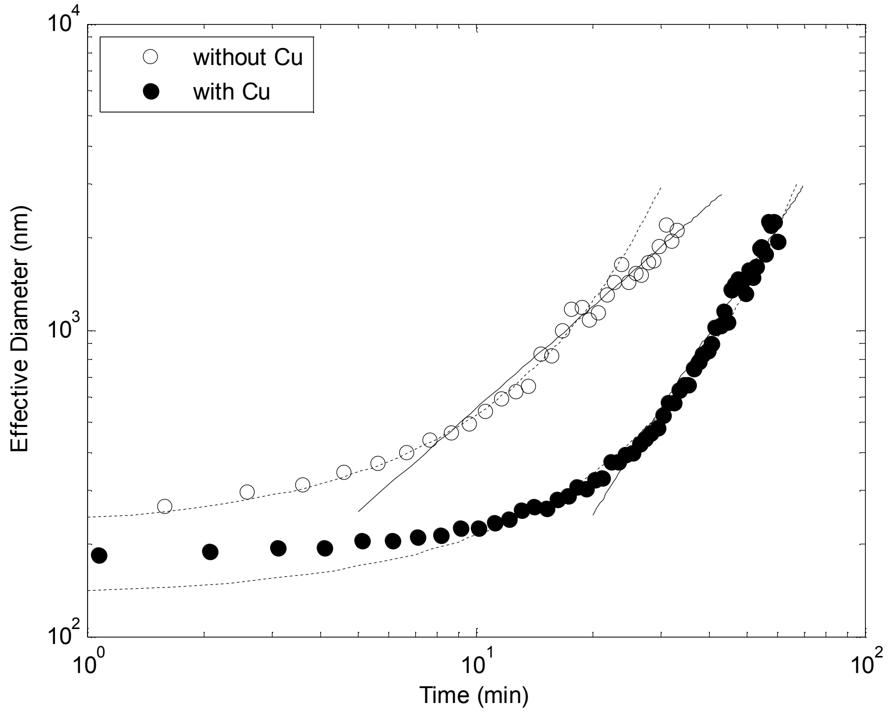

Figure 5.2. Aggregate size versus time for alumina particles in suspension E without and with 0.12mM copper at pH 8.0. Solid lines are power law fit and dotted lines are exponential fit.

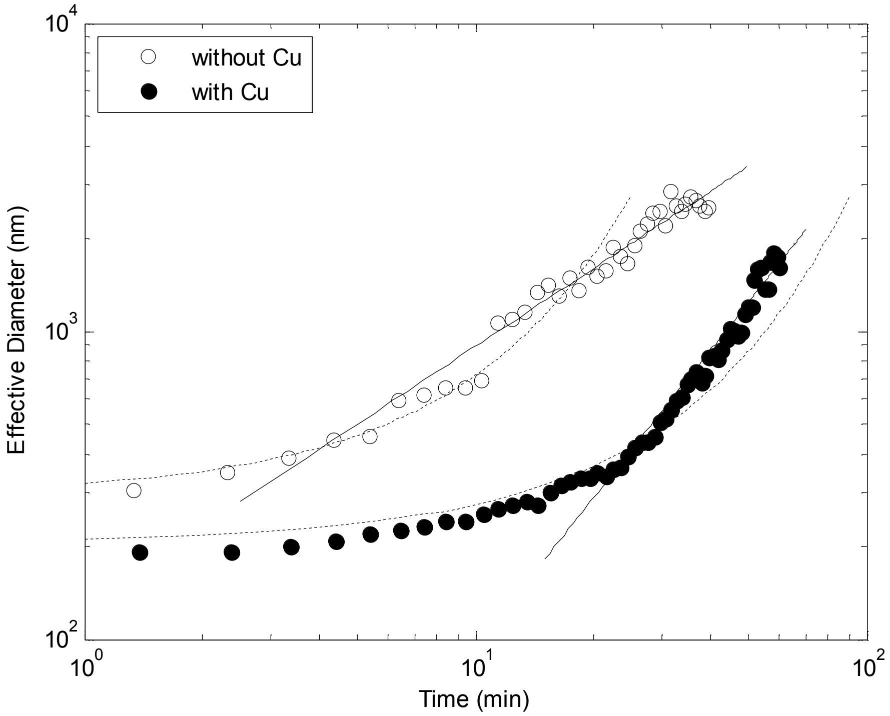

Figure 5.3. Aggregate size over time for alumina particles in suspension F without and with 0.12mM copper at pH 8.2 and 8.2 respectively. Solid lines are power law fit and dotted lines are exponential fit

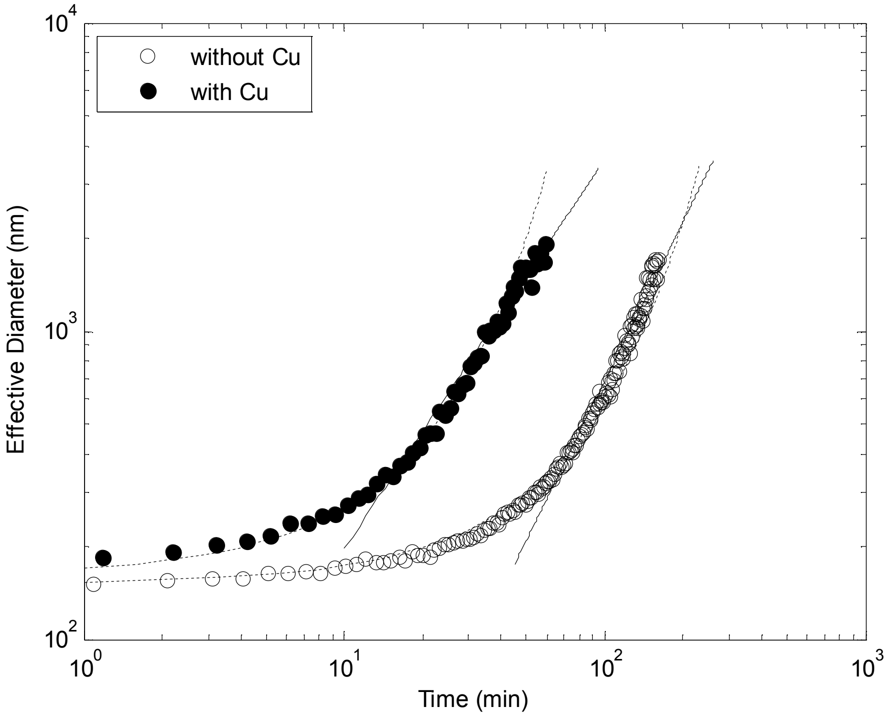

Figure 5.4. Aggregate size versus time for alumina particles in suspension C without and with 0.12mM copper at pH 8.4 and 8.8 respectively. Solid lines are power law fit and dotted lines are exponential fit.

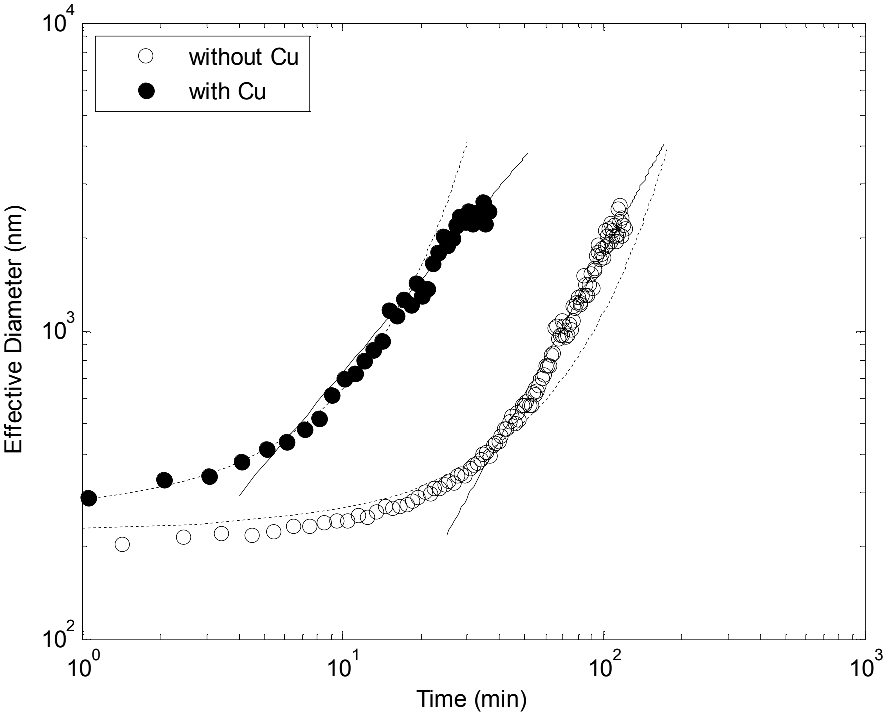

Figure 5.5. Aggregate size versus time for alumina particles in suspension G without and with 0.12mM copper at pH 8.1. Solid lines are power law fit and dotted lines are exponential fit.

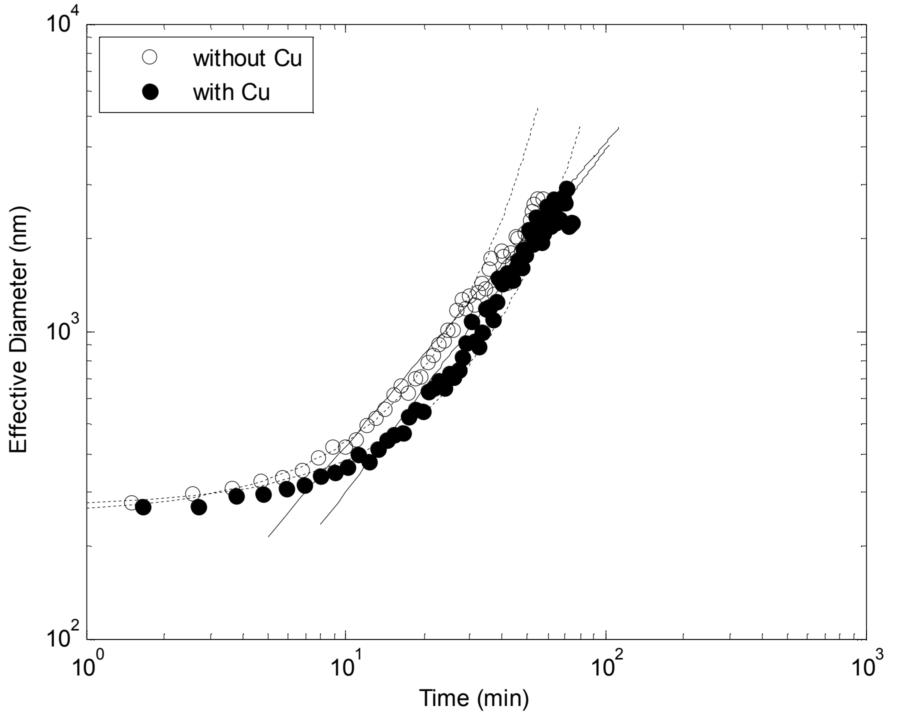

Figure 5.6. Aggregate size versus time for alumina particles in suspension H without and with 0.12mM copper at pH 7.4 and 7.2 respectively. Solid lines are power law fit and dotted lines are exponential fit.

Suspension A without copper aggregated most quickly of all the suspensions investigated, with an initial particle size of 336 nm and reaching an effective diameter of 1000 nm in 5.1 min. Without copper, particles in suspension A aggregated significantly slower, reaching a diameter of 1000 nm in 22.5 min and had an initial aggregate size of 233 nm. Also of note is that the shape of the plot for suspension A without copper is very much a power law, whereas the shape of suspension A with copper is exponential.

Suspension C with copper aggregates identically to suspension A without copper with an initial aggregate size of 246 nm and reaching an effective diameter of 1000 nm in 125 min. With copper, however, aggregation was faster with an initial aggregate size of 175 nm and reaching an effective diameter of 1000 nm in 36.3 min. The shapes of the plots are exponential, similar to suspension A with copper.

Suspension E without copper aggregated from an initial aggregate size of 208 nm and reaching an effective diameter of 1000 nm in 17.7 min. After the addition of copper, the initial aggregate size was 253 nm and the suspension reached an effective diameter of 1000 nm in 41.4 min. The shapes of both plots are also exponential.

Particles in suspension F without copper aggregated to a diameter size of 1000 nm in 11.4 min and had an initial aggregate size of 259 nm. The shape of the plot, however, is a power law, similar to suspension A without copper. Particles in suspension F with copper aggregated to a diameter size of 1000 nm in 44.7 min, had an initial aggregate size of 194 nm, and displayed an exponential shape.

Suspension G with copper also displayed an exponential shape in the plot. The particles in the suspension aggregated to 1000 nm in 15.2 min and had an initial aggregate size of 179 nm. Without copper, aggregation was significantly slower, aggregate diameters reaching 1000 nm in 65 min and had an initial aggregate size of 146 nm. The shape of the plot for suspension G without copper was also exponential. It should be noted that the pH was significantly different (8.4 vs 8.8 for without copper and with copper respectively) due to the instability of the suspensions.

Aggregation behavior of suspension H with and without copper is primarily exponential. Initial aggregate particle diameters of 251 and 255 were measured for H without and with copper respectively, as well as times of 24.8 and 30.3 minutes to aggregate to 1000 nm. Of note for H with and without copper is the similarity in the initial aggregate sizes and times to aggregate to 1000 nm along with the dissimilarity of pH (7.4 vs 7.2 for without and with copper respectively). At pH 7.4, a less stable suspension (aggregate sizes > 1000 nm observed in first measurement) is formed when copper is added, thus the pH where the suspension is stable enough for analysis is significantly lower than without copper.

To further analyze the aggregation data, exponential and power laws were fitted to the data, as shown in Figures 5.1-5.6, and stability ratio and fractal dimensions number were calculated. For the majority of the suspensions, an exponential growth describes the initial aggregation behavior (mean aggregate diameters <500 nm). A RLA mechanism is most likely in this region because the aggregate sizes increase exponentially and stability ratios were determined using equations 5.1 – 5.9. As listed in Table 1, the values of W vary from 3.6 to 21. Stability ratios varying by an order of magnitude is not uncommon [11]. A high stability ratio would indicate that the aggregation is occurring at a notably slower rate than if aggregation was limited by diffusion alone, indicating a high stability. Our calculated values of W > 1 (suspensions C, E with Cu, F with Cu, and G without Cu) indicate that the suspensions aggregate slower than by DLA alone and therefore, an energetic barrier to aggregation is present, although it is likely to be small. Indeed aggregate sizes aggregated at an exponential rate for these suspensions while aggregate sizes were < 500 nm.

Values of W for suspensions A, E without Cu, F without Cu, and G with Cu could not be calculated. As discussed in the background, the basis of the W calculation was by doublet formation but, for the suspensions mentioned above, aggregation proceeds so rapidly that clusters made up of a number of primary particles formed before the first measurement. Therefore it is probable that RLA is not occurring during the initial measurements as it is for the other suspensions, suggesting that DLA is the primary mechanism occurring for these suspensions.

Because it was impossible to keep pH consistent for all suspensions, some of the differences in the stability ratio can be attributed to differences in pH. Suspension A with Cu is more stable than without but it is also at a higher pH (8.2 vs 8.1 respectively). The IEP (listed in Table 5.1) is 9.6 and 9.7 for A with Cu and without Cu respectively. Since A with Cu is closer to the IEP than without Cu, it would be expected that the former would be less stable. However, since this is not the case, the Cu is stabilizing the slurry, although the mechanism is unknown.

Suspension C with Cu had a higher pH than without Cu (8.8 vs 8.4 respectively). The IEP of both suspensions are ~10 and C without Cu is more stable than without Cu (W of 21 and 4.2 respectively). Since C with Cu is at a pH closer to the IEP than without Cu, the decrease in suspension stability is not surprising. Suspensions E with and without Cu had identical pH (8.0) however did not have identical stability ratios (W of 5.7 for with Cu, W for without copper could not be calculated). The IEP for suspensions E were not identical (9.1 vs 9.9 for without Cu and with Cu respectively). Similar to suspension C, the more stable slurry is farther from the IEP than the less stable slurry. Suspensions F with Cu is at a higher pH than without (8.2 vs 8.1 respectively) and both have a measured IEP of 9.8. Therefore, based on pH alone it would be expected that F with Cu would be more unstable than without Cu and, based on calculated W, this is what is observed (W of 3.6 for F with Cu, W of F without Cu could not be calculated).

Suspensions G with and without Cu also had identical pH (8.1) and G with Cu was less stable than without Cu (W of 0.1 vs 7.1 respectively). The IEP for both suspensions also differ (8.0 and 8.4 for without and with Cu respectively). In this case, G without Cu is closer to the IEP than with Cu yet is more stable than when Cu is present. It is possible that Cu is dissolving and the ions are increasing the charge screening effect on the particles, promoting aggregation.

Values of W for suspension H with and without copper could not be calculated. However, due to the apparent exponential nature of the growth in the early measurements, it would reason that these suspensions have an almost insignificant barrier for aggregation and aggregate by DLA. However, the suspension pH of each differs by 0.2 as noted earlier. Since H with copper aggregates similarly to H without copper at a lower pH (7.2 vs. 7.4) it would reason that the presence of copper is destabilizing the slurry at pH 7.4. It can also be seen that the isoelectric point is lower with the presence of copper (9.0 vs 9.7). It is also of note that the pH where steady aggregation was occurring was considerably lower for suspension H than all other suspensions, even though its isoelectric point is comparable to all other suspensions.

Lattuada et al. noted that, for RLA, the aggregation data can be normalized for initial stability differences of each suspension, in our case caused by differing lag time from taking each suspension from sonication and to the DLS instrument for measurement, by using a dimensionless time, τ, defined as follows [11]:

$$\tau = \frac{tK_B N_0}{W} \qquad [5.10]$$

Then, when the effective aggregate diameter is plotted vs τ, the plots collapse to a master curve if the aggregation mechanism is the same [11]. Our data were normalized using equation 5.10 and suspensions with W > 1 were plotted in Fig 5.7. A master curve is observed in Fig 5.7 at dimensionless time < 10, which indicates that these suspensions are aggregating by the same mechanism. The spread in the values seen at high dimensionless time (>10) is typical [11]. The spread can be influenced by the additives present and the pH of the suspension.

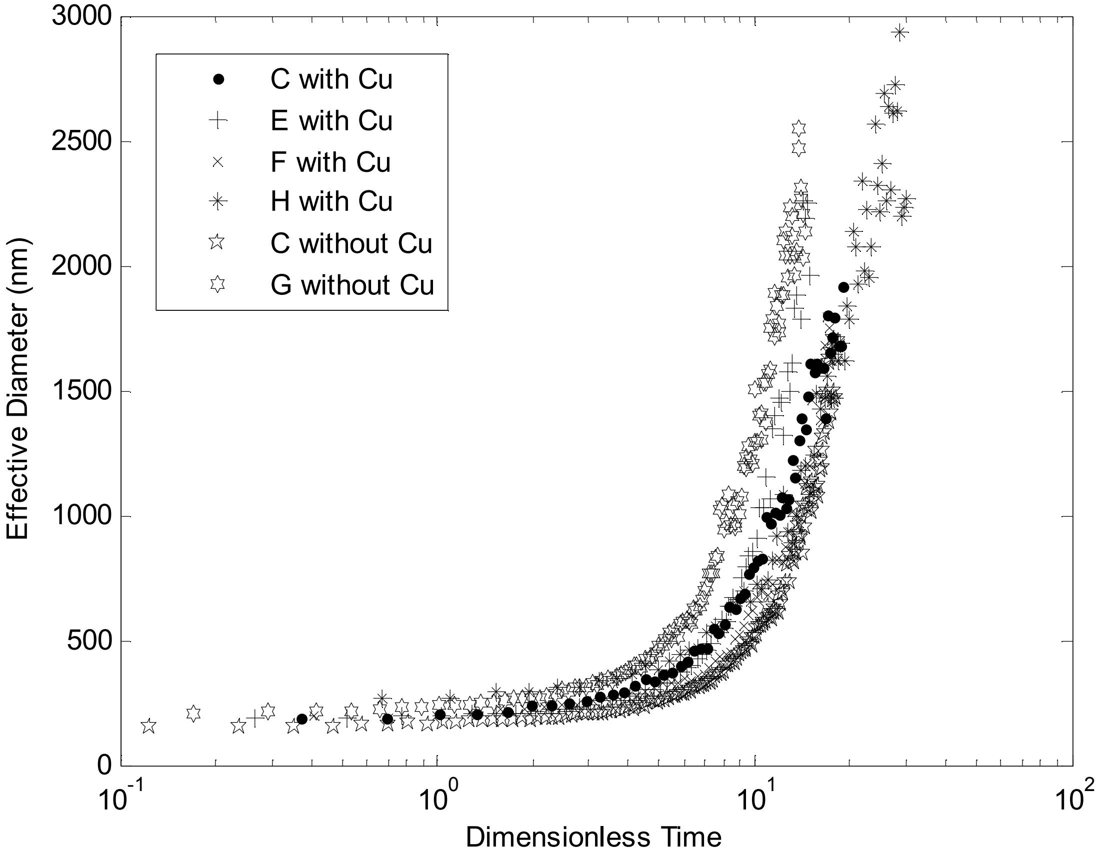

Figure 5.7. Aggregate size versus dimensionless time for suspensions with W >1.

To estimate the fractal dimension, d_f, a power law was fitted to the data shown in Figures 5.1-5.6. As mentioned above, an exponential growth describes the data until aggregate sizes are > 500 nm, after which aggregate sizes grow following a power law, indicating that a DLA mechanism is likely. This type of shift in mechanism has been observed by Hoekstra et al for nickel hydroxycarbonate particles, where a shift from RLA to DLA was noted after aggregate sizes grew to 700 nm [7]. This occurs as diffusion plays an increasing role in the aggregation kinetics as aggregation proceeds. The increased surface area of the cluster increases the probability of two clusters sticking upon collision [7]. For our data, it appears that for all suspensions, once the particles have aggregated to ~500 nm, DLA becomes the dominant mechanism. This suggests that a large population of aggregates is now present in the suspension and cluster-cluster agglomeration is significantly more frequent than cluster-particle agglomeration. Particle size distributions do show that a population of larger aggregates (~1000 nm) do form as aggregation proceeds until 10 min, after which smaller aggregates (<250 nm) are no longer detected. Because all suspensions exhibit the shift in aggregation mechanism at 500 nm, it is likely that this critical size is dependent on the physical properties of the particles and not affected by the chemistry of the suspension. The larger aggregate size of 700 nm observed by Hoekstra et al during crossover compared to 500 nm observed in this study may be due to the larger primary particle used by Hoekstra et al (40 to 100 nm vs 20 nm) [9]. The following estimations of the d_f number would describe only the region after particles have grown >500 nm which typically occurs after ~10 min (exact time varies for each suspension). Exceptions are the suspensions of A and F at pH 8.1 and 8.2

respectively where power law growth is observed immediately, indicating a DLA mechanism.

As listed in Table 5.1, the estimated d_f numbers vary widely from 1 to 1.7. Since all calculated d_f values are < 2, cluster-cluster aggregation is likely the primary mechanism occurring during DLA. For those suspensions that shift from RLA to DLA, adequate d_f numbers could not be calculated (suspensions A with copper, C, E, F with copper, and G without copper). These suspensions are likely very close to the transition point between RLA and DLA and proper calculation of the d_f number cannot be done with the analysis used. The measured isoelectric points (IEP), also listed in Table 5.1, of the different suspensions vary based on the additives as well. Some suspensions exhibit aggregation at pHs up to 2 unit less than the isoelectric point, an indicator that the range of instability for suspensions could be as large as 2 pH units, and possibly larger if the pH greater than the isoelectric point is considered. These results may indicate that pH ~8 is a transition pH where the aggregation mechanism is shifting from DLA to RLA, regardless of the additives present.

5.4 Conclusions

The aggregation rates of suspensions of alumina particles with various CMP additives were measured and analyzed. Exponential growth was observed in the initial regions of aggregate size < 500 nm for suspensions C, E with Cu, F without Cu, and G without Cu and calculated stability ratios ranged from 3.6 to 21, suggesting an RLA mechanism in this region. Calculated d_f values for these suspensions were not applicable (with the exception of A without Cu). A power law growth occurred for mean aggregate diameters > 500 nm, suggesting a shift from RLA to DLA once aggregate sizes exceeded 500 nm. Suspensions A, E without Cu, E with Cu, and G with Cu aggregated following a power law growth from the start of the measurements. Estimated d_f values ranging from 1 to 1.7, indicating a DLA for the entire duration of the measurements. Some suspensions, such as H, did not have an initial aggregate size < 500 nm however the period of aggregation under 500 nm is not sufficient for stability ratio analysis.

These results reinforce that pH control is crucial for optimal slurry development. The slurry pH must allow the chemical additives to react desirably with the substrate surface for optimal polishing. Effects of chemical additives on Cu surface hardness have been measured [20] and have been shown to affect the material removal rates of the slurries [18]. Additionally, as shown in our work, pH control is also required to keep the dispersion of alumina nanoparticles stable and prevent non-uniform polishing and defects.

Acknowledgements

This work was supported by University of California, Berkeley IMPACT program for its support along with the partner companies: Applied Materials, AMSL, Ebara Technologies, Global Foundries, IBM, Intel Corporation, KLA-Tencor, Marvell, Mentor Graphics, Novellus Systems, Panoramic Tech, SanDisk, Synopsys, Tokyo Electron Limited, and Xilinx Inc, along with matching support by the UC Discovery Grant ele07-10283.

This chapter in part is currently being prepared for submission for publication of the material; Neil Brahma and Jan B. Talbot. The dissertation author was the primary investigator and author of this material.

References

1. M. Bielmann, U. Mahajan, and R. K. Singh, *Electrochem. and Solid-State Lett.*, **2**, 401–403 (1999).

2. Y. Tateyama, T. Hirano, T. Ono, N. Miyashita, T. Yoda, *Chemical Mechanical Polishing (IV)*, The Electrochemical Society, Pennington, New Jersey (2001).

3. M. G. Song, J. Lee, Y. G. Lee, and J. Koo, *J. Colloid and Interface Sci.,* 300, 603-611 (2006).

4. M. Elimelech, J. Gregory, X. Jia, R. A. Williams, *Particle Deposition and Aggregation*, Butterworth-Heinemann, Oxford, England (1995).

5. C. Cametti, P. Codastefano, and P. Tartaglia, *Physical Review A*, 36 (10), 4916-4921 (1987).

6. R. J. Hunter, *Fundamentals of Colloid Science.*, Oxford University Press, 2001.

7. L. L. Hoekstra, R. Vreeker, and W. G. M. Agterhof, *J. Colloid Interface Sci.,* 151 (1), 17-25 (1992).

8. H. Holthoff, S. U. Egelhaff, M. Borkovec, P. Schurtenberger, and H. Sticher, *Langmuir.*, 12, 5541-5549 (1996).

9. T. M. Herrington and B. R. Midmore, *Colloids and Surfaces A: Physiochemical and Engineering Aspects,* 70, 199-202 (1993).

10. K. L. Chen and M. Elimelech, *Langmuir*, 22, 10994-11001 (2006).

11. M. Lattuada, P. Sandkühler, H. Wu, J. Sefcik, and M. Morbidelli, *Adv. Colloid Interface Sci.*, 103, 33-56 (2003).

12. P. C. Hiemenz, “Principles of Colloid and Surface Chemistry, ” Marcel Dekker, Inc., New York, NY (1977).

13. R. J. Hunter, “Zeta Potential in Colloid Science,” Academic Press, London (1981).

14. G. R. Wiese and T. W. Healy, *J. Colloid and Interface Sci.,* **51** (3), 427-433 (1975).

15. R. H. Ottewill and M. C. Rastogi, *Trans. Faraday Soc.,* **56**, 880-892 (1960).

16. R. Ihnfeldt and J. B. Talbot, *J. Electrochem. Soc.,* **155**, H412-H420 (2008).

17. F. J. Ansuini, J. R. Dimond, *Materials Performance,* **33** (11), 14-17 (1994).

18. R. Ihnfeldt and J. B Talbot, *J. Electrochem Soc.,* **154** (23), H1018-H1026 (2007).

19. R. Ihnfeldt and J. B Talbot, *J. Electrochem Soc.,* **155** (8), H582-H588 (2008).

20. N. Brahma, M.C. Chan, and J. B. Talbot, *ECS Trans.,* **19**(7), 25 (2009).

21. N. Brahma and J.B. Talbot*, ECS Trans.,* **33** (10), 53 (2010).

22. W. Brown and J. Zhao, *Macromolecules*, **26**, 2711-2715 (1993).

CHAPTER 6

SCANNING ELECTRON MICRSCOPY OF ALUMINA PARTICLES AND AGGREGATES

6.1 Introduction

Scanning electron microscopy (SEM) is an effective tool for the imaging of nanometer size particles and features. Electrons produced from a source (typically a thermionic emitter, although field electron emissions sources can be used) are focused through a series of lenses until a focused beam is achieved. The beam then scans over the sample and a portion of the electrical current leaving the sample is collected by the detector. Deflections of the electron beam occur as the beam passes through saw-tooth generators allowing the beam to scan across the sample and produce a raster of the surface [1]. Although transmission electron microscopy (TEM) had been developed before SEM and was shown to achieve higher resolutions, the ability of SEM to produce three dimensional images, revealing finer structures of a sample has proven to be invaluable [1].

SEM is a proven technology that is used in applications from microelectronics development to biological tissue analysis. The technique is also a common characterization method for nanoparticles, and as such numerous examples of imaged nanoparticles exist and will not be discussed in this chapter however extensive reviews of the technology are presented by Oatley et al.[1] and by Goldstein et al. [2].

A characteristic requirement for SEM is a high vacuum environment (10^{-6} torr) in the electron gun and sample chamber to ensure that excess scattering of electrons by the gaseous molecules does not occur [3]. Because of the high vacuum environment, adequate preparation of samples is needed such as drying and, especially in the case of insulating materials, coating with metal. Such preparation may alter the state of the sample, giving images that are not representative of the actual material being analyzed.

Development of a low vacuum SEM began as early as 1953 [3] with experimentation with differentially pumped, aperture-limited transmission electron microscopes (TEM) and with thin-film windows separating the electron source and sample chamber [3]. The first high-pressure SEM was developed from research in the 1970s and the first commercial environmental SEM (ESEM), as it came to be known, was available by the late 1980s [3].

To separate the electron gun from the sample chamber, a differential pumping scheme with small apertures separating regions of differing pressure is typically employed. When using a tungsten filament electron source, a two-stage differential pumping scheme is required [4]. Gas leaking into the electron source is pumped out while simultaneously being replenished in the sample chamber from an outside source via a control leak valve [4]. An electron transparent film can be used instead to separate the electron source and specimen chamber instead of differential pumping, however these films absorb and spread the electron beam very quickly in the low kV range [4].

As mentioned, the ability to backfill gas into the specimen chamber is the most unique feature of the ESEM and can allow for pressures from 0.1 to 10 torr within the chamber [3]. Because of the presence of gas, modified secondary-electron detectors (with positive potentials of at 300-500 V) are used (instead of the typical 10-12 kV Everhart-Thornley detectors used in conventional SEM) [3]. Low energy electrons are accelerated to the detector by the electric field present between the sample and the detector and can produce ionizing collisions with the gaseous molecules in the chamber. The additional secondary electrons generated in the collisions effectively amplify the signal and can also cause additional ionizing collisions, producing a cascading effect (gaseous amplification). Positive ion by products from the collisions can drift towards the specimen to compensate for negative charge buildup in insulating samples, thereby allowing for imaging of insulating samples without a metal coating [3]. The specimen chamber can be filled with a variety of gases (nitrous oxide, carbon dioxide, etc), however water vapor is most commonly used as it is the most efficient at gaseous amplification [3].

To prevent evaporation of water in hydrated samples in the low vacuum environment, samples must be cooled (achieved by a Peltier controlled cooling stage) to within a few degrees C. Typical operating temperatures for aqueous samples is 2 to 6^{o}C [3]. It is possible to operate at pressures below the equilibrium pressure (determined by the saturated vapor pressure at a given temperature) as samples can withstand dehydrating conditions for some time (minutes to hours) before drying out [3].

In this chapter, SEM images of alumina nanoparticle aggregates formed in suspensions of a variety of chemical compositions are presented. The purpose of this was to determine if aggregates formed by diffusion-limited (DLA) or reaction-limited (RLA) aggregation do have significant differences in structure.

The aggregation mechanism can have a significant effect on the aggregate structure, affecting its physical properties such as hardness and rigidity. The mechanism of aggregation has been observed to affect MRR by Basim and Moudgil. In their study, MRR of SiO_2 (2µm layer deposited on a silicon wafer) with 200nm sized silica particles from a dry powerd aggregated to 5-10µm by various methods. The methods included controlling ultrasonication during dispersion to allow for “dry” aggregates to remain in the slurry; flocculation induced by polyethylene oxide polymer; and aggregation caused by increasing salt concentration of the slurry with NaCl [5]. Significant differences in MRR were observed based on the aggregate used. They concluded that the increased MRR and surface roughness by the dry aggregates compared to the polymer flocculated aggregates was due to the increased rigidity of the dry aggregates [5]. Differences in MRR by the salt-induced aggregates was attributed to greater pad-particle-substrate interaction caused by charge screening by the ions from the dissolved salt [5].

The following investigation consisted of first experimenting with sample preparation techniques. After determining the most appropriate method, images of aggregates formed by RLA and DLA were collected and compared. Methods of imaging the aggregates while still wet were also explored.

6.2 Experimental

Suspensions of alumina particles were prepared by the procedure described in Chapter 3. For most cases, suspensions were left to sit for 10 minutes (the approximate residence time of a CMP slurry in the process) after sonication to allow for aggregates to form. For some experiments, where the aggregate structures formed by DLA and RLA were being imaged, suspensions were allowed to aggregate for longer times (up to 5 hours) to allow for large aggregates (> 1μm) to form in the cases of slow aggregation.

For initial imaging experiments alumina aggregates were loaded onto SiO_2 wafers by drop casting. However, because both the particles and substrate were insulating, metal coating was required to achieve submicron resolution. This was achieved by sputtering a small coating (~10 nm, Cr or Ir depending on availability). Alternatively, alumina aggregates were loaded onto ~1 cm^2 copper coated silicon wafer pieces. These substrates consisted of a 1000 nm sputter-deposited copper layer coated on a 30 nm tantalum layer on top of a silicon wafer. All images presented in this chapter are of alumina aggregates deposited on copper-coated substrates.

Imaging was done with a FEI XL30 SEM with a FEI Sirion column. This microscope has an ultra- high resolution (UHR) mode and a through lens detector allowing for resolutions up to 1 nm at 10 kV. SEM images of wet surfaces were collected on a Phillips XL30 ESEM with a field emission electron source and an electron transparent membrane separating the specimen chamber from the electron source column.

6.3 Results and Discussion

First, the method for applying the particles to the wafer substrates for SEM imaging was investigated. The first method was simple drop casting, a common method for applying particles to a substrate. This involved using a transfer pipette to put a single drop onto the wafer substrate and imaging the sample after drying. In a second method, samples were prepared by dipping the wafer piece into the suspension immediately after sonication for ~1 s followed by rinsing with water.

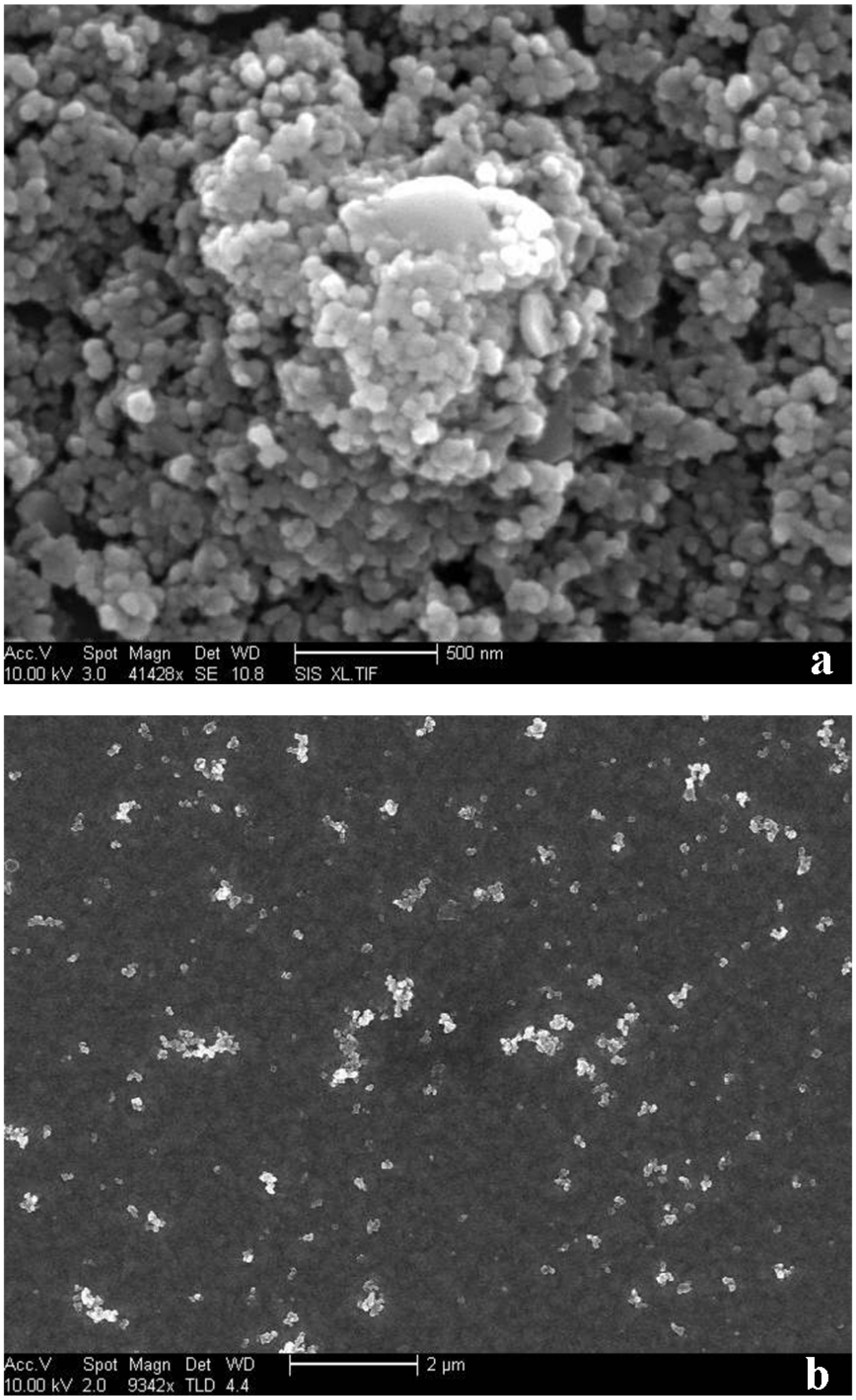

Figure 6.1. SEM images of alumina nanoparticle aggregates formed after being dispersed in water. Samples from the same suspension were prepared in separate methods: drop casting (a) and dip and rinse (b).

Figures 6.1 show SEM images of alumina nanoparticles on copper-coated silicon wafer pieces prepared from a suspension of 0.05 wt% alumina in deionized water with no additives. As can be seen in Figure 6.1a, samples prepared by drop casting were unsuitable for imaging of individual aggregates. Large area films of the primary alumina nanoparticles (~20 nm) were observed for these samples. As shown in Figure 6.1b, individual aggregates were imaged when samples were prepared by dipping of the wafer piece into the suspension followed by rinsing with DI water. It appeared that during drop casting, excess water on the copper surface caused oxidation of the copper, producing CuO particles. To prevent excess oxidation, a kimwipe was placed in contact with the water droplet to absorb excess water via capillary action after dipping and rinsing. Alumina particles on the copper surface were then imaged.

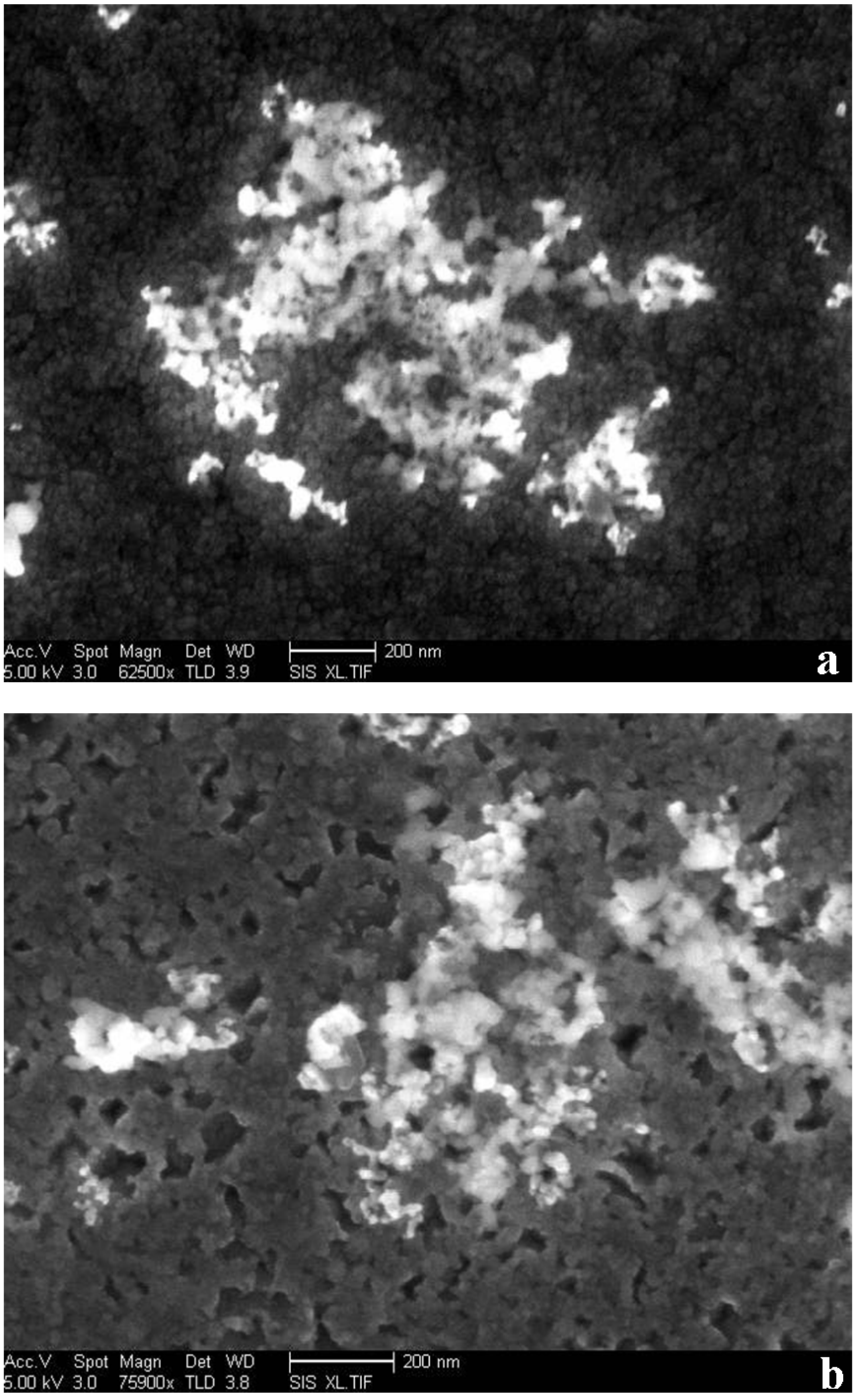

Figure 6.2. SEM images of alumina nanoparticle aggregates formed in suspensions with 1mM KNO_3, 0.1M glycine, and 0.12mM Cu at pH 8.0(a) and 8.4(b).

Images of alumina aggregates formed with significantly different aggregation rates are shown in Figures 6.2-6.4. Figures 6.5 and 6.6 show the aggregate sizes vs time for the suspensions from which the particles were imaged. Note that these aggregation rate data is not that which was presented in Chapter 5 as these suspensions were specifically prepared for the SEM imaging experiments. Figure 6.2 shows aggregates formed in suspensions of 1mM KNO_3, 0.1M glycine, and 0.12mM Cu at pH 8.0 and 8.4. As can be seen in Figure 6.5, aggregate sizes for the suspension at pH 8.4 are measured to be as large as 1μm almost immediately and aggregate to sizes > 3μm within 4 minutes. At pH 8.0, alumina aggregates reach sizes of ~1μm within 6 minutes and did not exceed 3μm until after 25 minutes. The aggregate size growth follows a power law and a fractal dimension of 1.5 was calculated, suggesting cluster-cluster aggregation following a diffusion-limited aggregation [6]. Particle size distributions measured at various stages of aggregation are primarily unimodal for both suspensions (bimodal distributions were observed at certain times for both, however both peaks were consistently > 3μm). The lack of any small aggregates in the late stage of aggregation would imply that cluster-cluster aggregation is occurring in both suspensions.

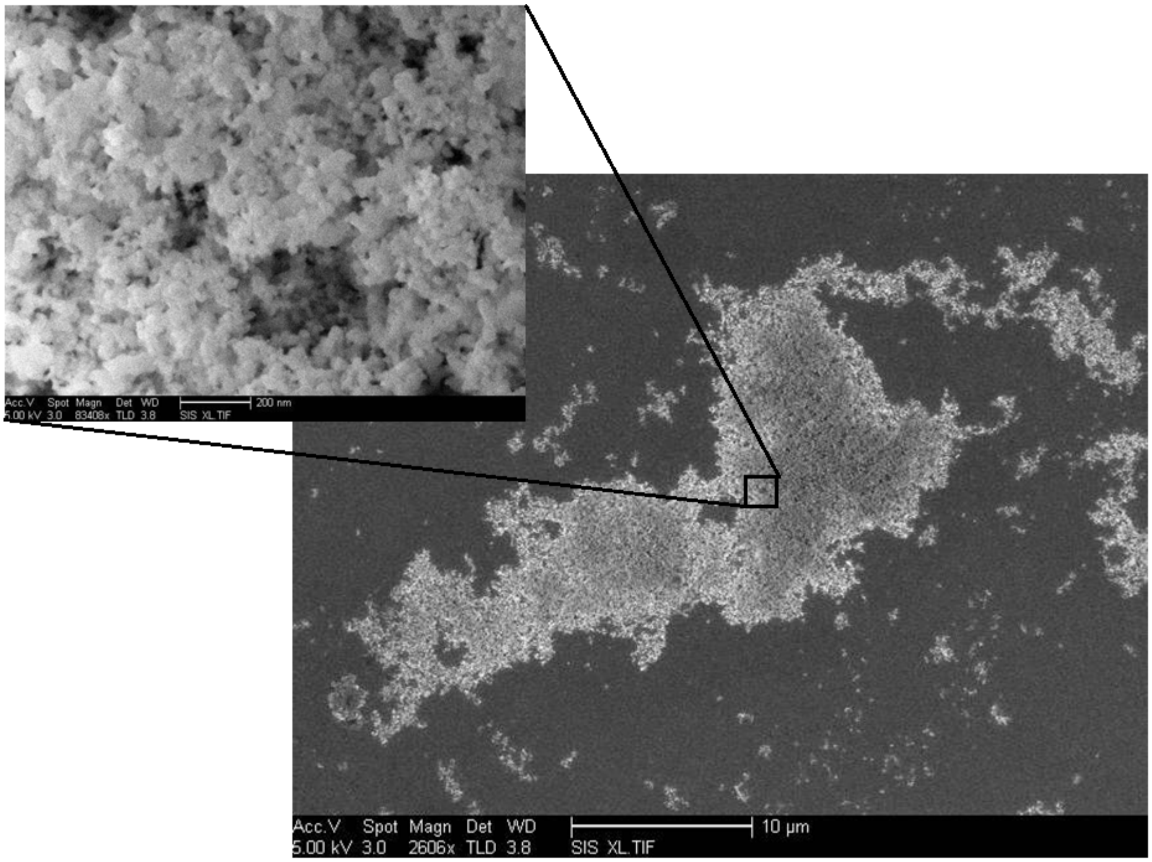

Figure 6.3. SEM images of a large alumina aggregate formed in a suspension of 1mM KNO_3 with 0.01wt% BTA at pH 8.4.

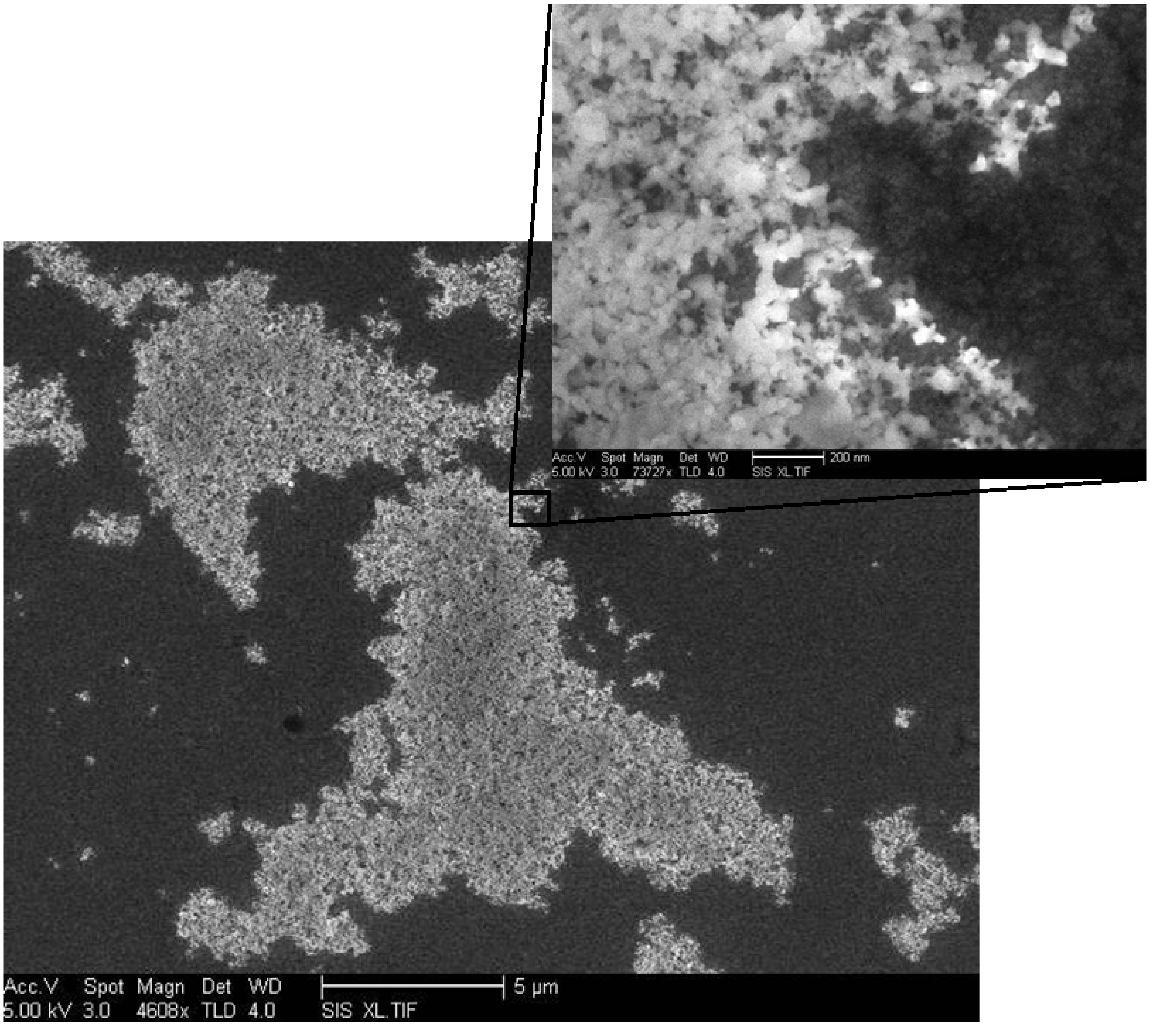

Figure 6.4. SEM images of a large alumina aggregate formed in a suspension of 1mM KNO_3 and 0.01wt% BTA at pH 8.8.

Comparisons of SEM images do not reveal any major differences. Aggregates formed in suspension at pH 8.0 and 8.4 both exhibit large aggregates, some exceeding 3µm. Figure 6.2 shows small aggregates formed in both suspensions and differences between the two structures are not apparent.

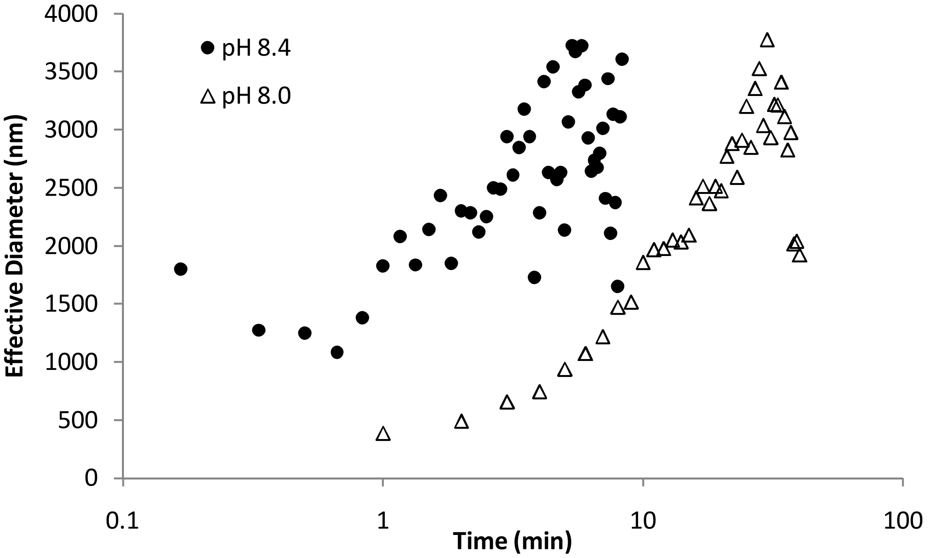

Figure 6.5. Mean particle diameter vs time for alumina aggregates suspended with 1mM KNO_3, 0.1M glycine, and 0.12mM Cu at pH 8.0 and 8.4.

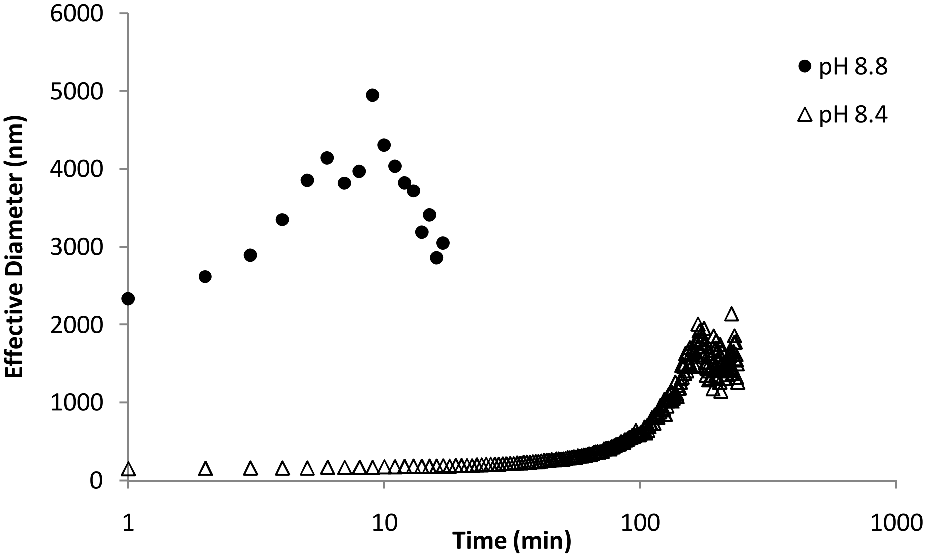

Figure 6.6. Mean particle diameter vs time for alumina aggregates suspended with 1mM KNO_3 and 0.01wt% BTA at pH 8.4 and 8.8.

A second slurry system investigated consisted of alumina dispersed in 1mM KNO_3 with 0.01 wt% BTA at pH 8.4 and 8.8. Figure 6.6 shows mean aggregate sizes over time for both suspensions. The suspension at pH 8.4 aggregated considerably slower than at pH 8.8; aggregate sizes reach a maximum mean size of 2140 ± 40 nm. The growth curve was exponential, suggesting reaction-limited aggregation as discussed in Chapter 5. To ensure that large enough aggregates to characterize the structure were present, the suspension was allowed to aggregate for ~4 hours before loading onto the substrate for imaging. Particle size distributions measured at various stages of aggregation are initially unimodal, but become bimodal after ~90 min with a smaller peak consistently in the range of 200-400nm; implying that particle-cluster aggregation is occurring. At pH 8.8, aggregation proceeds rapidly; mean aggregate sizes > 2μm are observed after the first minute and exceed 3μm within 4 minutes. Particle size distributions measured at various stages of aggregation are unimodal, implying that cluster-cluster aggregation is occurring.

As discussed in Chapter 5, aggregates formed by RLA are typically denser than those formed during rapid DLA and cluster-cluster aggregation. Because of the rapid aggregation occurring in the suspension at pH 8.8, it is expected that observed aggregates would be loosely packed compared to those formed by RLA (suspension at pH 8.4). SEM images of the large aggregates formed in these suspensions, shown in Figure 6.3 and 6.4, do not give evidence that this is indeed occurring. Extremely large aggregates, exceeding 10μm, as well as small aggregates (100 – 200nm) are observed in both samples. Magnified images of aggregates do not reveal differences in the aggregate structures.

The lack of difference in structure of the imaged particles may be attributed to the sample preparation. Because of the high vacuum environment required by SEM, as discussed in Section 6.1, slurry samples must be loaded onto the substrate and subsequently dried before imaging. The drying process may alter the state of the aggregates, potentially causing further aggregation or collapsing loosely packed structures. Descriptions of this effect in literature is limited, however Chang et al. observed clustering of silicon nanowire tips during drying after liquid immersion. They attributed this phenomenon to the effects of capillary forces of the liquid interacting with the van der Waals or electrostatic charges on the structures [7]. Chang et al. employed critical point drying to alleviate the problem. This particular technique requires rinsing the sample with a volatile solvent, typically ethanol.

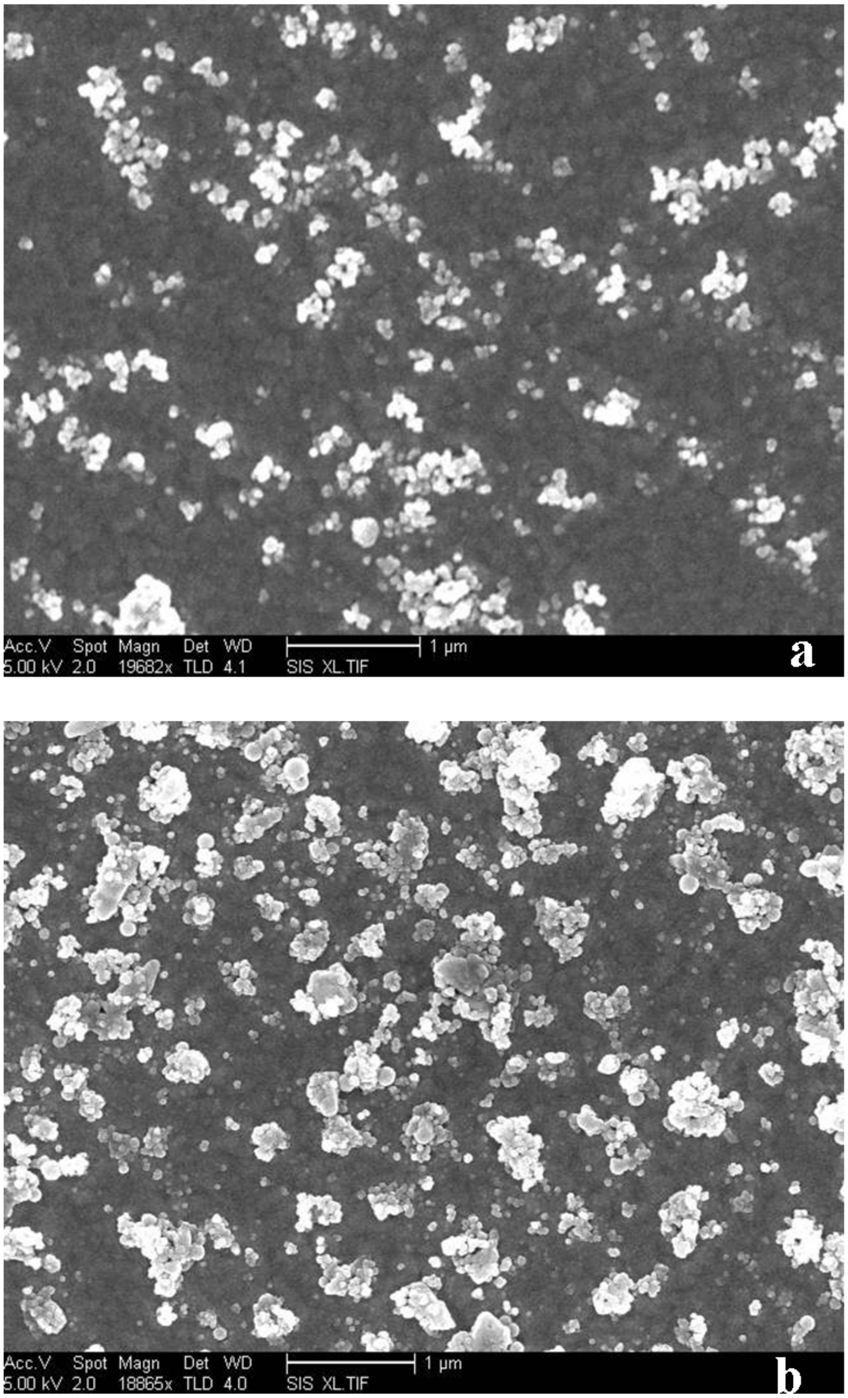

Figure 6.7. SEM images of alumina aggregates formed in suspensions with 1mM KNO_3, 0.1M glycine, 0.01wt% BTA, and 0.12mM Cu at pH 4. Samples were prepared by dipping wafer pieces into the suspension and then rinsing with DI water (a) or acetone (b).

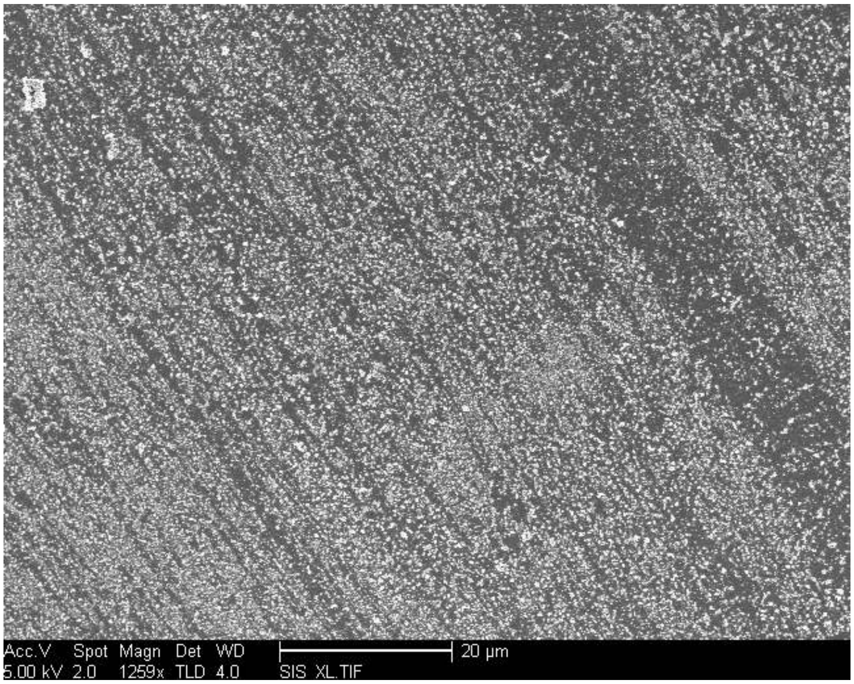

Figure 6.8. SEM image of alumina aggregates formed in a suspension of 1mM KNO_3, 0.1M glycine, 0.01wt% BTA, and 0.12mM Cu at pH 4. Sample was prepared with an acetone rinse. A uniform streaking pattern is seen that was not observed with samples that were rinsed with DI water.

Sample preparation using acetone as a rinsing agent was investigated. Alumina particles were dispersed in DI water with 1mM KNO_3, 0.1M glycine, 0.01wt% BTA, and 0.12mM Cu at pH 4. SEM samples were prepared by the dip and rinse method explained previously. A sample rinsed with DI water was compared to a sample rinsed with acetone. Images of alumina aggregates are shown in Figure 6.7. The sample rinsed with acetone had, on average, larger aggregates present. Additionally, large and dense agglomerates (> 4µm) were observed on the sample rinsed with acetone. It is likely that acetone has a greater capillary effect on the particles than water, causing further aggregation during the drying process. Aggregates arranged in streaking patterns (shown in Figure 6.8) were observed for samples rinsed in acetone, a feature not observed with samples rinsed with water, further suggesting enhanced capillary action with acetone as opposed to water. Furthermore, BTA crystals were observed on the sample rinsed with acetone, suggesting that acetone could alter the chemical state of the solution to allow precipitation.

The effects of solvent choice on aggregation of nanoparticles have been observed by others [8, 9]. Gacem and Diao observed increased tendency of polyvinylpyrrolidone-coated rhodium nanoparticles to aggregate with increased solvent polarity [8]. Sánchez-Iglesias et al. observed that gold nanoparticles stabilized with polystyrene chains would aggregate when shifting solvent from tetrahydrofuran to water due to hydrophobic interactions with water [9]. Because of this potential for altering the aggregate size and structure by changing solvent type, critical point drying was not used in our sample preparation. Instead, SEM techniques to image particles while still in suspension where investigated and will be discussed in the following section.

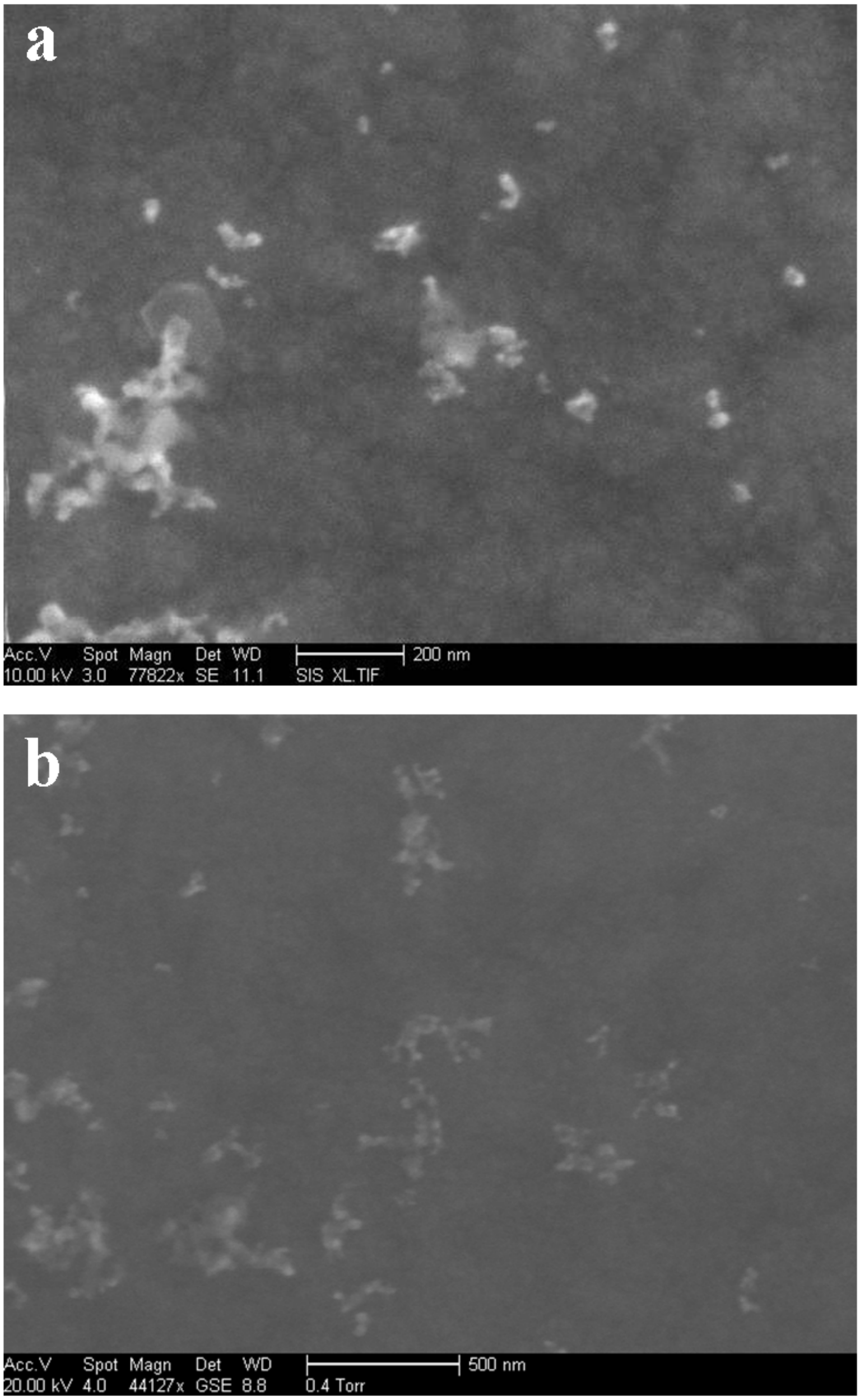

Figure 6.9. SEM (a) and ESEM (b) images of alumina nanoparticle aggregates prepared from suspensions in water.

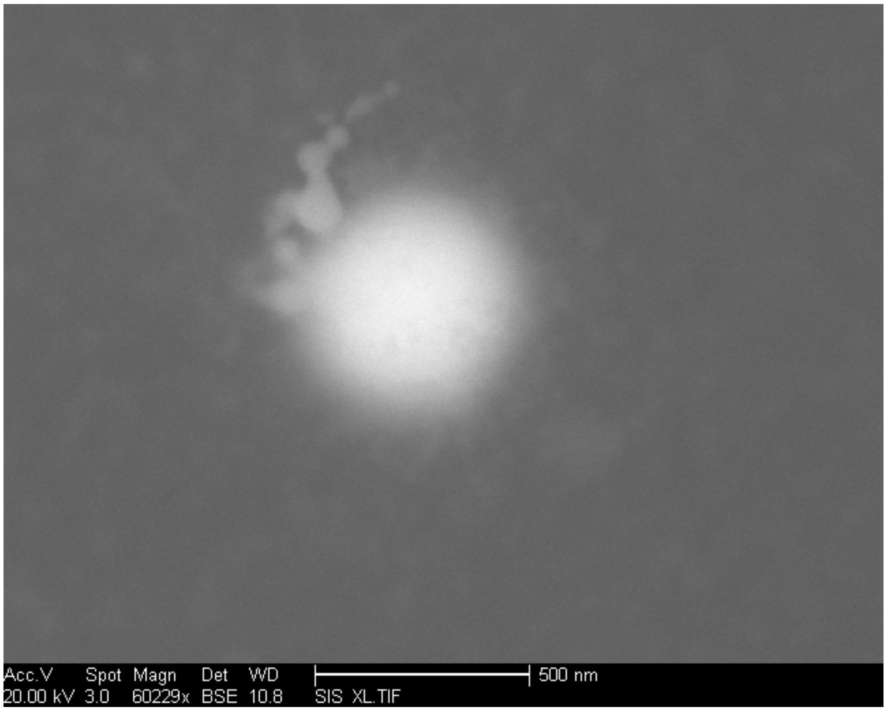

Figure 6.10. SEM image of alumina nanoparticle aggregate formed from a suspension of pure DI water with sample enclosed in a QuantomiX cell.

6.4 SEM of wet samples

Imaging of the alumina particles while in suspension was attempted. Figure 6.9 shows images of alumina nanoparticles prepared from a 0.05 wt% suspension with no other additives. As can be seen, individual particles can be resolved. However, due to the nature of the ESEM, high resolution and good contrast are difficult to achieve. A comparison of images of the alumina nanoparticle collected via ESEM with “dried” samples imaged by traditional SEM is shown in Figure B. Differences between the “dried” and “wet” samples are negligible; both show aggregates of alumina particles with comparable sizes, size distributions, and maximum aggregate sizes up to 500 nm.

Another explored alternative was using a QuantomiX SEM cell. Such a cell can be used in a traditional SEM and therefore useful for imaging wet samples. The

QuantomiX cell is enclosed from the environment with an air and water tight, electron transparent membrane at the top of the capsule [10]. Imaging can only be done in backscattered electron mode as secondary electrons are not transmitted through the membrane [10]. Energy dispersive spectroscopy can be done using a QuantomiX cell [10]. This cell, however, requires the samples to be attached to the membrane surface for proper imaging [11]. This is done by incubating the liquid dish located within the cell with a solution containing negatively or positively charged polymer (Poly(sodium-4-styrenesulfonate) and Poly-L-lysine respectively) followed by incubating with the sample itself [11].

Our attempts to utilize a Quantomix cell for particle imaging were unsuccessful. Attachment of particles to the membrane was difficult to achieve, possibly due to inadequate particle surface charge. Additionally, resolution was severely limited and visible structures could not be well resolved. Figure 6.10 shows an image of an alumina particle aggregate taken using a QuantomiX cell. The particle shown was the only observable particle from the entire sample. An artifact is also present on the sample.

6.5 Conclusions

SEM imaging of the alumina nanoparticles was performed, however, due to challenges with proper sample preparation, analysis of the aggregate structure was not possible. Although imaging of the primary particles and aggregates present in pure water was achievable, the drying process during sample preparation led to collapsing of loose aggregates as well as further aggregation of clusters.

SEM of wet samples was investigated as well. ESEM images had poor resolution and contrast. Use of a QuantomiX wet SEM cell had challenges of particle attachment to the electron transparent membrane.

Acknowledgements

This work was supported by University of California, Berkeley IMPACT program for its support along with the partner companies: Applied Materials, AMSL, Ebara Technologies, Global Foundries, IBM, Intel Corporation, KLA-Tencor, Marvell, Mentor Graphics, Novellus Systems, Panoramic Tech, SanDisk, Synopsys, Tokyo Electron Limited, and Xilinx Inc, along with matching support by the UC Discovery Grant ele07-10283. Also, I would like to thank Ryan Anderson and Aruni Suwarnasarn for their help with the SEM and ESEM experiments. Their invaluable guidance with using the SEM instrument is much appreciated. Additionally I extend my thanks to the Nano3 facility at CalIT2 along with its entire staff for providing and supporting the SEM used for imaging experiments.

References

1. C. W. Oatley, W. C. Nixon, and R. F. W. Pease, *Adv. Electronics Electron Phys.,* **21**, 181-247 (1966).

2. J. Goldstein, D. E. Newbury, D. C. Joy, C. E. Lyman, P. Echilin, E. Lifshin, L. Sawyer, and J. R. Michael, "Scanning Electron Microscopy and X-ray Microanalysis," Springer (2003).

3. D. J. Stokes, *Phil. Trans. R. Soc. Lond. A,* **361**(1813), 2771-2787 (2003).

4. G. D. Danilatos, P. L. Gai, "In-situ Microscopy in Materials Research," Kluwer Academic Publishers (1997).

5. G. B. Basim and B. M. Moudgil, *J. Colloid Interface Sci.,* **256**, 137-142 (2002).

6. R. J. Hunter, "Foundations of Colloid Science," Oxford University Press Inc., New York (2001).

7. S. W. Chang, V. P. Chuang, S. T. Boles, C. A. Ross, and C. V. Thompson, *Adv. Funct. Mater.,* **19**, 2495-2500 (2009).

8. N. Gacem and P. Diao, *Colloids and Surfaces A: Physicochem. Eng. Aspects,* **417**, 32-38 (2013).

9. A. Sánchez-Iglesias, M. Grzelczak, T. Altantzis, B. Goris, J. Pérez-Juste, S. Bals, G. V. Tendeloo, S. H. Donaldson Jr., B. F. Chmelka, J. N. Israelachvili, and L. M. Liz-Marzán, *ACSNano,* **6**(12), 11059-11065 (2012).

10. E. Gallucci and K. Scrivener, *Advances in Applied Ceramics,* **106**(6), 319-326 (2007).

11. QuantomiX Ltd. *QX-102 Applications Manual*, UQX003 Issue 2.1 (2005).

CHAPTER 7

MODELING COPPER CMP MATERIAL REMOVAL RATES USING COLLODAL BEHAVIOR OF THE ALUMINA SLURRY

7.1 Introduction

Modeling of the chemical mechanical planarization (CMP) process has been an area of research for the past two decades. Ihnfeldt [1] and Oliver [2] provide a comprehensive review of CMP models up to 2008 and Oliver provides a summary of metal CMP models [2]. One of the most well known CMP models is Preston's equation, equation 7.1, which shows a linear relationship between the material removal rate (MRR) and the wafer down pressure (P in Pa) and relative linear velocity (v in cm/s):

$$MRR = K_p P v \tag{7.1}$$

K_p (Pa^{-1}) incorporates the effects of all other variables and can vary depending on the chemical system [3]. This model is limited as it does not account for the slurry particle properties (size, distribution, concentration, etc.). Additionally, nonlinear relationships between MRR and down pressure and velocity have also been observed [3].

Models addressing the chemical nature of the slurry have been developed by numerous groups. Zhao et al. developed a mathematical model with the physical basis that chemical reactions weaken the bonds of surface atoms and using concepts including chemical reaction equilibrium, chemical kinetics, contact mechanics, molecular binding energy and random-process probability [4]. Paul et al. also utilized chemical reaction kinetics to model chemical effects of the slurry on the wafer surface, notably the role of oxidizers [5]. Chen and Wang extended their model by including corrosion inhibitors and incorporating the ratio of the concentrations of oxidizer to inhibitor to account for the non-Prestonian behavior observed experimentally [6] while Wang and Zhao further developed the model to include complexing agents [7]. Others have also included effects of slurry hydrodynamics and mass transport of the chemical components [8, 9]. DeNardis et al. proposed a one dimensional-model incorporating etching effects of a slurry on a copper oxide surface, noting that rate of copper dissolution was a function of the reaction byproduct film thickness [10].

More comprehensive models have recently been developed that account for the synergy of the chemical and mechanical effects of the slurry by assuming a chemically modified thin layer formed on the wafer surface by chemical effects of the slurry that is removed by mechanical action of the particles [11-13]. Models that address the colloidal aspects of the slurry have also been developed [14, 15]. More recently, Lee et al. have integrated distributions of relative velocity and normal stress between the wafer and polishing pad with existing MRR models to produce a unified MRR distribution model for SiO_2 CMP, predicting material removal rates as a function of position on the wafer surface [16]. Their semi-empirical model shows good agreement with experiment experimentally measured SiO_2 MRR using silica abrasive particles [16].

The Luo and Dornfeld model of CMP is a comprehensive model that utilizes a solid-solid contact mode for mechanical removal instead of a hydrodynamic mode used by others [17]. Along with the variables of down pressure and velocity, key variables such as wafer hardness, pad hardness, pad roughness, abrasive size, abrasive size distribution, and abrasive geometry were integrated into the model [18]. A detailed derivation of the model can be found elsewhere [17]. The simplified model equation is shown below:

$$MRR = \rho_w NV + C_o \qquad [7.2]$$

where ρ_w is the wafer density, N is the number of active abrasives, V is the volume of material removed by a single abrasive particle, and C_o is the material removal rate by chemical etching (typically negligible compared to the overall removal rate as it is generally <5% of the overall MRR) [17, 19, 20]. The model assumes a plastic contact mode at the wafer-abrasive interface, elastic contact at the pad-abrasive surface, a normal distribution of particles, and periodic roughness of the pad surface [17]. The bulk of material is removed from the surface by quasi-static abrasion, which is removal of material from sliding of the wafer surface over abrasive particles embedded in the pad [17].

The MRR (thickness/time) as a function of mean abrasive size (x_{avg}), standard deviation (σ), wafer hardness (H_w) and pad hardness (H_p) is given by the following equation:

$$MRR = \underbrace{\left(\frac{B_1}{H_w^{3/2}}\right)\left(\frac{1}{x_{avg}}+\frac{6\sigma}{x_{avg}^2}+\frac{9\sigma^2}{x_{avg}^3}\right)}_{\text{Thickness Removed by Single Abrasive}}\underbrace{\left[1-\Phi\left(3-B_2\left(\frac{1}{H_P}+\frac{2}{H_W}\right)\frac{\left(x_{avg}+3\sigma\right)}{\sigma}\right)\right]}_{\text{Number of Active Abrasives}}$$

$$+\underbrace{C_0}_{\text{Material Removed by Chemical Etching}} \qquad [7.3]$$

In equation 7.3, C_0 is the chemical etch rate (thickness/time) and Φ is the normal probability density function, defined below:

$$\Phi(x) = \tfrac{1}{2\pi}\int_{-\infty}^{x} e^{\left(-1/2\right)t^2}\,dt \qquad [7.4]$$

In equation 7.3, B_1 and B_2 incorporate properties of the slurry and are given by:

$$B_1 = \frac{8\sqrt{2}d_s\rho_s m_{s-a}D_{SUM}^{1/2}alE_P}{3R\rho_a\pi^{5/2}}\sqrt{P_0}v \qquad [7.5]$$

$$B_2 = \frac{1}{4\pi}\left(\frac{4}{3}\right)^{4/3}\left(\frac{E_P}{R}\right)^{2/3}\left(\frac{P_0}{D_{SUM}}\right)^{1/3} \qquad [7.6]$$

Definitions and values for the parameters used in equations 7.5 and 7.6 are given in Table 7.1. The values listed were based on those used by Ihnfeldt for her copper CMP MRR measurements and modeling [19]. Because the modeling presented in this chapter is an extension of that done by Ihnfeldt, the same values used were chosen. Based on the parameters, B_1 is 3.18 x 10^7 $nm^2GPa^{1.5}/min$ and B_2 is 1720 kPa [20].

Table 7.1. Values for parameter used in Luo and Dornfeld model (Equation 7.3) [from 16].

Parameter	Value
Dilution Ratio - d_s	0.1
Down Pressure - P_0 (psi)	1
Wafer Diameter (mm)	100
Young's Modulus for pad – E_P (MPa)	2.3
Number of asperities per unit area of pad D_{SUM} (cm^{-2})	27
Mean asperity area – a (μm^2)	18,500
Asperity height – l (μm)	58
Asperity radius – R (μm)	6.5
Density of alumina abrasive – ρ_a (g/cm^2)	3.7
Linear wafer velocity – v (m/s)	0.3
Hardness of IC1000 polishing pad – H_P (MPa)	100
Density of slurry – ρ_s (g/cm^3)	1.4
Slurry concentration – $m_{s\text{-}a}$ (%)	40

The product of the first two terms in equation 7.3 represent the thickness removed per unit time, while the third term represents the number of active abrasives. Because the model assumes a Gaussian distribution of particles, the size of the active abrasives that is removing material must be larger than the mean abrasive particle size x_{avg}. Therefore the relation shown in equation 7.7 must be satisfied:

$$\frac{x_{avg}}{\sigma} < \frac{3\left[1 - B_2\left(\frac{1}{H_P} + \frac{2}{H_W}\right)\right]}{B_2\left(\frac{1}{H_P} + \frac{2}{H_W}\right)} \qquad [7.7]$$

Based on the parameters listed above, x_{avg}/σ must be less than 165.

The Luo and Dornfeld model has successfully predicted MRR for CMP of SiO_2 compared to experimentally measured MRR (± 7%) for various down pressures, pad hardness, etc. It has also estimated MRR for tungsten CMP to some success as well [17, 18]. Gopal simplified equation 7.3 to:

$$MRR \propto \frac{(x+3\sigma)^2}{x^3} \qquad [7.8]$$

Based on this relationship, she noted that for large aggregate diameters ($x_{avg} > \sim 750$nm) MRR does not vary significantly with small variations of σ, but for small aggregate diameters the model predictions vary notably with small variations in σ [18]. Ihnfeldt incorporated experimentally determined average aggregate size, aggregate standard deviation, copper surface hardness, and etch rate data into the Luo and Dornfeld model. She found that copper CMP MRR predictions improved with inclusion of this data, however the model could not predict MRRs for highly chemically active slurries, that is slurries at acidic pH or with high etch rates (Co> 8nm/min) [20].

This chapter presents copper CMP MRR predictions made using the Luo and Dornfeld model. The purpose of this analysis was to determine the effects of the growth of aggregates on the MRR of copper CMP. Until now, all CMP MRR predictions have been calculated using a single set of particle size distribution data collected at a certain point in time and used to predict MRR using the model described above. For example, Ihnfeldt measured the particle size distribution of alumina particles 10 minutes after the particles were suspended [19].

7.2 Results and Discussion

Table 7.2 shows pH and zeta potential for three different suspensions of 1mM KNO_3, 0.1M glycine, and 0.12mM Cu (A); 1mM KNO_3, 0.1M glycine, 0.1 wt% H_2O_2, and 0.12mM Cu (B) ; and 1mM KNO_3, 0.1M glycine, 0.1wt% H_2O_2, 0.01wt% BTA, 0.1mM SDS, and 0.12mM Cu (C). Ihnfeldt measured MRR of 1µm copper films on 30nm of sputtered tantalum on 100 mm silicon wafers (with the conditions of 1 psi down pressure, 30 rpm platen and wafer rotational speed, 150 mL/min slurry delivery rate, and 2 min polishing time) using the same slurry compositions in Table 7.2 [20]. Ihnfeldt also measured copper hardness and etch rates with the same slurry compositions as well, which are reported in Table 7.2.

Table 7.2. Values of pH, zeta potential wafer hardness, and etch rate used in model.

Suspension	**pH**	**Zeta Potential (mV)**	**H_w (±0.3 GPa) [from 17]**	**C_0 (± 4nm/min) [from 17]**
A) 1mM KNO_3 + 0.1M glycine + 0.12mM Cu	8.2	29 ± 3	2.99	7.6
B) 1mM KNO_3 + 0.1M glycine + 0.1wt% H_2O_2 + 0.12mM Cu	8.0	19 ± 7	2.92	33.0
C) 1mM KNO_3 + 0.1M glycine + 0.1wt% H_2O_2 + 0.01wt% BTA + 0.1mM SDS +0.12mM Cu	8.5	16 ± 5	5.29	0.0

Ihnfeldt noted that the predicted MRR decreased with increasing mean aggregate size and standard deviation up to a critical size (dependent on the slurry conditions), after which MRR began to increase [20] as expected from equation 7.3. A plot of equation 7.3 is illustrated in Figure 7.1 with x_{avg} held constant (150 nm) and varying σ as well as with σ held constant (10, 50, and 200 nm) and varying x_{avg}. Calculated MRR show a U-shaped curve as a function of x_{avg} or σ for all conditions.

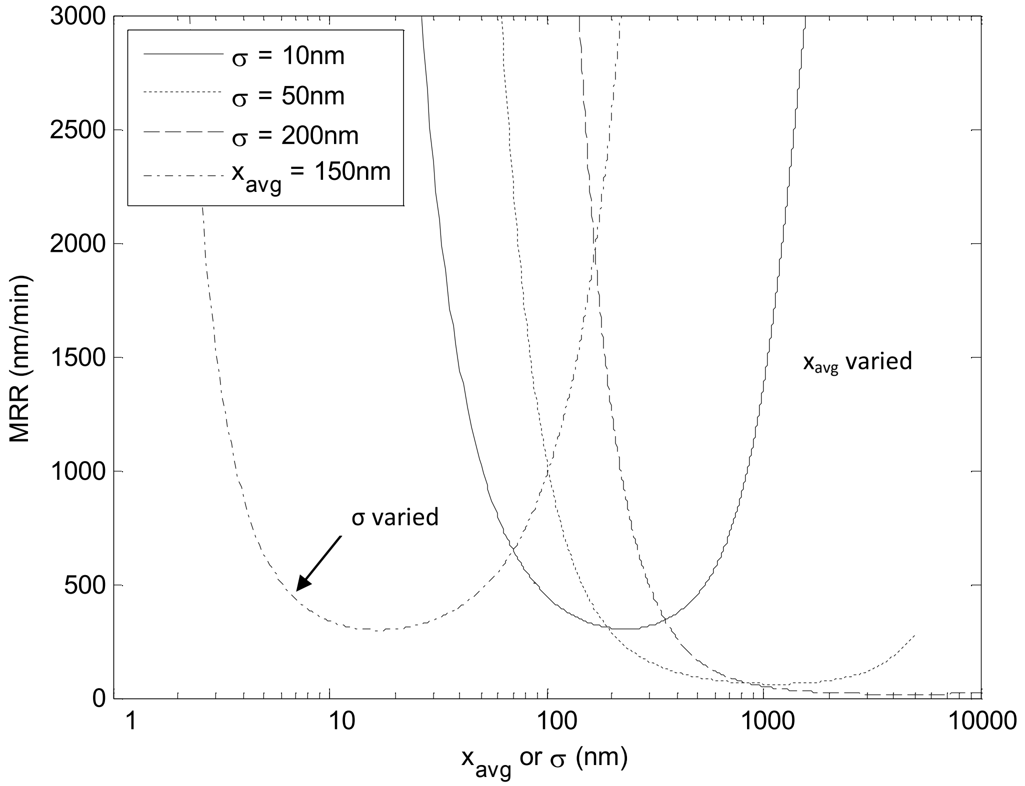

Figure 7.1. Predicted material removal rates from equation 7.3 with varying standard deviation with fixed mean aggregate sizes (dot and dashed line) and varying mean aggregate sizes with fixed standard deviation (all other lines). All other values are listed in Table 7.1 ($H_W = 2.3$, $C_0 = 0.0$).

Table 7.3 shows measured initial and final particle size and standard deviation along with predicted MRRs. To make the predictions more comparable with measured MRR data from Ihnfeldt [20], the predicted MRR were time averaged over 10 minutes. This essentially done by taking a moving average over the time series and the iterative algorithm is shown below:

$$\overline{x_t} = \overline{x}_{t-1} + \frac{x_t - \overline{x}_{t-1}}{t} \qquad [7.9]$$

Ihnfeldt's CMP experiments had a polishing time of 2 min due to slurry waste restrictions. However, she had determined that typical slurry residence time on the CMP instrument of ~ 10 min [1] and therefore made her particle size distribution measurements 10 min after sonication. For this reason, only the first 10 minutes of predicted MRR calculated for this chapter were time averaged. Due to inconsistencies in standard deviation caused by settling of large aggregates (described in detail later), suspension C predicted MRR were not time averaged.

Table 7.3. Initial and final x_{avg} and σ of alumina particles from the suspensions investigated. Initial and final predicted MRR are also shown, corresponding to model predictions made using the initial and x_{avg} and σ. Time averaged (first 10 minutes) predicted MRR and measured MRR are also shown.

Suspension	**$x_{avg} \pm \sigma$ Initial (nm)**	**$x_{avg} \pm \sigma$ Final (nm)**	**Predicted MRR Initial (nm/min)**	**Predicted MRR Final (nm/min)**	**Time Averaged Predicted MRR (nm/min)**	**Measured MRR (± 14 nm/min) [From 17]**
A	197 ± 44	3360 ± 736	190	18	93	9
B	145 ± 13	2850 ± 711	250	47	178	287
C	1570 ± 25*	3871 ± 30*	62*	184*	NA	11

***Inconsistent standard deviation due to settling of very large aggregates**

Comparison of time-averaged MRR with measured MRR is shown in Table 7.3. The predicted MRR is still considerably larger for suspension A. This may be due to the sensitivity of the suspension stability to pH at levels near the isoelectric point (~9.7, as discussed in chapter 5). Although the pH level was adjusted to be as close to those used by Ihnfeldt [20], obtaining the exact value was difficult and the pH used in suspension A was lower than that used by Ihnfeldt (8.2 vs 8.5) and farther from the IEP; therefore it is not surprising that Ihnfeldt's suspension exhibited larger aggregate diameters and smaller MRR as a consequence. For suspension B, the time-averaged predicted MRR is significantly lower than that measured. As Ihnfeldt noted, for chemically active slurries the model is not predictive.

Figure 7.2 shows predicted MRR (nm/min) vs time (min) for suspension A. The initial predicted MRR (t = 1min) was significantly larger than experimental measured (190 nm/min vs 9 ± 14 nm/min [20]), but decreases to 37 nm/min within 10 min as the mean particle sizes and standard deviation increases and levels off to ~18 nm/min by 30 min. The results shown in Figure 7.2 are consistent with a decreasing MRR with increasing aggregate size described earlier. The U-shaped curve is not observed, likely because the critical size after which predicted MRR increases was never reached as the mean aggregate sizes stop growing as shown in Figure 3.1 in Chapter 3.

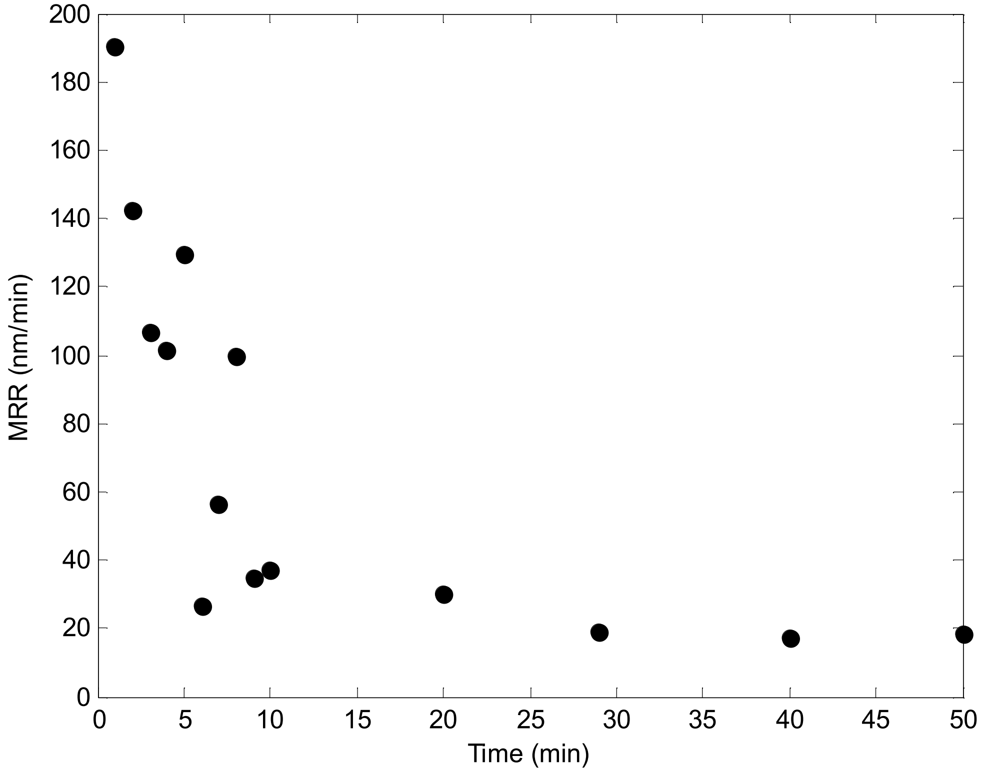

Figure 7.2. Material removal rate predictions vs. time for mean aggregate size and standard deviation measured of alumina suspensions with 1mM KNO_3, 0.1M glycine, and 0.12mM Cu.

Ihnfeldt predicted a MRR of 16 nm/min for a slurry of the same composition using a mean aggregate size and standard deviation of the particles measured 10 minutes after sonication (x_{avg} of 3750nm and σ of 319nm) [19]. Because the measurement was taken 10 minutes after sonication, the small aggregates present during the early stages of aggregation, responsible for larger MRR, are not considered and therefore, the large predicted MRR is not observed.

Figure 7.3 shows predicted MRR vs time for suspension B. The initial predicted MRR (t = 1min) was 250 nm while the measured MRR was 287 ± 14 nm/min. Similar to the previous suspension, the MRR decreases as the mean aggregate size and standard deviation increases, reaching a minimum of ~47 nm/min after 50min. This also agrees with equation 7.3 and Fig 7.1 [20]. Ihnfeldt predicted a MRR of 57 nm/min, significantly lowered than the measured, although she noted that the model was not predictive for chemically active slurries (etch rates > 8nm/min).

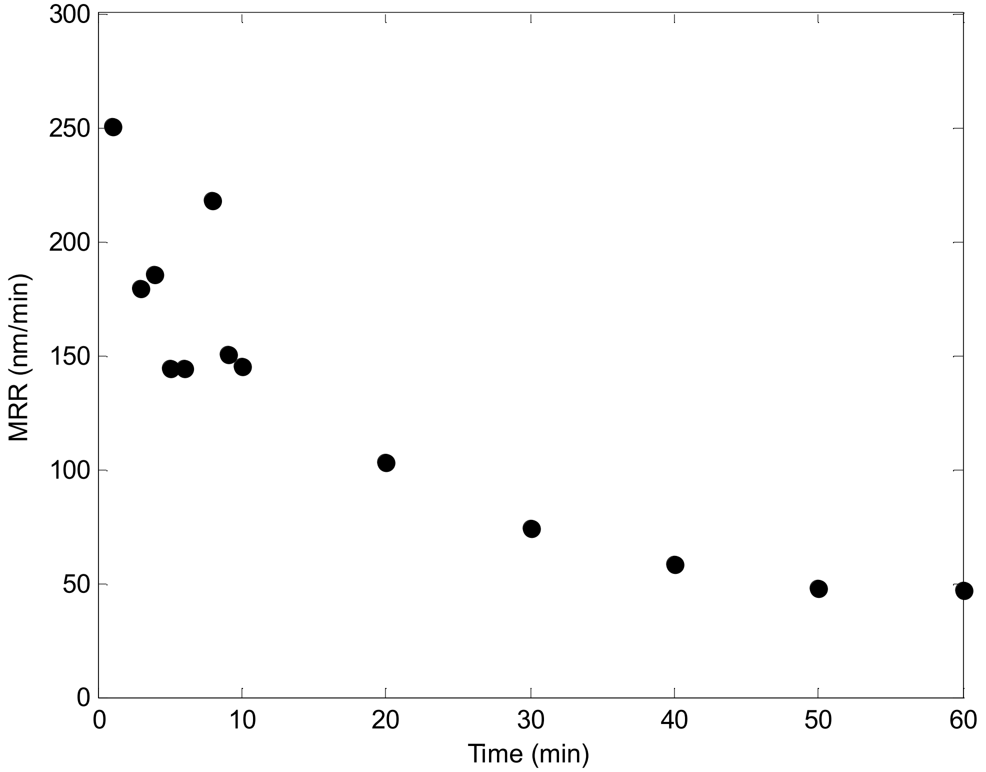

Figure 7.3. Material removal rate predictions vs. time for mean aggregate size and standard deviation measured of alumina suspensions in 1mM KNO_3, 0.1M glycine, 0.1wt% H_2O_2, and 0.12mM Cu.

Predicted MRR vs time for suspension C (not shown) do not agree with the measured MRR by Ihnfeldt (11 ± 14nm/min). The measured σ was considerably lower (< 40nm vs 94nm measured by Ihnfeldt) at most particle size measurements, which is likely the reason for the predicted large MRR. Because aggregate sizes were measured under quiescent conditions, it is likely that very large aggregates were settling to the bottom of the cuvette leading to the measurement of small σ. By using Stoke's law of drag force, the settling velocities of the aggregates based on aggregate sizes were calculated [21] using equation 7.10:

$$v_s = \frac{2(\rho_p - \rho_f)}{9\mu} gR^2 \qquad [7.10]$$

In equation 7.10, the variables displayed are as follows: v_s is the settling velocity (cm/s), ρ_p is alumina particle mass density (3.7 g/cm^3 [1]), ρ_f is fluid (water) density (1 g/cm^3), g is the acceleration due to gravity (981 cm/s^2), μ is the dynamic viscosity of the fluid (8.9 x 10^{-4} Pa*s), and R is the radius of the aggregate (cm). The distance the particle can settle before no longer being detected by the DLS machine was taken as the distance from the laser port to the bottom of the cuvette (0.3 cm). By dividing the distance to settle by the settling velocity, the time to settle as a function of particle diameter was calculated and plotted in Figure 7.4. Primary aggregates (150 nm in diameter) will settle after ~21 hours and the time to settle decreases parabolically (1/d^2). Aggregates greater than 3μm settle to the bottom after ~ 3 minutes, after which these large aggregates will no longer be detected by the machine. Aggregates larger than 5μm will settle within ~1 minute, therefore it is not surprising that such large aggregates that form during the early stages of aggregation are not detected by the DLS at later times and therefore are excluded during reporting of the particle size distribution.

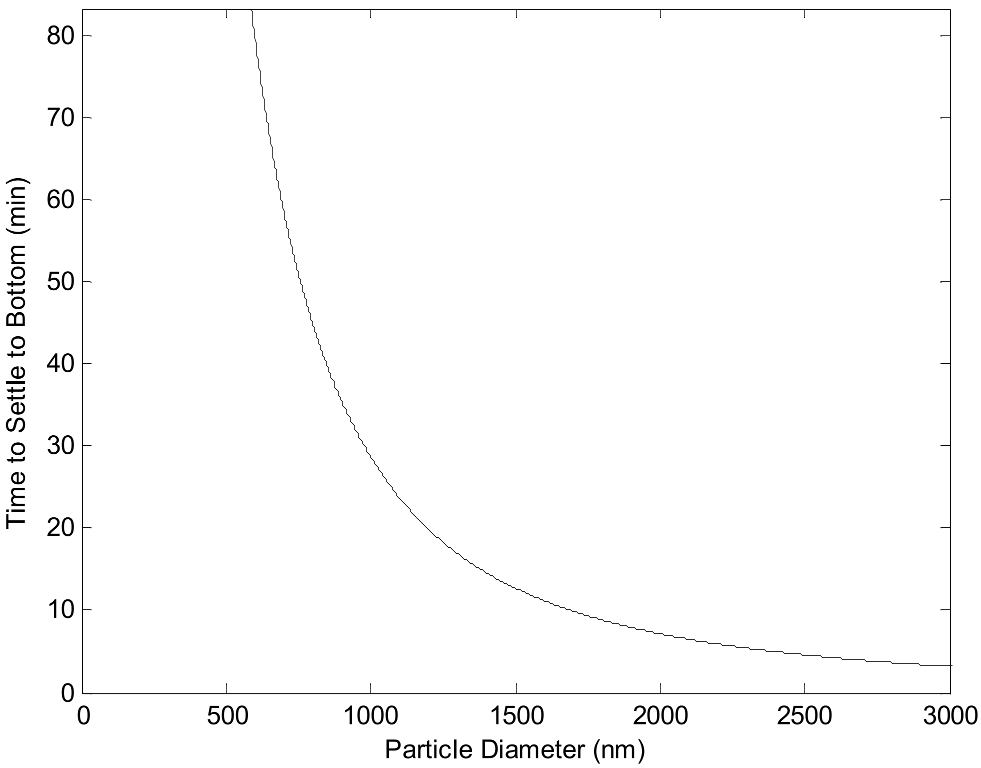

Figure 7.4. Time for aggregate particles to settle to bottom of cuvette as a function of particle diameter.

7.3 Conclusions

Experimentally determined mean aggregate size and standard deviation measurements were incorporated into the Luo and Dornfeld model of CMP. Copper surface hardness and etch rate data collected by Ihnfeldt were also used. In general, predicted MRR were initially large (~200-250 nm/min) but reduced to <50 nm/min over time. Suspensions with 1mM KNO_3, 0.1M glycine, 0.1wt% H_2O_2, 0.01wt% BTA, 0.1mM SDS, 0.12mM Cu showed MRR predictions which varied greatly by as much as a hundred nm/min. This is most likely due to small standard deviations caused by settling of extremely large aggregates during measurement.

The time dependent predictions suggest that MRR may be significantly reduced over time if abrasive particles are allowed to aggregate to large sizes. This result is consistent with Ihnfeldt's observation that increasing mean aggregate size and standard deviation will result in reduced predicted MRR in the Luo and Dornfeld model. However, the U-shaped curve of the predicted MRR on mean aggregate size and standard deviation was not observed, likely because the aggregates stop growing before reaching the critical size beyond which the model predicts increasing MRR with increasing particle size.

Acknowledgements

This chapter in part is currently being prepared for submission for publication of the material; Neil Brahma and Jan B. Talbot. The dissertation author was the primary investigator and author of this material

References

1. R. Ihnfeldt, PhD Thesis, University of California, San Diego (2008).
2. M. T. Oliver, *Chemical-Mechanical Planarization of Semiconductor Material*, Springer-Verlag, Berlin (2004).
3. T. J. Gopal and J. B. Talbot, *J. Electrochem. Soc.,* **154**(6), H507-H511 (2007).
4. Y. Zhao, L. Chang, and S. H. Kim, *Wear*, **254**, 332 (2003).
5. E. Paul, F. Kaufman, V. Brusic, J. Zhang, F. Sun, and R. Vacassy, *J. Electrochem. Soc.*, **152**, G322 (2005).

6. K. W. Chen and Y. L. Wang, *J. Electrochem. Soc.*, **154**, H41(2007).

7. Y. Wang and Y. Zhao, *Appl. Surf. Sci.*, **254**, 1517 (2007).

8. L. Zhang and R. S. Subramanian, *Thin Solid Films*, **397**, 143 (2001).

9. D. G. Thakurta, D. W. Schwendeman, R. J. Gutmann, S. Shankar, L. Jiang, and W. N. Gill, *Thin Solid Films*, **414**, 78 (2002).

10. D. DeNardis, D. Rosales-Yeomans, L. Borucki, and A. Philipossian, *Thin Solid Films*, **518**, 3910-3916 (2010).

11. K. Qin, B. Moudgil, and C. W. Park, *Thin Solid Films*, **446**, 277 (2004).

12. J. Li, X. Lu, Y. He, and J. Luo, *J. Electrochem. Soc.*, **158**, H197 (2011).

13. J. Xin, W. Cai, and J. A. Tichy, *Wear*, **268**(5-6), 837-844 (2010).

14. A. R. Mazaheri and G. Ahmadi, *J. Electrochem. Soc.*, **150**, G233 (2003).

15. P. H. Chen, B. W. Huang, and H. Shih, *Thin Solid Films*, **476**, 130 (2005).

16. H. S. Lee, H. D. Jeong, D. A. Dornfeld, *Precision Engineering*, **37**(2), 483-490 (2013).

17. J. Luo and D. A. Dornfeld, *IEEE Trans. Semicond. Manuf.*, **14** (2), 112-133 (2001).

18. T. J. Gopal and J. B. Talbot, *J. Electrochem. Soc.,* **154**(6), H507-H511 (2007).

19. R. Ihnfeldt and J. B. Talbot, *J. Electrochem. Soc.,* **154**(12), H1018-H1026 (2007).

20. R. Ihnfeldt and J. B. Talbot, *J. Electrochem. Soc.*, **155**(8), H582-H588 (2008).

21. H. Lamb, *Hydrodynamics,* Cambridge University Press, Cambridge, UK (1994).

CHAPTER 8

CONCLUSIONS AND FUTURE WORK

8.1 Conclusions

Chemical mechanical planarization has proved to be a very effective process for the planarization of heterogeneous materials. The mechanical removal due to the abrasive particles in concert with the chemical effects of the ingredients within the slurry produces a synergistic effect that produces nearly globally planar surfaces. To achieve high MRR and uniformity, abrasive particles must be on the size order of nanometers to produce the minimal roughness needed, but may aggregate in the slurry. The presence of large agglomerates reduces CMP performance (i.e, decreasing material removal rates and increasing overall surface roughness) and can also increase the number of defects present on wafers.

The purpose of this study was to investigate the fundamentals of the aggregation phenomenon of alumina particles used in copper CMP slurries. The work presented in this dissertation is a continuation of the work done by Drs. Tanuja Gopal [1] and Robin Ihnfeldt [2] on the effects of chemistry on the aggregation of alumina particles. The effects of different slurry additives on the agglomeration behavior and rate of aggregation of alumina nanoparticles were studied. Zeta potential measurements of the particles in suspensions of different chemistries were also conducted to further elucidate the effects of the slurry additives.

In general three behaviors for the alumina slurries were observed: no aggregation, reversible aggregation where large agglomerates (>2.5 μm) formed almost instantaneously, and steady aggregation from the initial aggregate size. As also reported by Gopal and Ihnfeldt, pH was observed to have the largest effect on aggregation, an expected result since alterations of H^+ ion concentrations in suspension greatly affects the surface charge, and consequently zeta potential of the particles. Different aggregation behavior was observed when SDS was added to the suspensions. Significant aggregation was observed at acidic pH (<6.5), a region where aggregation was not observed for all other additives. The aggregation with slurries with SDS at low pH was so fast that very large aggregates (>1 μm) were observed almost immediately and was observed regardless of any other additives present, suggesting that SDS was promoting aggregation. The likely reason for the enhanced aggregation was the higher concentration of adsorbed SDS onto the alumina particle surface at low pH. At high enough concentrations or ionic strength [8], the hydrophobic hydrocarbon chains of the adsorbed SDS molecules can bridge across particles in an attempt to lower their free energy and attract the particles. Typical copper CMP slurries containing alumina abrasives operate at acidic conditions and therefore, the ionic strength would need to be decreased appropriately so aggregation would be prevented [9].

Zeta potential, as expected, had highly positive values at acidic pH and negative values at basic pH for all suspensions, except when SDS was present. With SDS in the slurry the zeta potential was close to 0 mV at acidic pH (<6.5). Isoelectric points (IEP) varied from 8 – 10 depending on the additives present and aggregation was only observed for suspensions where zeta potentials were close to the IEP (absolute value < 25 mV), as expected. Aggregation and zeta potential were not affected by 0.1 wt% hydrogen peroxide in the slurry, however higher IEP's (~10) were measured when 0.01 wt% benzotriazole (BTA) and/or 0.1M glycine were present, likely due to the shielding effect (described in Chapter 3).

For most suspensions tested, the observed zeta potential and aggregation behavior did not change with the presence of 0.12 mM copper. However, a shift in IEP was observed when copper was added to the suspension containing all additives. These effects may be attributed to a similar shielding effect described for BTA and glycine by the copper complexes formed with the various additives.

It is well known that the temperature of the slurry during the CMP process can increase due to friction from the abrasive particles and the substrate, leading to temperatures up to 40^{o}C [10]. The effect of temperature from 25 to 40^{o}C on the CMP process was studied [10, 11] and a decreased zeta potential and particle size of silica particle were observed [11]. This was the first time measurements of alumina nanoparticle aggregate sizes and zeta potentials as a function of temperature were measured. Zeta potential measurements showed no significant changes in the isoelectric point for most suspensions tested, except when all additives (KNO_3, glycine, BTA, H_2O_2, and SDS) were present in the dispersion. For this suspension, the zeta potentials and isoelectric point were observed to decrease with increasing temperature, which has been observed previously for metal oxide particles [12, 13]. The likely explanation for this behavior is due to changes in surface oxygen protonation/deprotonation reactions and additive adsorption/desorption at higher temperatures as well as increases in the double layer thickness.

Aggregation rate experiments were performed to develop an understanding of the effects of the additives on the aggregation mechanism. Experiments were performed with suspensions at pH close to the IEP of pH ~8. For the majority of suspensions reaction-limited aggregation was observed, characterized by the exponential growth of the aggregate sizes. It was observed that once aggregate sizes reached ~500nm, the aggregate size growth followed a power law, suggesting a shift to diffusion-limited aggregation. Some suspensions that exhibited diffusion-limited aggregation from the beginning of the measurement, with fractal dimension numbers ranging from 1 to 1.4. These values suggest that the aggregate structure formed under these conditions have a large degree of openness and likely were produced by a cluster-cluster agglomeration mechanism.

Imaging of the structure of the aggregates formed in CMP slurries was attempted by SEM. Aggregates formed in slurries via RLA and DLA were imaged and compared. However, differences in structure could not be observed. This is likely due to capillary forces causing excess aggregation of the particles and collapse of open aggregate structures during sample preparation for the high vacuum environment present in the specimen chamber of a SEM. SEM methods for wet samples, including ESEM and QuantomiX wet SEM cell, were explored, however, results were unsatisfactory. Images collected by ESEM had low resolutions and poor contrast. For the QuantomiX cells, particle attachment to the membrane window was poor, preventing imaging of the particles.

Particle size distribution data at various times were incorporated into the Luo and Dornfeld model of CMP to investigate the dependence of material removal rate on time. Copper surface hardness and etch rate data, measured by Ihnfeldt [14], were also used. For suspensions of 1mM KNO_3 + 0.1M glycine and 1mM KNO_3 + 0.1M glycine + 0.1wt% H_2O_2, material removal rates were initially large (~200-250 nm/min), but decreased to <50 nm/min after ~30 min. This result is consistent with observations of decreasing MRR with increasing particle size observed by Ihnfeldt in testing the Luo and Dornfeld model [14], although a minimum MRR and subsequent increased were not observed, likely because aggregates stopped growing before reaching the critical particle size beyond which material removal rates increase (due to increasing volume of material removed by a single particle).

8.2 Future Work

The colloidal behavior of alumina nanoparticles was investigated in this study. However, the CMP process is used in a variety of applications and, as such, utilizes an array of abrasive particle materials in their respective slurries. Therefore, characterizing the colloidal behavior of suspensions composed of other abrasive particles (silica, ceria, etc.) would be useful. The tests discussed in this dissertation can be easily done for other particle types by simply preparing the slurries with the desired particle of interest. The colloidal behavior of mixed abrasive slurries as well as composite particle slurries may also be examined.

To gain a more complete understanding of the electrokinetic effects of CMP additives on the abrasive particles, knowledge of the surface charge is essential.

Measurement of zeta potential is useful in the analysis of colloidal stability, however it ignores the effects of additives on the surface of the particles themselves. If H^+ and OH^- ions are the only ions present in suspension, the zeta potential is equal to the surface charge [3], however when other ions are present, the relationship between the zeta potential and surface charge becomes more complex. To fully understand the effect of slurry additives on the particle themselves, the interaction of the additives with the particle surface should be determined by analysis of the surface charge.

An effective method to determine surface interaction of slurry additives could begin with measuring the point of zero charge of the particles in slurries of different chemistries. A method for measuring surface charge is potentiometric titrations where a measured amount of particles is titrated with a base while the pH is monitored [4]. The collected titration data could then be used to construct plots of surface charge versus pH aiding in determination of the adsorption of slurry additives to the particle surface. Adsorption of slurry additives on the particle surface can also be determined using other characterization methods such as energy-dispersive X-ray spectroscopy.

Knowledge of the aggregate structure can provide evidence of the aggregation method as well as determining if “hard” or “soft” aggregates are forming [5]. Currently scanning electron microscope (SEM) imaging of particles is difficult as the substrates need to be dried adequately before imaging. The drying process can disturb the structure of the aggregates as they collapse once the water is removed. Supercritical drying could be useful but it requires the use of a volatile solvent; utilization of this solvent can itself disturb the nature of the aggregates being observed.

STEM of wet samples is a relatively new type of imaging technology that has been shown to successfully image colloidal particles in suspension [6]. This technique requires the use of an ESEM with some modifications. A transmission electron micrograph grid, on which a droplet of the suspension of interest is deposited, is placed on the sample stage. The dipolar detector utilized for backscattered electron detection is relocated directly below the grid, allowing for transmission electron detection [6]. Careful pump-down must be done to ensure that the liquid drop does not evaporate completely. Once the partial pressure is reached, temperature and pressure can be adjusted to evaporate a controlled amount of the liquid until a layer thin enough to allow incident electrons to pass through is achieved [6]. Bogner et al. have demonstrated this type of wet-STEM imaging system. Using this system, they have successfully imaged suspensions of gold, silica, styrene, and poly-styrene particles ranging from 20 to 100nm in addition to others [6].

References

1. T. J. Gopal and J. B. Talbot, *J. Electrochem. Soc.,* **153**(7), G622-G625 (2006).
2. R. Ihnfeldt and J. B. Talbot, *J. Electrochem. Soc.,* **153**(11), G948-G955 (2006).
3. R. J. Hunter, "Zeta Potential in Colloid Science: Principles and Applications," Academic Press Inc., London (1981).
4. K. Bourikas, J. Vakros, C. Kordulis, and A. Lycourhiotis, *J. Phys. Chem. B*, **107**, 9441-9451 (2003).
5. G. B. Basim, J. J. Adler, U. Mahajan, R. K. Singh, and B. M. Moudgil, *J. Electrochem. Soc.*, **147**(9), 3523-3538 (2000).
6. A. Bogner, G. Thollet, D. Basset, P. –H. Jouneau, and C. Gauthier, *Ultramicroscopy*, **104**, 290-301 (2005).

7. D. Kristt and A. Nyska, *J. Toxicol Pathol*, **20**, 1-11 (2007).

8. P. C. Pavan, E. L. Crepaldi, G. A. Gomes, J. B. Valim, *A. Physiochemical and Engineering Aspects*, **154**, 399-410 (1999).

9. B. J. Palla and D. O. Shah, *J. Colloid Interface Sci.,* **223**, 102-111 (2000).

10. S. Mudhivarthi, P. B. Zantye, A. Kumar, A. Kumar, M. Beerbom, and R. Schalf, *Electrochemical and Solid State Letters*, 8, G241-G245 (2005).

11. N. H. Kim, Y. J. Seo, and W. S. Lee, *Microelectronic Engineering*, **83**, 362-370 (2006).

12. P. Jayaweera, S. Hettiarachchim, and H. Ocken, *Colloids and Surfaces* A, **85**, 19-27 (1994).

13. P. H. Tewari and A. W. McLean*, J. Colloid and Interface Sciences*, **40**, 267-272 (1972).

14. R. Ihnfeldt and J. B. Talbot, J. Electrochem. Soc., **155**(8), H582-H588 (2008).